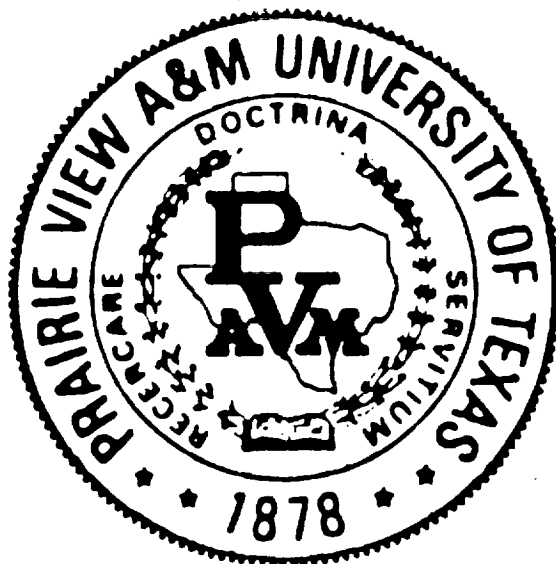


NAG 9-310

IN 44-CR  
58219  
p. 97



A

REPORT

FROM

THE

THERMAL SCIENCE

**FLOW BOILING WITH  
ENHANCEMENT DEVICES FOR  
COLD PLATE COOLANT CHANNEL DESIGN**

**FINAL REPORT  
December 27, 1991**

Submitted to:

National Aeronautics and Space Administration(NASA)  
Lyndon B. Johnson Space Center

From the:  
THERMAL SCIENCE RESEARCH CENTER(TSRC)

by

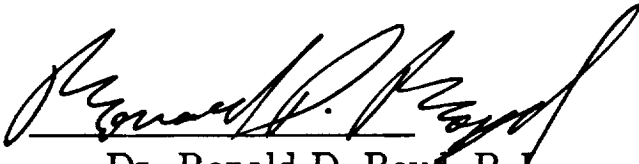
Dr. Ronald D. Boyd (P.I.)  
Honeywell Endowed Professor of Engineering and  
Director of Thermal Science Research Center  
College of Engineering and Architecture  
Prairie View A&M University  
Prairie View, TX 77446  
(409) 857-4811, 2827 or 4023

Contract No. NAG 9-310  
Purchase Request No: 89235009  
Appropriation Symbol: 809/00105  
992-15-MV-04-5A-BL-2511-AJ

**FLOW BOILING WITH  
ENHANCEMENT DEVICES FOR  
COLD PLATE COOLANT CHANNEL DESIGN**

FINAL REPORT  
December 27, 1991

PRAIRIE VIEW A&M UNIVERSITY  
Thermal Science Research Center(TSRC)



Dr. Ronald D. Boyd, P. I.,  
Honeywell Endowed Professor  
and Director of the TSRC.

# FLOW BOILING WITH ENHANCEMENT DEVICES FOR COLD PLATE COOLANT CHANNEL DESIGN

Ronald D. Boyd, P.I.

## TABLE OF CONTENTS

EXECUTIVE SUMMARY . . . . .	1
PART I: MULTI-DIMENSIONAL WALL TEMPERATURE MEASUREMENT AND HEAT TRANSFER ENHANCEMENT FOR TOP-HEATED HORIZONTAL CHANNELS WITH FLOW BOILING . . . . .	3
ABSTRACT . . . . .	4
NOMENCLATURE . . . . .	5
INTRODUCTION . . . . .	7
EXPERIMENTAL INVESTIGATION . . . . .	8
Flow Loop . . . . .	9
Test Section . . . . .	10
Data Reduction . . . . .	11
RESULTS . . . . .	14
Overall Heat Transfer . . . . .	14
Two-D Wall Temperature Distributions . . . . .	15
Circumferentially Mean, Axially Distributed Heat Transfer .	16

CONCLUSIONS . . . . .	19
ACKNOWLEDGMENTS . . . . .	20
REFERENCES . . . . .	21
TABLE 1: TEST SECTION INTERNAL CONFIGURATIONS	23
FIGURE CAPTIONS . . . . .	24
Figure 1: Freon-11 Flow Loop . . . . .	25
Figure 2: Cross Section of the Heated Portion of the Test Section . . . . .	26
Figure 3: Location of Outside Wall Temperature Measurements . . . . .	27
Figure 4: Control Volume for the Heated Hydraulic Diameter Model . . . . .	28
Figure 5: Comparison of the Overall Heat Transfer Coefficients for Different Internal Configurations . . . . .	29
Figure 6: Power vs Temperature for Large Pitch Spiral Fins . . . . .	30
Figure 7: Power vs Temperature for Large Pitch Sprial Fins with Twisted Tape . . . . .	33
Figure 8: Axial and Circumferential Wall Temperature Distributions for Small Pitch, Sprial Fins . . . . .	36
Figure 9: Axial Distribution of the Circumferentially- Averaged Heat Transfer Coefficient . . . . .	40
APPENDIX . . . . .	43
Uncertainty Analysis . . . . .	43
Sample Calculation . . . . .	49

<b>Discussion . . . . .</b>	<b>51</b>
<b>Experimental Design . . . . .</b>	<b>52</b>
<b>References . . . . .</b>	<b>53</b>

# PART II: IMPROVED ANALYTICAL HEAT TRANSFER DATA

## REDUCTION FOR A SINGLE-SIDE HEATED

COOLANT CHANNEL . . . . .	54
ABSTRACT . . . . .	55
NOMENCLATURE . . . . .	56
INTRODUCTION . . . . .	58
PROBLEM SPECIFICATION AND FORMULATION . . . . .	60
Case I: $q''(\phi)=q_o = \text{constant}$ . . . . .	62
Case II: $q''(\phi)=q_o \sin(\phi)$ . . . . .	64
Formulation Verification . . . . .	65
RESULTS . . . . .	65
Parametric Temperature Distribution . . . . .	66
Inside Wall Heat Flux Distribution . . . . .	67
CONCLUSIONS . . . . .	68
ACKNOWLEDGMENTS . . . . .	69
REFERENCES . . . . .	69
FIGURE CAPTIONS . . . . .	70
Figure 10: Circumferentially Averaged Temperature at $R=R_o$ , vs the Biot Number, $Bi$ . . . . .	71
Figure 11: Local Temperature as a Function of $R$ , $Bi$ , and $R_o$ for $\phi = 0$ and $\pi$ . . . . .	72
Figure 12: Circumferential Variation of the Ratio of the Inside to the Outside Wall Dimensionless Temperatures	

as a Function of $Bi$ for $R_o = 3.0$ . . . . .	84
Figure 13: Circumferential Variation of the "Local"	
Dimensionless Radial Temperature Gradient as a	
Function of $Bi$ and $R_o$ . . . . .	85
DISTRIBUTION . . . . .	88



# FLOW BOILING WITH ENHANCEMENT DEVICES FOR COLD PLATE COOLANT CHANNEL DESIGN

*Dr. Ronald D. Boyd (P.I.)*

*Honeywell Endowed Professor of Engineering and  
Director of the Thermal Science Research Center*

*College of Engineering and Architecture*

*Prairie View A&M University*

*Prairie View, TX 77446*

*(409) 857-4811, 2827 or 4023*

## EXECUTIVE SUMMARY

Future space exploration and commercialization will require more efficient heat rejection systems. In order to accommodate the required heat transfer rates, such systems must employ advanced heat transfer techniques. Forced two-phase flow boiling heat transfer with enhancements falls in this category. However, moderate to high quality two-phase systems tend to require higher (compared to single-phase systems) pressure losses. Previous investigators have studied a variety of two-phase flow (with Freon-11) regimes in uniformly-heated (or cooled) flow channels. It has been demonstrated that various degrees of heat transfer enhancement are possible depending on the: (1) enhancement device used, (2) predominating flow regime, (3) geometry (e.g., orientation, heat flux distribution), and (4) specific localized thermophysical processes.

Since many space applications will involve single-side (top- side) heating, it is essential to extend the literature to assess any enhancement of such heating alone and with other enhancement techniques. Experiments, using freon-11, were used primarily to examine top-side heating with and without enhancements. The objective of this work was to expand the existing freon-11 flow loop capabilities to include both saturated and subcooled flow boiling experiments. The experiments include: (1) measurements of local (axial) heat transfer coefficients, (2) evaluation of the effectiveness of combined (e.g., combined helical fins and twisted tapes) and single heat transfer enhancements, (3) assessment of the effects on heat transfer of single-side heating, and (4) development of heat transfer data reduction techniques.

Although most flow boiling experiments documented in the technical literature deal with uniform heating of the coolant channel walls, actual cold-plate components will always be heated from one side. In addition, the coolant channels of these components are likely to have a horizontal orientation. However, the magnitude of the gravitational vector will be usually small or nonexistent. Although stratification will not occur in actual cold plate channels due to gravity, some form of stratification may occur due to: (1) circumferential surface tension gradients, and (2) localized or single-side heat flux.

Thermal systems designers, for the most part, are using data from uniformly heated experiments to design components which are subjected to single-side heat fluxes. Under certain flow conditions such heat flux distributions can significantly affect the heat transfer

and hence the ability of the component to transport thermal energy. The present work has increased the heat transfer data for single-side heated channels with enhancement devices.

This final report is divided into two major parts: (1) Part I: Multidimensional Wall Temperature Measurement and Heat Transfer Enhancement for Top-Heated Horizontal Channels with Flow Boiling, and (2) Part II: Improved Analytical Heat Transfer Data Reduction for a Single-Side Heated Coolant Channel.

Part I summarizes over forty experiments which involve both single-phase convection and flow boiling in a horizontal channel heated externally from the top side. The following experimental parametric effects were included: (1) inside wall enhancement [smooth, spiral fins with small pitch, spiral fins with large pitch (LP) combined enhancements which include LP and a twisted tape], (2) channel inside diameter, (3) inlet subcooling, and circumferential heat flux distribution [uniform and top-side heating]. Part I also has an appendix, where the experimental uncertainty analysis was summarized. The resulting uncertainty in the mean heat transfer coefficient was  $\pm 14.6 \text{ W/m}^2\text{K}$ .

Part II contains parametric dimensionless curves with parameters such as the coolant channel radius ratio, the Biot number, and the circumferential coordinate. These curves directly relate the measured circumferentially averaged temperature to an equivalent mean heat transfer coefficient. For the case of non-uniform circumferential heat transfer distribution on the outside of the coolant channel, most designers desire to know the equivalent non-uniform heat flux distribution on the inside of the coolant channel. This inside surface heat flux distribution has been obtained for the case of constant external heat flux on the top of the coolant channel with the bottom half insulated. The inside wall heat flux distribution is presented in terms of dimensionless radial temperature gradients.

This report only summarizes many of the activities of the students and the principal investigator. More details can be found in students individual reports and theses. This work has supported four (4) graduate students and five (5) undergraduate students. However, many more students have been exposed indirectly to this project through technical presentations to student groups and tours of the laboratory. As a result, more students have considered and/or made plans to pursue a graduate education or improve their academic performance.

Finally, the continual support of this work by NASA and funded research from other agencies have assisted in the creation of the **Thermal Science Research Center (TSRC)** at Prairie View A&M University. This Center is interdisciplinary in that professors from Engineering, Physics, Chemistry, Mathematics, Computer Science and Engineering Technology will focus their vast backgrounds on thermal science related research and design. This includes heat transfer, thermodynamics, thermal control, fluid mechanics, mass transport, thermo-chemical processes, micro-heat transfer, two-phase flows, and non-intrusive optical diagnostics.

**PART I:**

**MULTI-DIMENSIONAL WALL  
TEMPERATURE MEASUREMENTS  
AND HEAT TRANSFER ENHANCEMENT  
FOR TOP-HEATED HORIZONTAL CHANNELS  
WITH FLOW BOILING**

# MULTI-DIMENSIONAL WALL TEMPERATURE AND HEAT TRANSFER ENHANCEMENT FOR TOP-HEATED HORIZONTAL CHANNELS WITH FLOW BOILING

Ronald D. Boyd<sup>1</sup>, Alvin Smith<sup>2</sup>, and  
Jerry C. Turknett<sup>3</sup>

Mechanical Engineering Department  
P. O. Box 397  
Prairie View A&M University  
Prairie View, TX 77446

## Abstract

Two-dimensional (circumferential and axial) wall temperature distributions have been measured for top-heated coolant channels with different internal geometries which include smooth walls, spiral fins, and both twisted tape and spiral fins. Freon-11 was the working fluid. The flow regimes studied include: (1) single phase, (2) subcooled flow boiling, and (3) stratified flow boiling. The inside diameter of all test sections was near 1.0 cm. Circumferentially averaged heat transfer coefficients at several axial locations were obtained for selected coolant channels for a mass velocity of  $210 \text{ kg/m}^2\text{s}$ , 0.19 MPa (absolute) exit pressure, and  $20.8^\circ\text{C}$  inlet subcooling. Overall (averaged over the entire channel) heat transfer coefficients were compared for the above channel geometries. This comparison showed that the channel with large pitch spiral fins had higher heat transfer coefficients at all power levels. However, the results appear to indicate that if the twist ratio (ratio of the twisted tape period to the inside diameter) was decreased, the configuration employing

---

<sup>1</sup> Honeywell Endowed Professor of Engineering and Director of the Thermal Science Research Center

<sup>2</sup> Harrison Division, General Motors Corp.; 200 Upper Mountain Rd; A&E, Bldg 6; Lockport, NY 14094

<sup>3</sup> Westinghouse Savannah River Company; P. O. Box 616; Bldg 705-1c; Aiken, SC 29802

both fins and a twisted tape would have had greater enhancements.

## NOMENCLATURE

$A_s$	Surface area, $m^2$
$D$	Thermal hydraulic diameter, m
$Ec$	Eckert number, $\frac{G^2}{\rho_{liq}^2 c_p (T_m - T_{sat})}$
$h$	Circumferentially and axially averaged heat transfer coefficient (HTC), $W/m^2 K$
$h_m$	Axially-distributed but circumferentially-averaged HTC, $W/m^2 K$
$h_\infty$	HTC due to natural convection (see Figure 4), $W/m^2 K$
$i_{fg}$	Specific latent heat of vaporization, kJ/kg
$i_{subliq}$	Enthalpy subcooling of the fluid, kJ/kg
$Ja^*$	Jakob number, $\frac{\Delta i_{subliq}}{i_{fg}}$
$k$	Thermal conductivity, W/mK
$Pe$	Peclet number, $Re Pr$
$P_p$	Net power generation, W
$q_c$	Heat flux due to natural convection from outside of test section (see Figure 4), $W/m^2$
$q_R$	Heat flux due to radiation from the outside of the test section, $W/m^2$
$r$	Radial coordinate for the data reduction model (see Figure 4), m
$T_f$	Bulk temperature of the flowing fluid (see Figure 2), $^{\circ}C$
$T_m(\phi, Z)$	Local measured outside wall temperature of the test section (see Figures 3 and 4), $^{\circ}C$
$T_w(\phi, Z)$	Outside wall temperature of the test section = $T_m(\phi, Z)$ , $^{\circ}C$
$T_{sat}$	Saturation temperature (316 K at 0.19 MPa for Freon-11), $^{\circ}C$

$T_{\infty}$  Ambient temperature,  $^{\circ}C$

$We^*$  Modified Weber number,  $\frac{\rho_g G^2 D}{\rho_{liq}^2 \sigma}$

$Z$  Axial coordinate for the heated portion of the test section (see Figure 3), cm

### *Subscripts*

$A, B, \text{ and } C$  Denotes Domains A, B, or C (see Figure 4)

$i$  = 1 through 7 for each axial location (see Figure 3)

### *Greek*

$\phi$  Circumferential coordinate; see Figures 2, 3, and 6 ("Phi")

$\pi$  Half of a full rotation or 180 degrees; in some figures,  $\pi$  is also referred to as "Pi."

$\rho_g$  Density of gaseous phase of fluid,  $kg/m^3$

$\rho_{liq}$  Density of liquid phase of fluid,  $kg/m^3$

## INTRODUCTION

Space commercialization will require efficient heat transfer systems. The future success of many efforts will be based on our understanding of the behavior of two-phase flow boiling in both the space (zero-g or reduced-g) and earth environments. This was emphasized in the Workshop on Two-Phase Fluid Behavior in a Space Environment, sponsored by NASA (Swanson, et al., 1989). Flow boiling heat transfer offers an enhancement alternative to forced-primed and capillarity heat management systems. Essential to better understanding factors affecting flow boiling in heated tubes is the following effects: (1) non-uniform heat flux distribution, (2) local (axial and circumferential) distributions of the heat transfer coefficient, (3) resulting pressure drop and pumping power requirements, (4) single and double enhancement devices, (5) the relative advantages of saturated and subcooled flow boiling regimes, (6) flow channel aspect ratio effects, (7) the relative effects of heat transfer enhancement techniques, and (8) correlations for mean and local heat transfer, and pressure drop. In addition to being applicable to several gravitational levels, future research efforts must also include basic phenomena such as: (1) orientation (e.g., vertical flow and bottom-heated flow channels) and Marangoni effects, (2) other working fluids such as ammonia, (3) flow stability, (4) binary fluids, and (5) identification of the threshold inertia (Froude number) beyond which gravity effects would be negligible. For example, threshold inertia determination is necessary to identify when orientation and/or Marangoni effects become important. Although it is not apparent, the development of improved data reduction models is also essential to the accurate representation and interpretation of the heat transfer data.

This work will assist the development of fundamentally-based heat transfer correlations which include effects of: (1) enhancement device configurations for fluids other than air (Carnovos, 1977), (2) basic flow parameters which are fluid independent, and (3) complex heat flux distributions.

This paper examines, experimentally, two-dimensional wall temperature variations for highly turbulent horizontal channel flows, which are heated from the top. Freon-11 was the working fluid. The temperature measurement were used to obtain axial variations in the circumferentially averaged heat transfer coefficient ( $h_m$ ). The over-all heat transfer coefficient ( $h$ ) was determined and compared for four different internal channel enhancement configurations (see Table 1): (1) smooth wall, (2) spiral fins with a small pitch (SP, 6.52 fins per cm), (3) spiral fins with a larger pitch (LP, 4.0 fins per cm), and (4) doubly enhanced spiral fins with both large pitch fins and a twisted tape.

## EXPERIMENTAL INVESTIGATION

In this section, brief descriptions are given of the freon-11 flow loop, test section, and the data reduction procedure.



### Flow Loop

The flow loop (see Figure 1) was a closed system, which operates between 0.1 MPa ( $T_{sat} = 24^{\circ}C$ ) and 1.3 MPa ( $T_{sat} = 124^{\circ}C$ ). The total power generation was 2.6 kW, and the maximum mass velocity was  $1.0 \text{ Mg/m}^2\text{s}$ . Under special circumstances, the loop can be operated at a pressure near 0.04 MPa ( $T_{sat} = 0^{\circ}C$ ). The loop has two reservoirs ( $0.25 \text{ m}^3$  each). The reservoirs have separate heat exchanger jackets for secondary temperature control. The flow loop tubing was 2.5 cm (inside diameter) stainless steel. The flow loop consists of: (1) the freon loop, (2) air lines for pneumatically controlling valves and pulsation damper, and (3) vacuum lines for system evacuation.

The freon loop was designed to study both saturated and subcooled flow boiling regimes. After the loop was evacuated, it was filled with freon until the pressure was slightly above the atmospheric pressure. After the charging process, the fluid was circulated through the loop at the desired operating conditions. Bled valves were used to purge the loop and transducers of any gases, and the flow conditions were reestablished. During a given test, the heater tape power output was adjusted to a given level. The flow rate of the isothermal bath (50%-50% mixture of ethylene glycol and water) was adjusted until the test section inlet temperature was at the desired level. A steady-state was then allowed to occur. After all the desired flow conditions were again verified, the test section's axial and circumferential wall temperature measurements were recorded along with all the flow conditions.

Referring to Figure 1, the freon flowed from reservoir 1 through a filter to the main pump (positive displacement), which required a net positive suction pressure of at least

0.02 MPa. After leaving the pump, the fluid passed near a pulsation damper, which reduced the pressure and flow oscillations. When the damper was used, a pneumatically controlled metering valve was used to stabilize the flow. After exiting the metering valve, the fluid passed through a turbine flowmeter and then through an unheated flow developing section (upstream portion of the test section) which had a length greater than 40 times the test section's diameter. This flow developing section had the same diameter as the heated portion of the test section. As the fluid flowed through the test section, the inlet and exit temperatures and pressures were monitored. The downstream portion of the test section was heated (with a heater tape) on its top half. A downstream valve was used to control the test section's exit pressure. The fluid then passed through the heat exchanger where the energy generated in the test section was removed. For these tests, the working fluid bypassed reservoir 2 and the charging pump and then flowed back to reservoir 1.

### Test Section

The test section was 223.0 cm long and is shown in Figures 2 and 3. The upstream unheated portion of the test had smooth walls and the downstream heated portion (121.9 cm long) had either smooth or an enhanced wall configuration (spiral fins and/or a twisted tape). The entire test section was insulated, and had three main ports (with a fourth extending from the center one), mounted facing downward on either end of the test section. These ports were used to monitor the inlet and exit fluid pressures, temperatures, and test section differential pressure. Each test section had twenty-eight (28) Type-K thermocouples mounted on the outside surface of the copper flow channel. Seven thermocouples were used to make temperature measurements ( $T_m$ ) at specific axial locations (see Figure 3)

on the wall of the coolant channel. Figure 3 also shows the four circumferential locations ( $\phi = 0, \frac{\pi}{4}, \frac{3\pi}{4},$  and  $\pi$  radians) at which wall temperature measurements were made for each of the seven axial locations. All measurements were made for flow conditions of: (1) 0.19 MPa (absolute) exit pressure, (2) 22.2°C inlet temperature, and (3) a mass velocity of 210 kg/m<sup>2</sup>s. These wall temperature measurements were used, along with other measured conditions and the data reduction analysis, to determine the unknown steady-state heat transfer coefficients ( $h$ , and  $h_m$ ).

### Data Reduction

The data reduction approach was based on a heated hydraulic diameter (Boyd and Turknett, 1989) assumption. Figure 4 shows the model used for this approach. This model was used to compute a circumferentially averaged heat transfer coefficient from the circumferentially averaged wall temperature. This latter temperature was computed from the four wall temperature measurements made on the outside of the test section at each of the seven axial locations.

Briefly, this approach involves estimating the inside flow channel's wall temperature by using an equivalent uniformly heated tube, whose diameter is equal to the ratio of four times the actual flow channel cross sectional area to the heated perimeter. This was done using the model in Figure 4, by accounting for the temperature drop across the flow channel wall, and the heat losses (convection and radiation) from the test section to the ambient. An iteration scheme was necessary to compute the inside wall temperature. After accounting for finite heat losses, the circumferentially averaged heat transfer coefficient was given by

$$h_m = \frac{A}{B}, \quad (1)$$

where

$$A = \left(\frac{k_A}{r_A}\right) B_1 \left[\ln\left(\frac{r_D}{r_c}\right) + \frac{k_C}{h_\infty r_D}\right] - \left(\frac{k_C}{r_A}\right)(T_m - T_\infty),$$

$$B = B_2 + B_3 + B_4,$$

$$B_1 = \frac{P_p r_C}{A_s k_B},$$

$$B_2 = [T_m - T_\infty] \left[ \ln\left(\frac{r_D}{r_C}\right) + \frac{k_C}{h_\infty r_D} + \left(\frac{k_C}{k_B}\right) \ln\left(\frac{r_C}{r_B}\right) \right],$$

$$B_3 = [T_m - T_\infty] \left[ \frac{k_C}{k_A} \ln\left(\frac{r_B}{r_A}\right) \right] - \left[ \ln\left(\frac{r_D}{r_C}\right) + \frac{k_c}{h_\infty r_D} \right] [T_f - T_\infty],$$

and

$$B_4 = B_1 \left[ \ln\left(\frac{r_C}{r_B}\right) + \left(\frac{k_B}{k_A}\right) \ln\left(\frac{r_B}{r_A}\right) \right].$$

In the above expression for the circumferentially-averaged heat transfer coefficient ( $h_m$ ), the magnitude of the bulk temperature,  $T_f$ , is dependent on  $T_{av}$ , which is the circumferentially-averaged wall temperature at  $r = r_C$  (see Figures 3 and 4).  $T_f$  was determined based on the magnitude of  $T_{av}$  relative to the wall temperature,  $T_{w_{ONB}}$  which is the temperature required for the onset of nucleate boiling. The bulk fluid temperature is given by,

$$T_f = \begin{cases} T_f(z), & \text{for } T_{av} < T_{w_{ONB}}; \\ T_{sat}, & T_{av} \geq T_{w_{ONB}} \end{cases}. \quad (2)$$

For a given axial location, the measured circumferential values of  $T_m$  were related to  $T_{av}$  by

$$T_{av} = \frac{T_m(\theta = 0) + 3T_m(\theta = \frac{\pi}{4}) + 3T_m(\theta = \frac{3\pi}{4}) + T_m(\theta = \pi)}{8}, \quad (3)$$

Finally, the temperature  $T_{w_{ONB}}$  was computed using the correlation by Frost and Dzakowic (Collier, 1981),

$$1.0 = 8.0 St_{ONB} Pe We^{*-1} Ec Ja^*. \quad (4)$$

Using equation (4), the superheat required for the onset of nucleation was  $5.9^\circ C$  (for a pressure of 0.19 MPa).

In some cases, the heat transfer coefficient was not only averaged circumferentially but also axially. Although there were seven axial locations at which wall temperature measurements were made, those measurements near either end of the test section heated length were influenced by end losses. Hence, the averaged heat transfer coefficient,  $h$ , was obtained using the five central axial locations ( $Z_2$ ,  $Z_3$ ,  $Z_4$ ,  $Z_5$ , and  $Z_6$ ),

$$h = \frac{h_{m_2} + 2h_{m_3} + 2h_{m_4} + 2h_{m_5} + h_{m_6}}{8}, \quad (5)$$

so that the values of  $h_{m_i}$  (where  $i = 2, 3, 4, 5$ , and  $6$ ) correspond to the various locations at  $Z_i$ .

An uncertainty analysis was developed using the above formulae to estimate the uncertainty,  $\delta h_m$ . Using the approach suggested by Moffat (1988, 1990),  $\delta h_m$  was found to be  $\pm 14.6 W/m^2 K$ .

## RESULTS

For the various internal channel configurations noted above, comparisons were made of the two-dimensional wall temperature distributions, axial distribution of the mean (circumferentially-averaged) heat transfer coefficient ( $h_m$ ), and the totally averaged (circumferentially and axially) or overall heat transfer coefficient ( $h$ ).

### Overall Heat Transfer

Figure 5 shows a comparison of the overall heat transfer coefficient for the four internal configurations. These comparisons show that the spiral fins with the large pitch resulted in a higher heat transfer coefficient at all power levels. The discontinuities in each curve are due to either nucleate boiling or severe flow structure change at certain axial or circumferential locations for a given power level. Since the test section was horizontal and since the mass velocity level was relatively low (low Froude number), stratification effects were expected and found to be significant. Stratification conditions reduced the enhancement effectiveness for all internal configurations. Preliminary estimates indicated that these reductions could be as high as an order of magnitude relative to vertical flow.

### Two-D Wall Temperature Distributions

Figures 6 (6a-6c) and 7 (7a-7c) show the power generation as a function of measured outside wall temperature at different circumferential and axial locations for the cases of large pitch spiral fins without and with a twisted tape, respectively. The three figures in each of these sets are for three of the four circumferential locations ( $\phi = 0, \frac{\pi}{4}, \text{ and } \pi$ ; see Figure 3). As  $\phi$  varied from 0 to  $\frac{\pi}{4}$ , the peak wall temperatures for the case of large pitch fins with the twisted tape were consistently higher than those for the channel with only the large pitch spiral fins. This was displayed more dramatically in Figure 8, which shows the axial distribution of  $T_W (= T_m)$  for the four circumferential locations and constant power. While the wall temperature distributions were essentially identical for  $\phi = \frac{3\pi}{4}, \text{ and } \pi$ , there were significant differences at  $\phi = 0 \text{ and } \frac{\pi}{4}$  (compare Figures 8a and 8b). It is apparent from these figures that the addition of a tape increased mixing and reduced stratification at downstream locations. For the case without the twisted tape and for  $\phi = 0$ , the wall temperature in the upstream portion of the test section between  $Z_2$  ( $Z=20.32 \text{ cm}$ ) and  $Z_4$  ( $Z=60.98 \text{ cm}$ ) was consistently lower than that with the twisted tape. However, this trend reversed downstream of  $Z_5$  ( $Z=81.28 \text{ cm}$ ). Since the power level for the large pitch finned tube in Figure 8a ( $P_p = 653 \text{ W}$ ) was greater than that for the large pitch finned tube with a twisted tape (shown in Figure 8b with  $P_p = 611.0 \text{ W}$ ), the profiles for the former case will be consistently lower than that for the latter case at the same power level. With the exception of the differences noted at  $\phi = 0 \text{ and } \frac{\pi}{4}$ , the two profiles were similar. Further, for the case with the twisted tape and the large pitch fins and at  $\phi = \frac{\pi}{4}$ , the wall temperature varied axially in a periodic manner between maxima

of  $155^{\circ}\text{C}$  (upstream) and  $90^{\circ}\text{C}$  (downstream). Since there were only seven axial locations in which measurements were made, it was not possible to determine the period of this variation. However, the present measurements indicate that the period was less than 40.0 cm. As implied above, the amplitude of the fluctuations decreased as  $Z$  increased. These latter trends were caused by: (1) periodic liquid wetting near  $\phi = \frac{\pi}{4}$  (off center from the top of the channel) due to the swirl flow, (2) liquid entrainment into the vapor flow, and (3) circumferential conduction in the tube.

From Figures 8a and 8b, stratification effects can be seen to have been significant in that: (1) the wall temperatures at  $\phi = 0$  remained significantly above the saturation temperature ( $T_{sat} = 43^{\circ}\text{C}$ ), and (2) those wall temperatures at  $\phi = \frac{3\pi}{4}$  and  $\pi$  were consistently below  $T_{sat}$ . However, the tubes with the large pitch fins (with and without the twisted tape) reduced stratification much more than the small pitch finned wall tube. As  $Z$  was increased, the stratification decreased more for the former two configurations than for either the smooth tube or the small pitch fins (compare Figures 8a and 8b with 8c and 8d). Although the power levels for the latter two figures are lower than that of the former two, a comparison of the axial distribution of the circumferentially-averaged wall temperatures clearly shows significant reductions in  $T_w$  with respect to  $Z$  for the large pitch finned wall. In fact, the large pitch spiral fin with the twisted tape was more effective than all other cases.

In all tube configurations, the wall temperature increased (from  $22.2^{\circ}\text{C}$ ) with  $Z$  near the entrance ( $Z_1$ ) and later decreased (to near  $25.0^{\circ}\text{C}$ ) as  $Z$  approached  $Z_7$ , near the exit of the test section.



### Circumferentially Mean, Axially-Distributed Heat Transfer

Figures 8a and 8b emphasize the significance of the circumferential temperature variations in systems with single-side heating. It is apparent that in cases where stratification is important, the addition of a twisted tape will, at some locations, exacerbate (compare Figures 8a and 8b, for  $\phi = \frac{\pi}{4}$ ) the already large wall temperature and small heat transfer coefficient. However, the data also indicated that the twisted tape will enhance, rather than inhibit, the heat transfer in some cases. Before this enhancing effect is discussed, the adverse influence of the twisted tape on the heat transfer coefficient will be discussed.

The detrimental influence on  $h_m$  due to the addition of the twisted tape was emphasized by considering the circumferential averaged heat transfer coefficients as a function of the power generation, with  $Z$  as a parameter. At each axial location, a sudden rise in  $h_m$  was a manifestation of the inside wall temperature (computed from the measured outside wall temperature) exceeding the absolute wall superheat required for the onset of nucleate boiling. Relatively speaking, larger values of  $h_m$  (1,500 to 2,000  $W/m^2 K$ ) were obtained at both the entrance ( $Z_1$ ) and the exit ( $Z_7$ ) than at intermediate locations. This is due to: (1) entrance effects, (2) the presence of the single-phase liquid at the bottom of the tube, (3) axial conduction losses, and (4) the absence of heating from the heater tape near the exit. Therefore, the data near the test section exit and entrance may not be representative of the actual behavior. Nevertheless, when the values of  $h_m$  at the intermediate axial locations were compared, one finds that the levels of  $h_m$  before and after ONB were higher for the tube without the twisted tape.

The above trends could possibly be reversed by reconfiguring the twisted tape. The

twisted tapes's twist ratio ( $t_T$ , ratio of the axial period to the inside diameter) appears to be the underlying factor which could improve the enhancement capabilities of the tube with both fins and a twisted tape. Supporting evidence for this possibility can be observed by comparing either Figures 6b with 7b or 8a with 8b for  $\phi = \frac{\pi}{4}$ . As noted earlier, the effect of the twisted tape is to raise the local wall temperature at some axial locations and lower it at other locations. In cases where the wall temperature was lowered, these lower values (as well as the peak values) decreased with increasing  $Z$ . It would appear that if the period of these temperature fluctuations could be decreased, the lower levels of the wall temperature would prevail over a large portion of the flow channel. Lower temperatures, and hence larger  $h_m$ , would result due to increased mixing between the stratified fluid layers. This overall trend, of enhanced heat transfer accompanying reduced  $t_T$ , has been pointed out in the literature (e.g., see Kirishenko, 1980; and Hong and Bergles, 1976) but has never [to the authors' knowledge] been documented by local measurements on top-heated tubes. However, to verify that this is also true for stratified flows, the present work should be extended to include lower values of  $t_T$ .

The axial distribution of the circumferentially mean heat transfer coefficient ( $h_m$ ) is shown in Figure 9 for three of the four internal tube configurations. The axial trends for the smooth wall case in Figure 9c form a basis for the other cases. The trends in the axial variation of  $h_m(Z)$  become increasingly irregular as the internal enhancement progresses from smooth wall tube to the small pitch fins and eventually to the large pitch fins with the twisted tape. There was a reduction and subsequent increase in  $h_m(Z)$  as  $Z$  increased, which is similar to observations made by Reid et al. (1987) for the case of uniform heating.

From Figure 9c, there was a local (axial) peak in  $h_m(Z)$ , which moved downstream as the power increased. This may be representative of a slug-type flow and may be a unique consequence of the top-heated boundary condition. The width of the axial distribution and the magnitudes of  $h_m(Z)$  increased with the power. For the smooth wall case, all curves appeared to approach an asymptote as  $Z$  increased. The addition of enhancement devices disrupted these rather regular trends. The fluctuations of  $h_m(Z)$  with increasing  $Z$  still existed but became more irregular and greater in amplitude.

## CONCLUSIONS

The present work provides experimental data characterizing the localized thermal transport in top-heated horizontal coolant channels with enhancement devices. The present local wall temperature measurements form a basis for future comparisons with both three-dimensional numerical predictions. Such comparisons will be useful in explaining the underlying local flow conditions which are favorable to both local and overall heat transfer enhancement in top-heated configurations. This can be demonstrated in a limited way by noticing the behavior for  $h_m$  for  $\phi = \frac{\pi}{4}$  in Figures 8a, and 8b. The effect of adding a twisted tape was to move the peak wall temperature upstream. The present cases should be expanded to include additional circumferential and axial resolution of the wall temperature variations, and comparisons at additional levels of mass velocity. The two-dimensional wall temperature measurements were used to determine the circumferentially-mean but axially-dependent heat transfer coefficient. The flow in the coolant channel was hydrodynamically developed but thermally developing with regions of: (1) single phase convection, (2) local subcooled boiling, and (3) a predominating stratification flow over most of the channel's

length.

The results show that the coolant channel with the large pitch spiral fins had a larger overall heat transfer coefficient than smooth tubes, or tubes with either small pitch spiral fins or a combination of large pitch spiral fins and a twisted tape. However, local measurements indicated that the effectiveness of the latter case will improve for stratified flow as the period of the twisted tape is reduced. Although similar observations have been made in the literature for non-stratified flows, the present local measurements not only documents this effect, but: (1) provides a basis for comparisons with three-dimensional, two-phase, numerical models, and (2) forms a basis for assessing present and evolving heat transfer correlations.

## ACKNOWLEDGMENTS

The authors would like to acknowledge Dr. Joseph Atkinson, Russ Long, John Thornborrow, and Dr. Y. Freeman for their support and assistance. The authors are especially appreciative to NASA (JSC and Headquarters) for supporting this work under contract 9-310. In addition, the authors are grateful to Mark Martin, and David Ogbuaku for their assistance and their willingness to consider and complete graduate school.

## REFERENCES

1. Boyd, R. D., and Turknett, J. C., 1989, "Forced Convection and Flow Boiling with and without Enhancement Devices for Top-Side-Heated Horizontal Channels," NASA Space Science and Engineering Research Forum Proceedings, Alabama A&M University, Huntsville, Alabama, March 22-23, pp. 363-370.
2. Carnovos, T. C., 1977, "Cooling Air in Turbulent Flow with Internally Finned Tubes," **Process Heat Transfer**, AIChE HT & EC Division, National Heat Transfer Conference, pp 32-37.
3. Collier, J. G., 1981, **Convective Boiling and Condensation**, 2nd ed., McGraw-Hill, New York.
4. Hong, S. W., and Bergles, A. E., 1976, "Augmentation of Laminar Flow Heat Transfer in Tubes by Means of Twisted-Tape Inserts," **Journal of Heat Transfer**, May issue, pp. 251-256.
5. Kiricheuko, Yu. A. et al., 1980, "Investigation of Effect of Subcooling on Centrifugal Acceleration on Nucleate Boiling Heat Transfer to Cryogenic Fluids," **Heat Transfer-Sov. Res.**, **12** (2), p. 57.
6. Moffat, R. J., 1990, "Estimating the Credibility of Experimental Work," Department of Mechanical Engineering, Stanford University, Stanford, CA 94305.
7. Moffat, R. J., 1988, "Describing the Uncertainties in Experimental Results," **Experimental Thermal and Fluid Science**, Vol 1, pp. 3-17.
8. Reid, R. S., Pate, M. B., and Bergles, A. E., 1987, "Evaporation of Freon-113 Flowing Inside Smooth Tubes," National Heat Transfer Conference, Pittsburgh, Pennsylvania,

ASME 87-HT-51, August, 1987.

9. Swanson, T. D., et al., 1989, **Workshop on Two-Phase Fluid Behavior in a Space Environment**, NASA Conference Publication 3043.

**Table 1: Test Section Internal Configurations\*.**

<b>Tube Type</b>	<b>O.D.</b>	<b>I.D.</b>	<b>No. Fins</b>	<b>Fin Height</b>	<b>Fin Width</b>	<b>Fins/cm</b>
Spiral Fin L.P.	1.27 cm	0.95 cm	16	0.056 cm	0.30 cm	4
Spiral Fin L.P./Tape	1.27 cm	0.95 cm	16	0.056 cm	0.3 cm	4
Spiral Fin S.P.	1.27 cm	1.13 cm	26	0.056 cm	0.30 cm	6
Smooth Walls	1.27 cm	1.07 cm	–	–	–	–

**\*Note:** L.P., and S.P. denote large and small pitch fins, respectively.

## Figure Captions

Figure 1. Freon-11 Flow Loop for Both Subcooled and Saturated Flow Boiling Experiments.

Figure 2. Cross Section of the Heated Portion of the Test Section.

Figure 3. Wall Temperature Measurement Locations.

Figure 4. Control Volume for the Heated Hydraulic Diameter Model.

Figure 5. Comparison of the Overall Heat Transfer Coefficients for Circular Coolant Channels With Different Internal Configurations.

Figure 6. Measured Outside Wall Temperature Axial Distribution as a Function of the Net Power Generation for the Spiral Fin, Large Pitch Internal Geometry at: (a)  $\phi = 0$ , (b)  $\phi = \frac{\pi}{4}$ , and (c)  $\phi = \pi$ .

Figure 7. Measured Outside Wall Temperature Axial Distribution as a Function of the Net Power Generation for the Spiral Fin, Large Pitch With a Twisted Tape Internal Geometry at: (a)  $\phi = 0$ , (b)  $\phi = \frac{\pi}{4}$ , and (c)  $\phi = \pi$ .

Figure 8. Axial Distribution of the Wall Temperature for the Four Circumferential Locations for the: (a) Large Pitch Spiral Fins, (b) Large Pitch Spiral Fins With Twisted Tape, (c) Small Pitch Spiral Fins, and (d) Smooth Tube.

Figure 9 Axial Distribution of the Circumferentially Averaged Heat Transfer Coefficient for: (a) Large Pitch Spiral Fins With a Twisted Tape, (b) Small Pitch Spiral Fins, and (c) Smooth Wall.



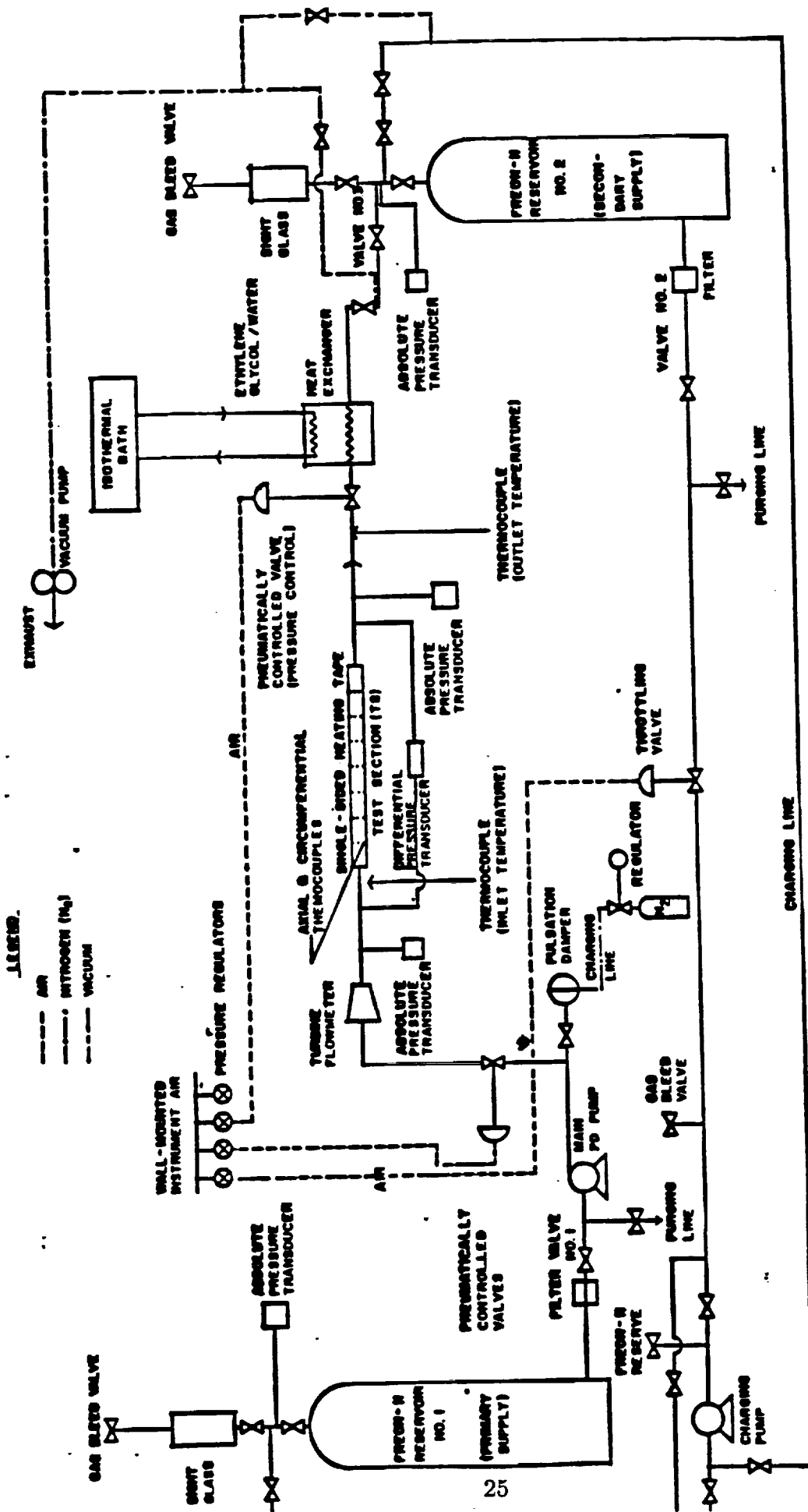
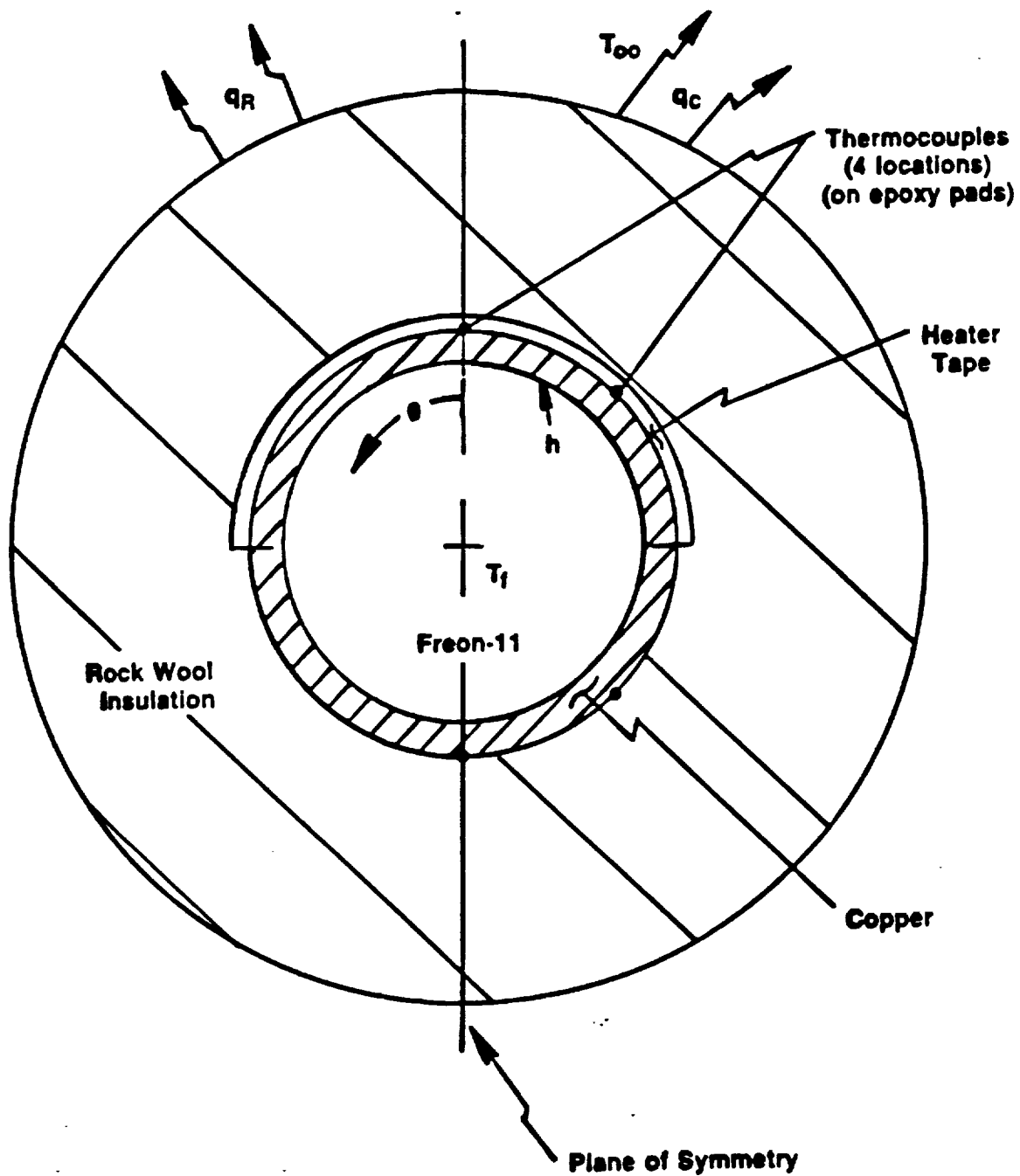


Figure 1: Freon-11 Flow Loop for Both Subcooled and Saturated Flow Boiling Experiments.

ORIGINAL PAGE IS  
OF POOR QUALITY



**Figure 2.** Cross Section of the Heated Portion of the Test Section.

LOCATION MEASUREMENTS (cm)						
Z1	Z2	Z3	Z4	Z5	Z6	Z7
0.00	20.32	40.64	60.96	81.28	101.60	121.9

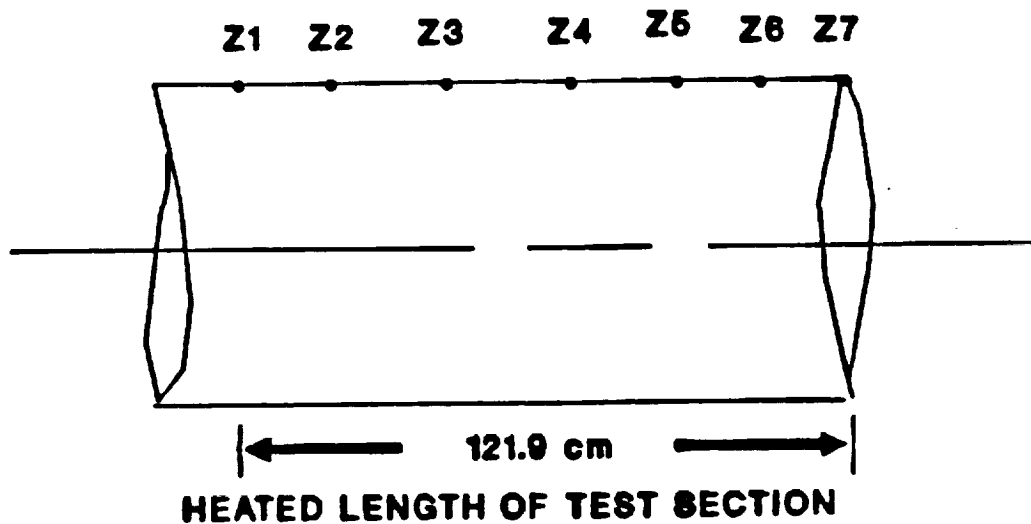
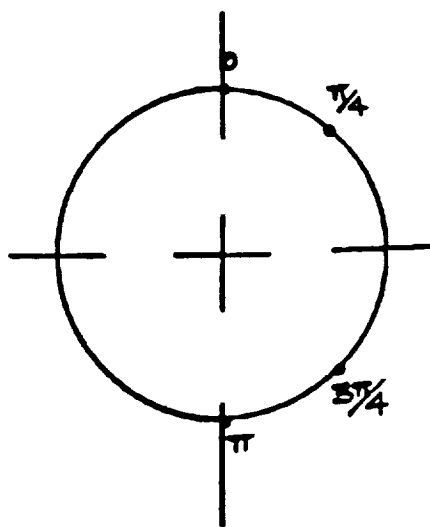


Figure 3.: Locations in which Local Outside Wall Temperature Measurements were Made.

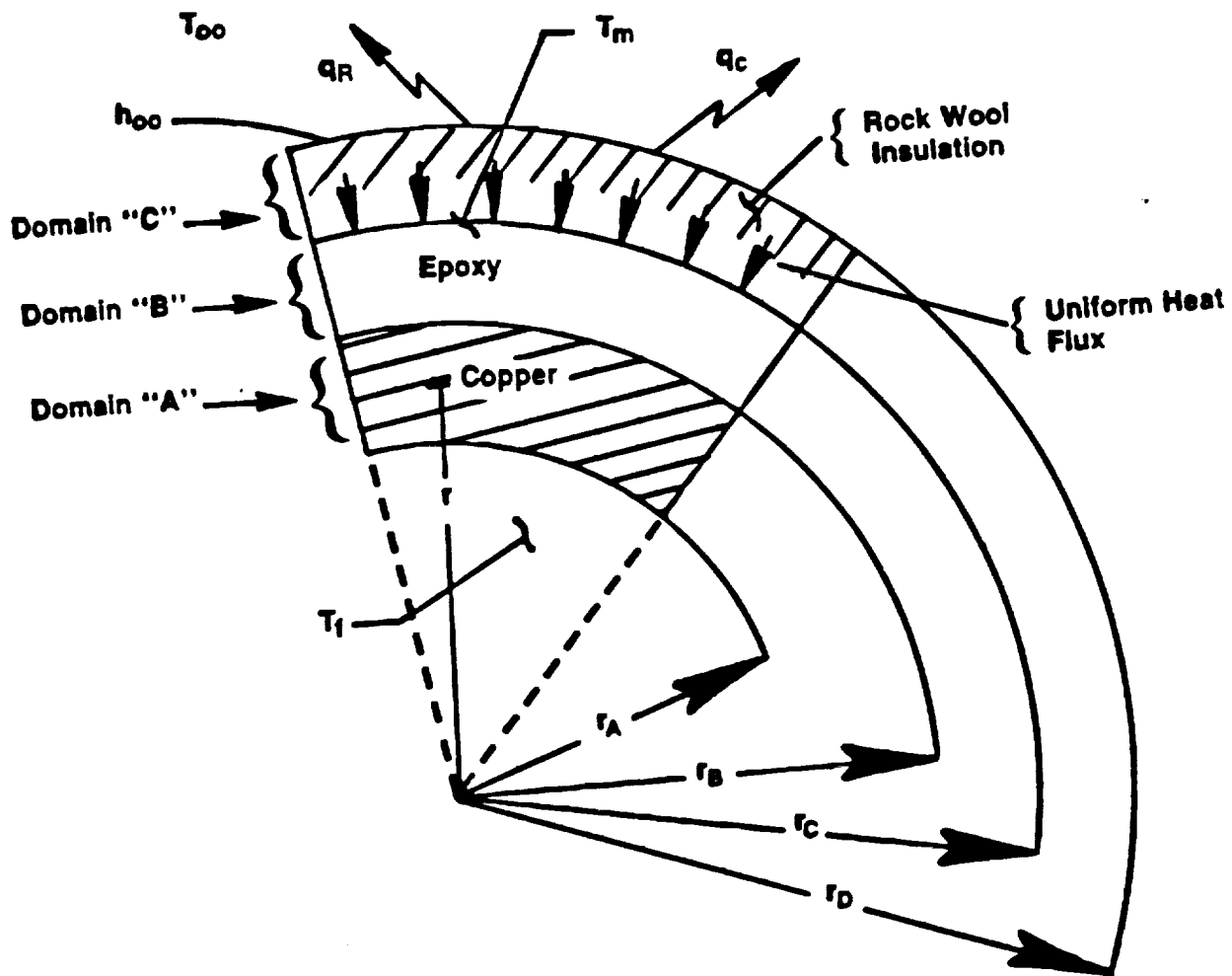


Figure 4.: Control Volume for the Heated Hydraulic Diameter Model.

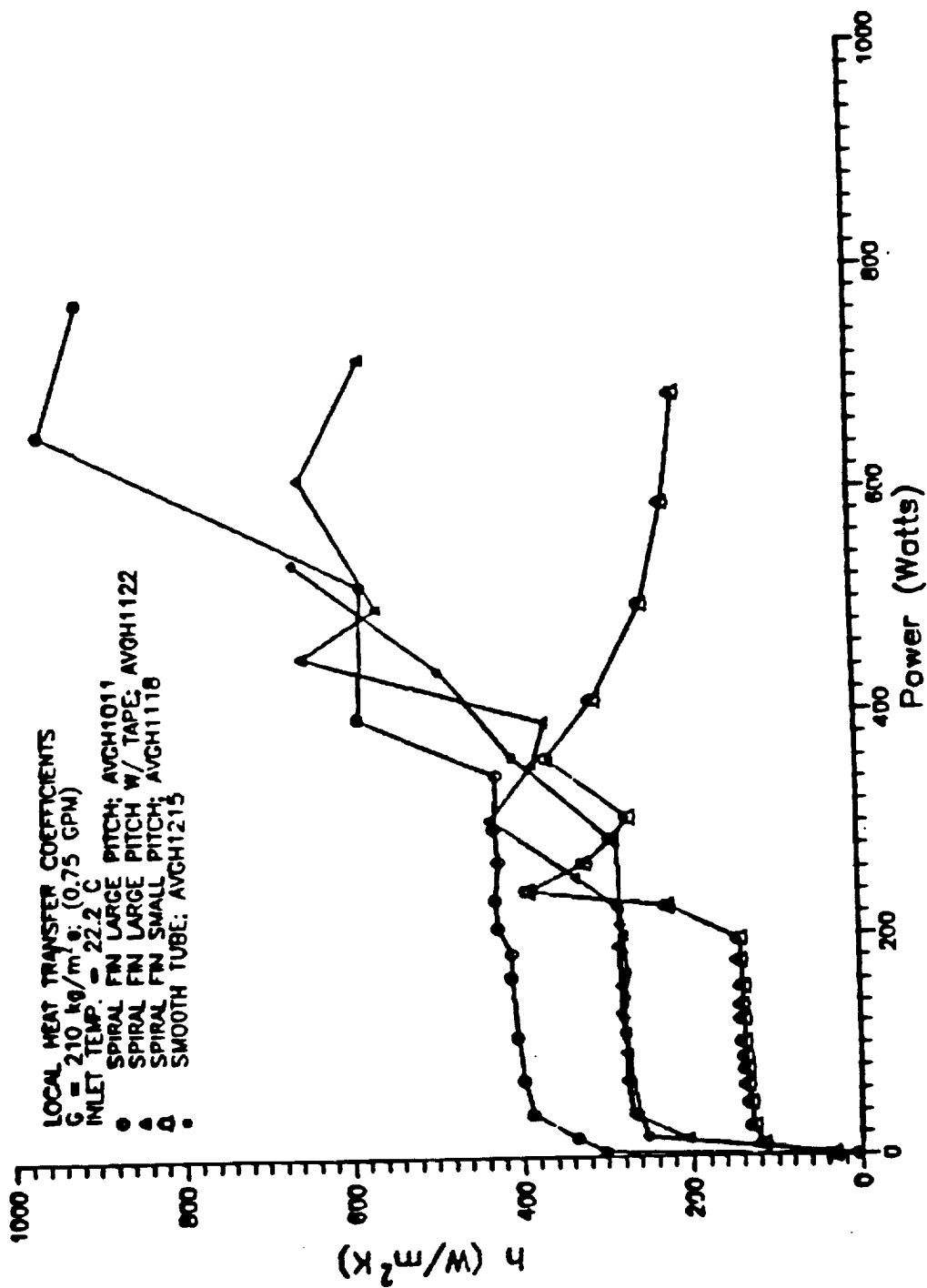


Figure 5.: Comparison of the Overall Heat Transfer Coefficients for Circular Coolant Channels with Different Internal Configurations.

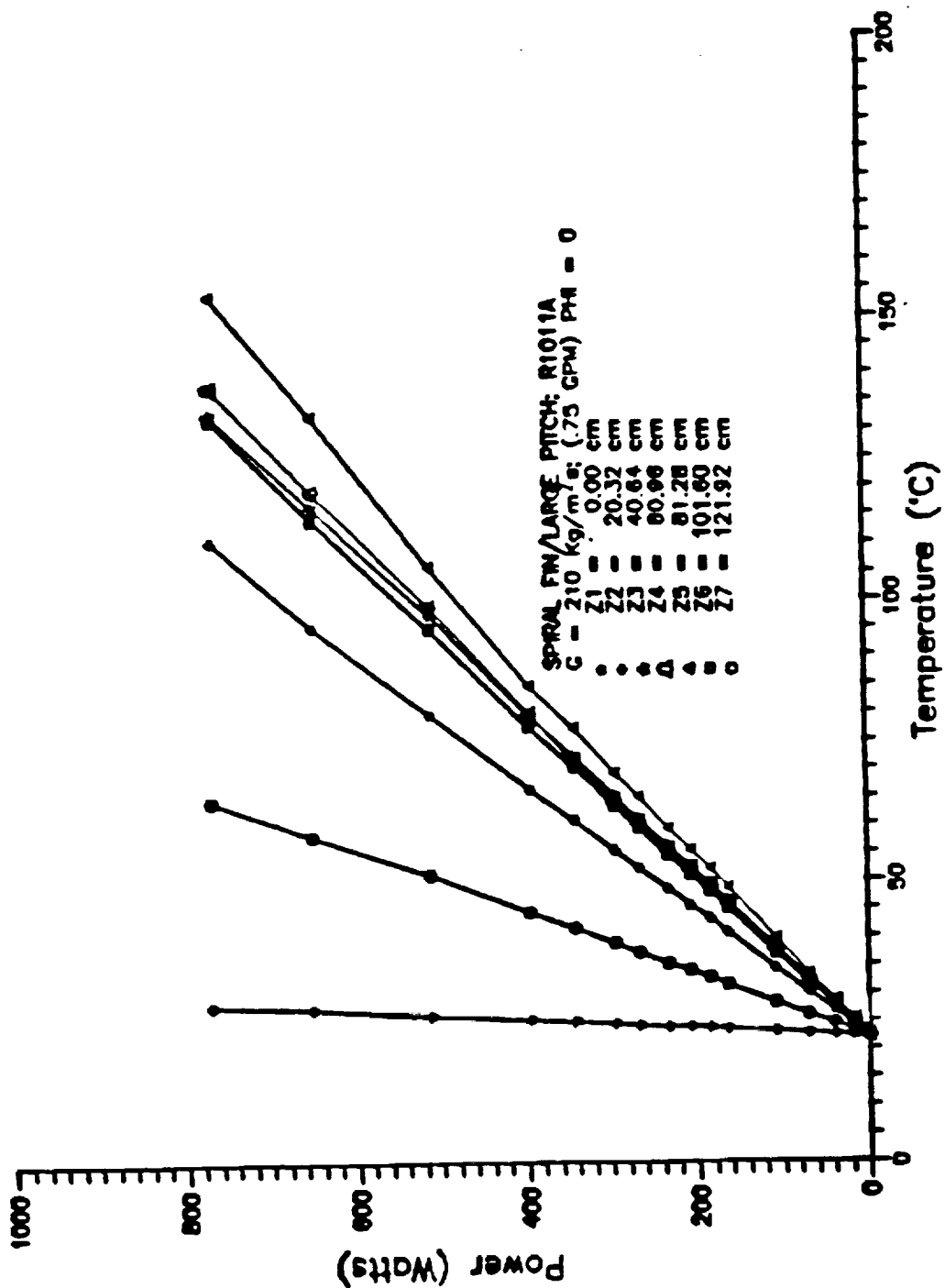


Figure 6. (a)  $\phi = 0$ ,

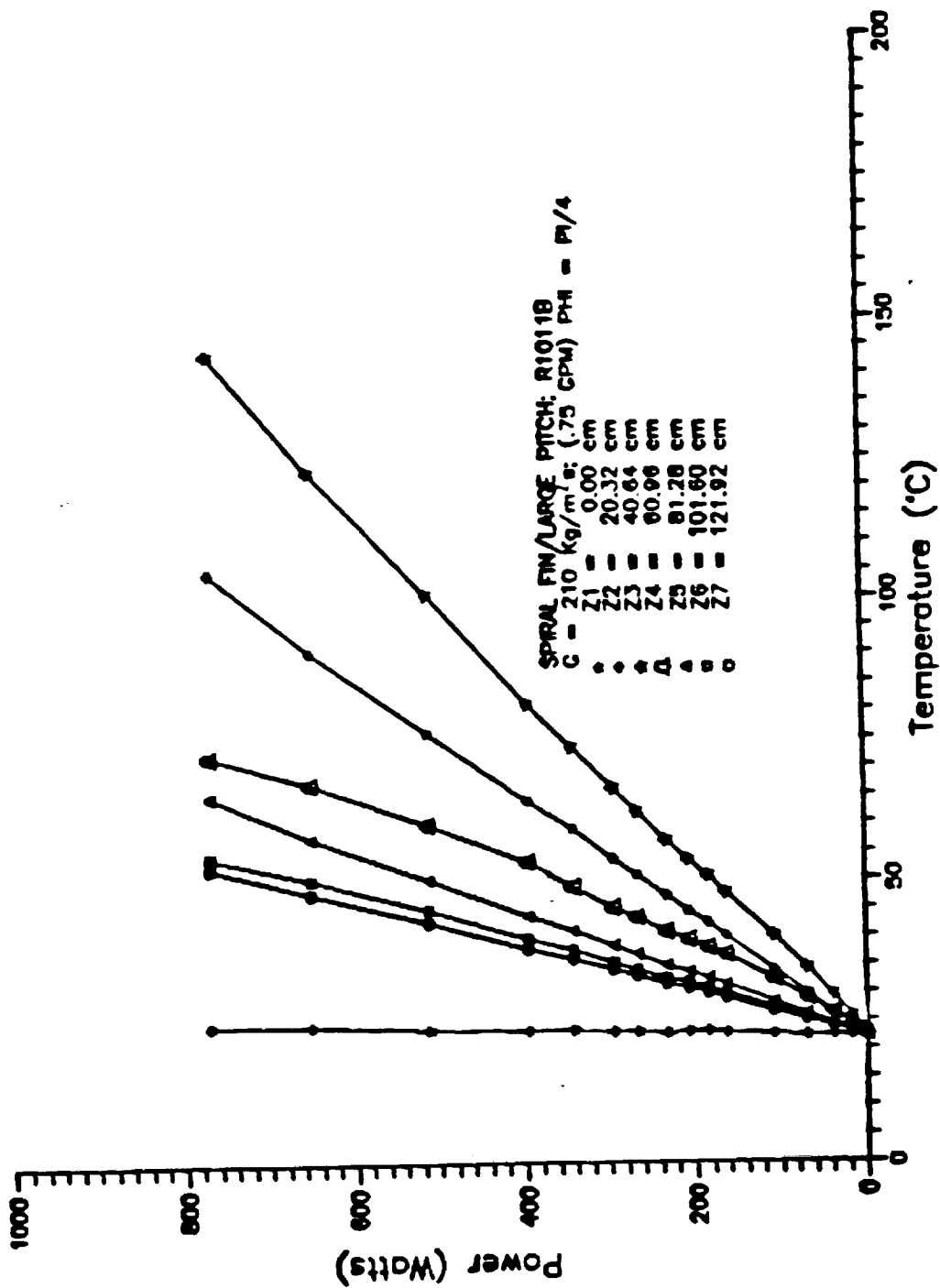


Figure 6. (b)  $\phi = \frac{\pi}{4}$

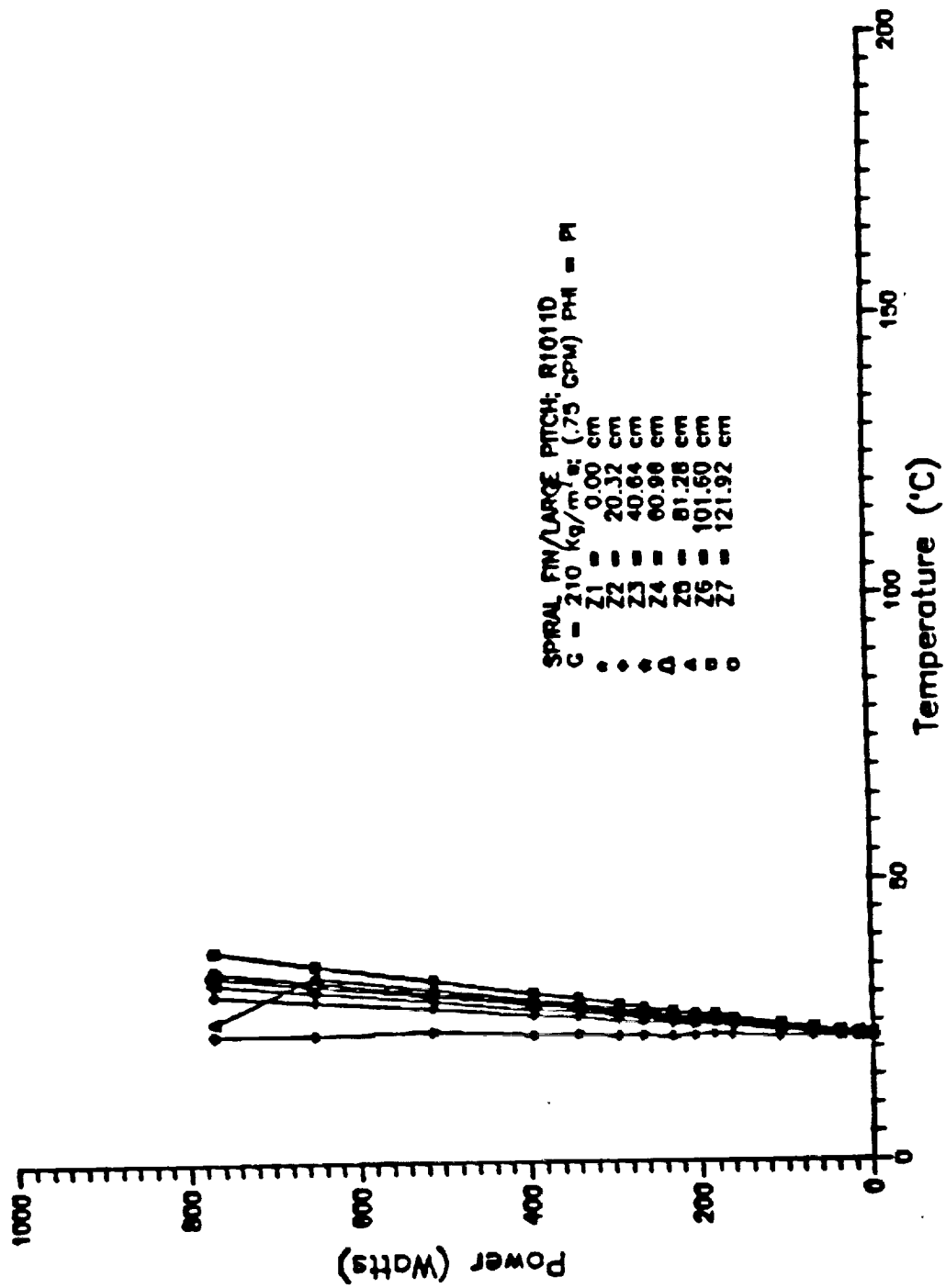


Figure 6. (c)  $\phi = \pi$ .



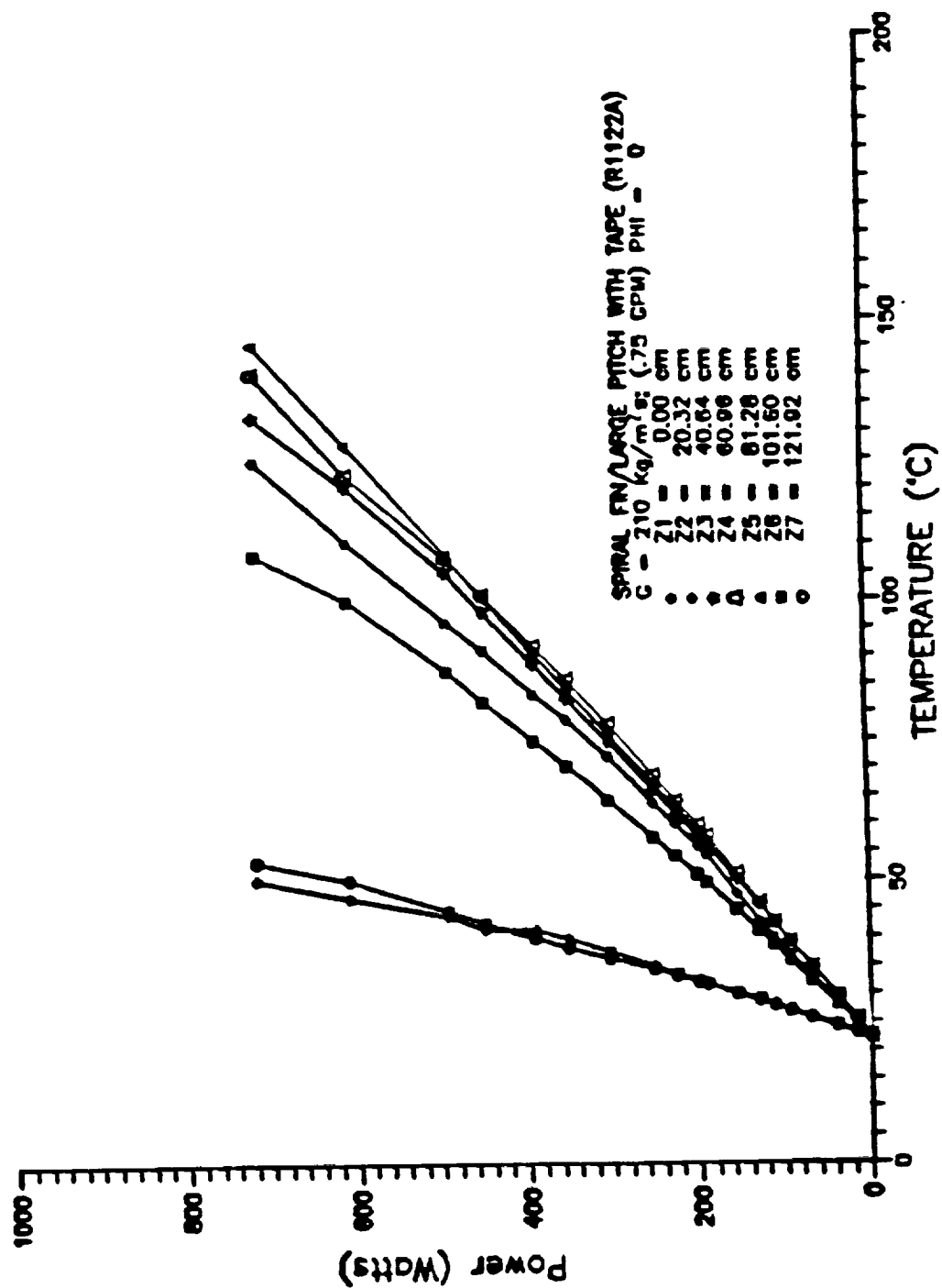


Figure 7. (a)  $\phi = 0$ ,

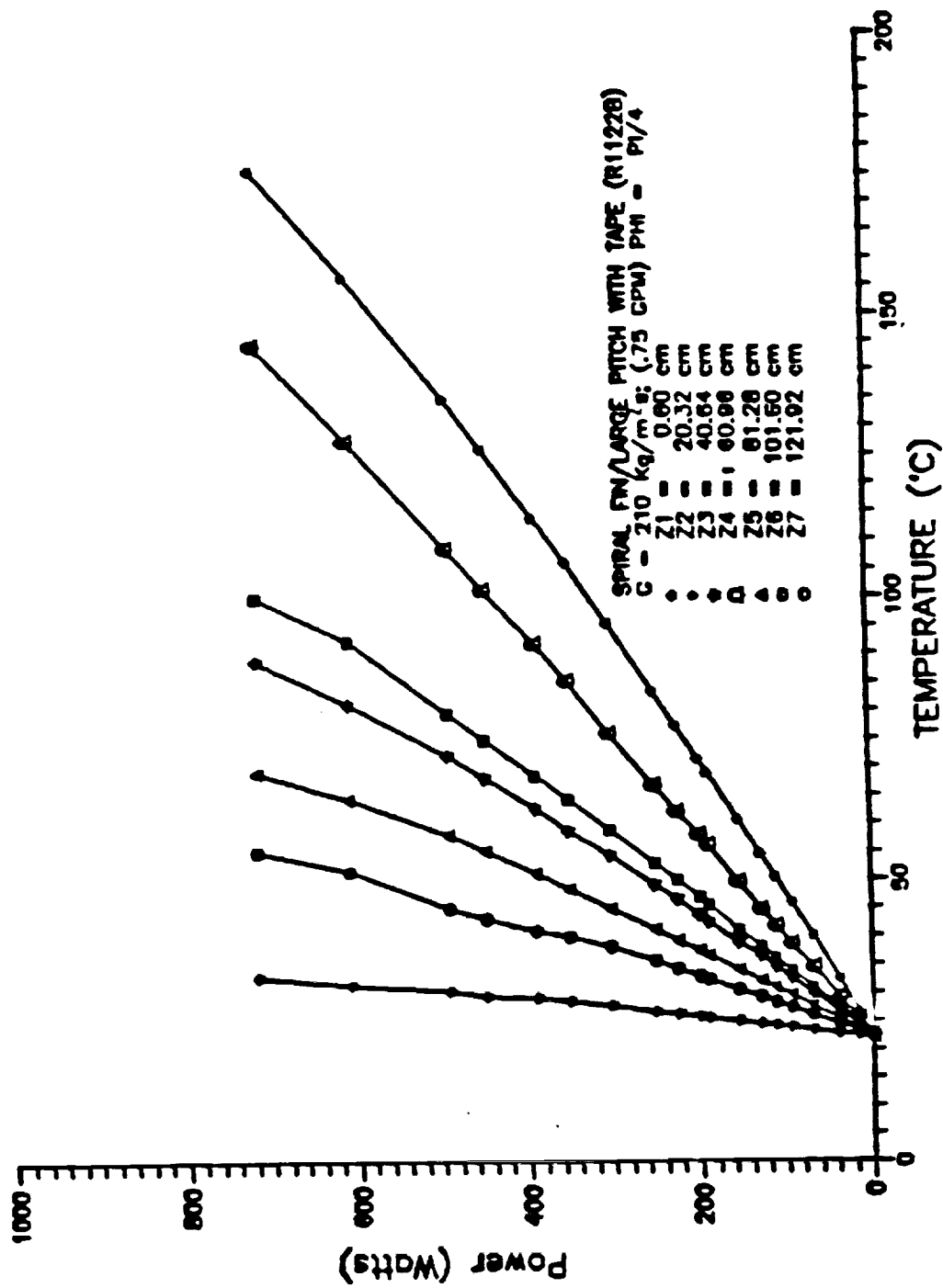


Figure 7. (b)  $\phi = \frac{\pi}{4}$ ,

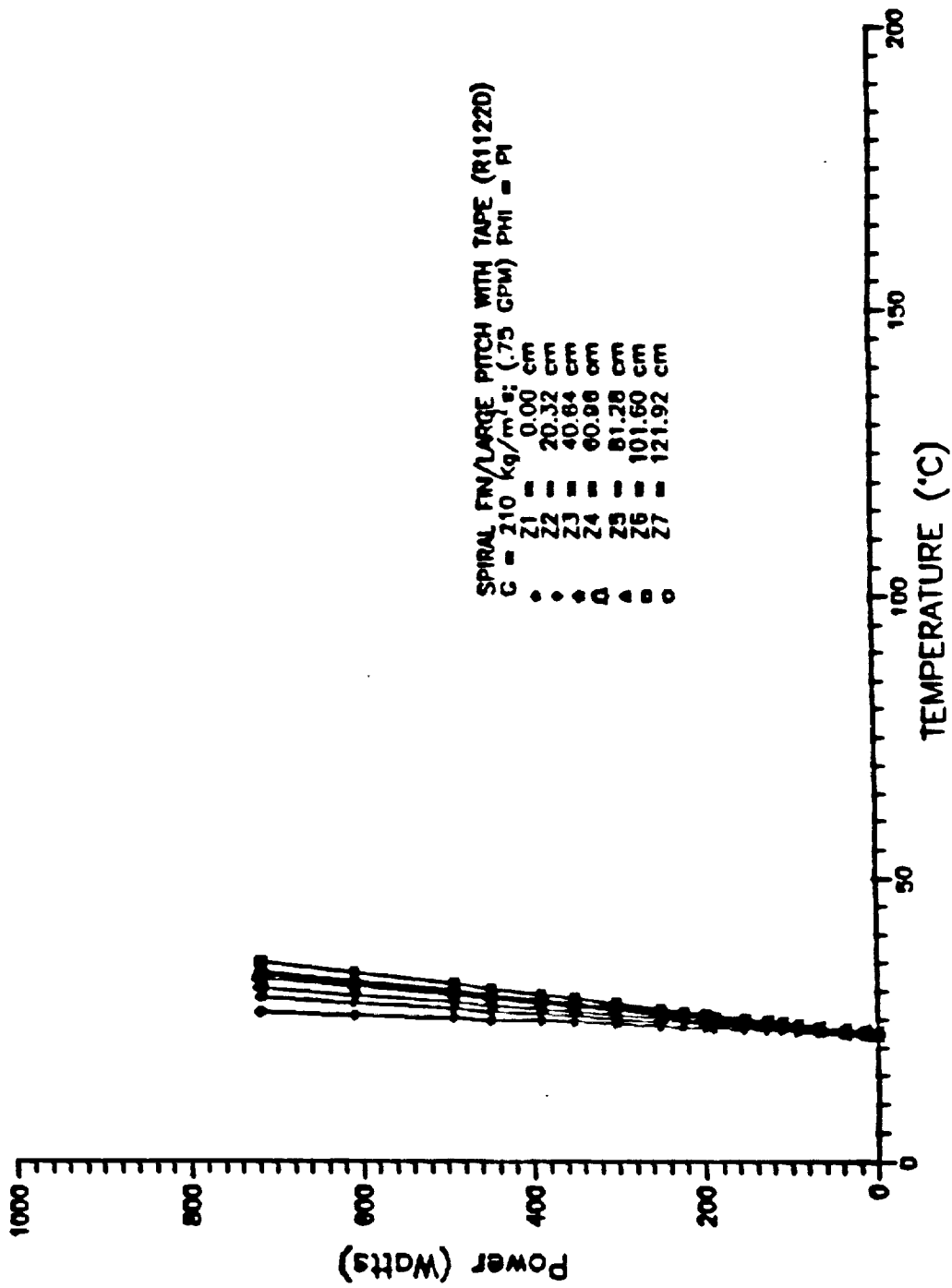


Figure 7. (c)  $\phi = \pi$ .

SPIRAL FIN LARGE PITCH; Z1011  
 $G = 210 \text{ kg/m}^2\text{s}$ ; INLET TEMP. =  $22.2^\circ\text{C}$   
 POWER = 653 Watts; TOP-HEATED 1.27cm TUBE

\* CIRCUMFERENTIAL LOCATION 0  
 □ CIRCUMFERENTIAL LOCATION  $\pi/4$   
 △ CIRCUMFERENTIAL LOCATION  $3\pi/4$   
 ▲ CIRCUMFERENTIAL LOCATION  $\pi$   
 ○ CIRCUMFERENTIALLY AVERAGED

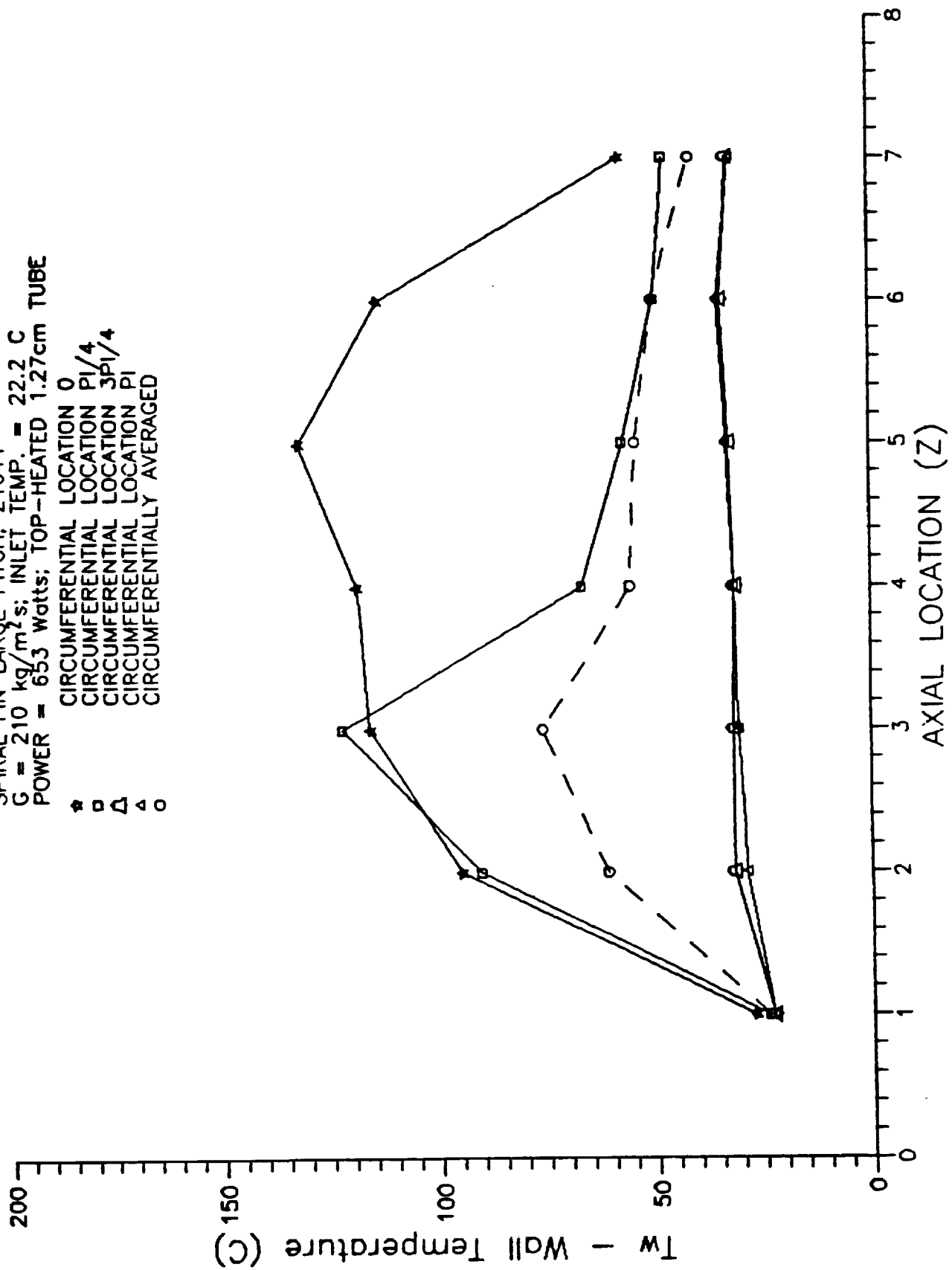


Figure 8. (a) Large Pitch Spiral Fins,

SPIRAL FIN/LARGE PITCH WITH TAPE : Z1122  
 $G = 210 \text{ kg/m}^2\text{s}$ ; INLET TEMP. =  $22.2^\circ\text{C}$   
 POWER = 611 Watts; TOP-HEATED 1.27cm TUBE

\* CIRCUMFERENTIAL LOCATION 0  
 □ CIRCUMFERENTIAL LOCATION  $\pi/4$   
 △ CIRCUMFERENTIAL LOCATION  $3\pi/4$   
 ▲ CIRCUMFERENTIAL LOCATION  $\pi$   
 ○ CIRCUMFERENTIALLY AVERAGED

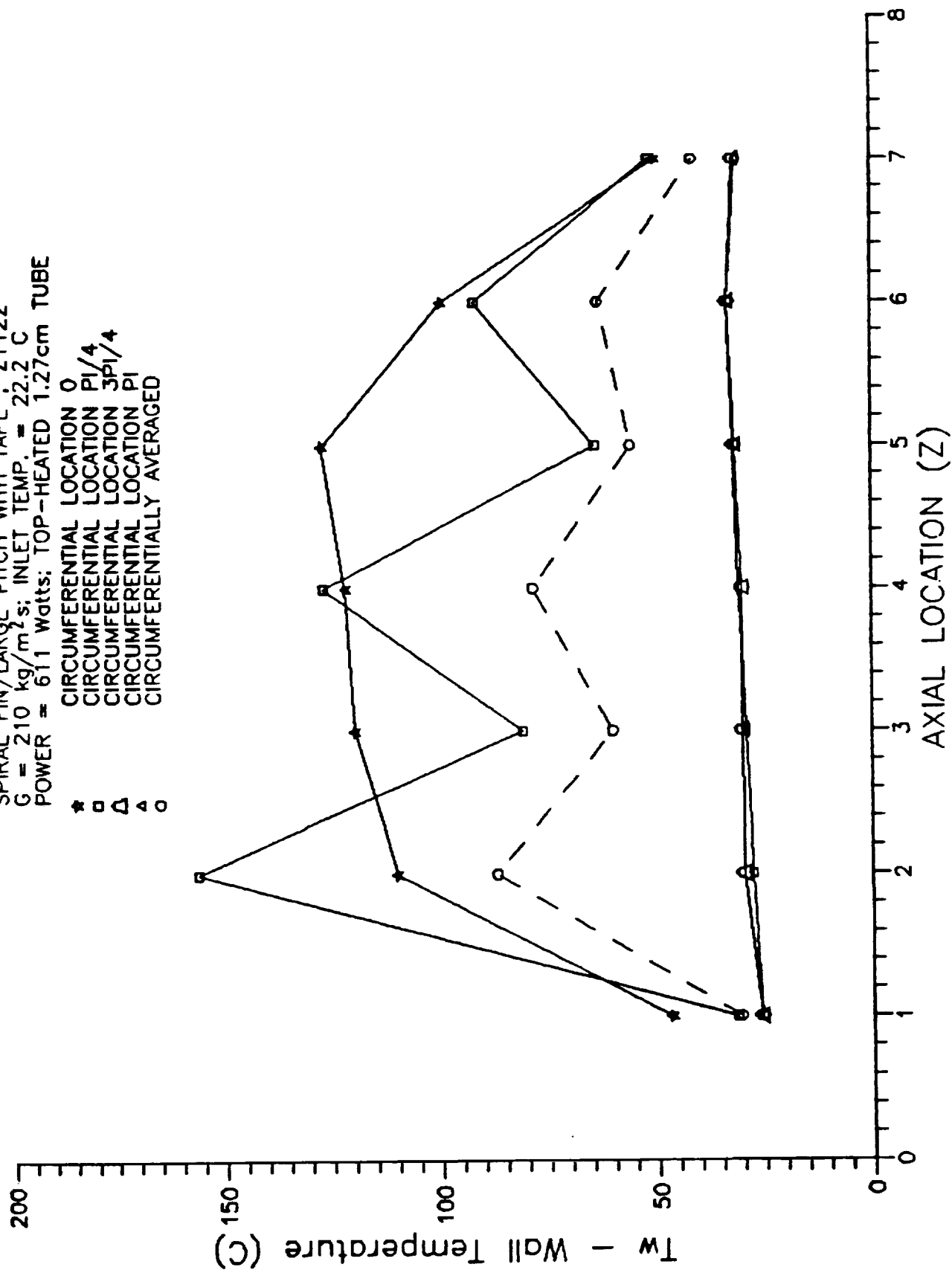


Figure 8. (b) Large Pitch Spiral Fins With Twisted Tape,

SPIRAL FIN SMALL PITCH; Z1118  
 $G = 210 \text{ kg/m}^2\text{s}$ ; INLET TEMP. =  $22.2^\circ\text{C}$   
 POWER = 410 Watts; TOP-HEATED 1.27cm TUBE

\* CIRCUMFERENTIAL LOCATION 0  
 □ CIRCUMFERENTIAL LOCATION  $\pi/4$   
 △ CIRCUMFERENTIAL LOCATION  $3\pi/4$   
 ▲ CIRCUMFERENTIAL LOCATION  $\pi$   
 ○ CIRCUMFERENTIAL LOCATION AVERAGED

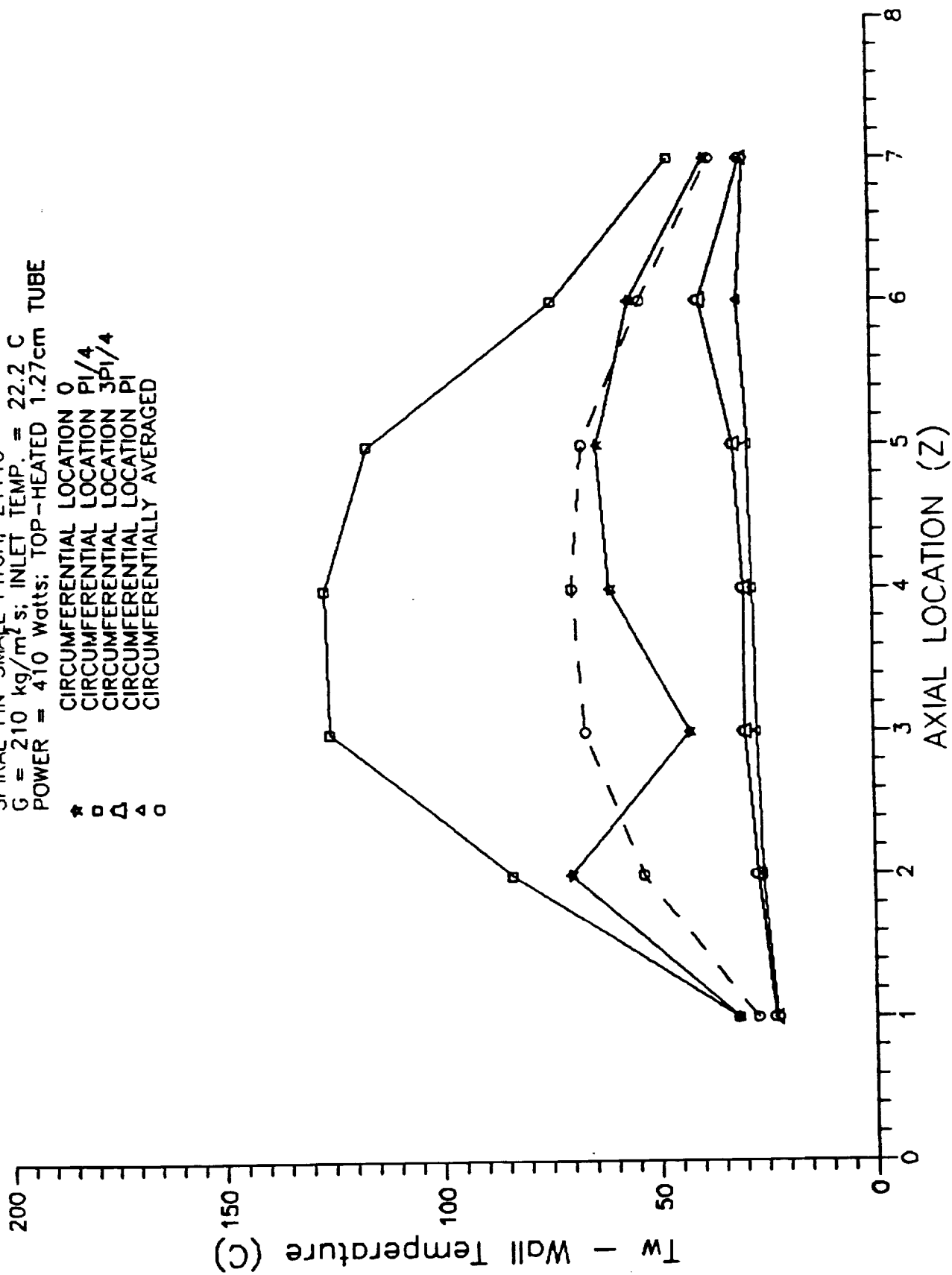


Figure 8. (c) Small Pitch Spiral Fins,

TOP-HEATED 1.27cm SMOOTH TUBE; Z1215  
 $G = 210 \text{ kg/m}^2\text{s}$ ; INLET TEMP. =  $22.2^\circ\text{C}$   
 POWER = 535 Watts

★ CIRCUMFERENTIAL LOCATION 0  
 □ CIRCUMFERENTIAL LOCATION  $\pi/4$   
 △ CIRCUMFERENTIAL LOCATION  $3\pi/4$   
 ▲ CIRCUMFERENTIAL LOCATION  $\pi$   
 ○ CIRCUMFERENTIAL LOCATION AVERAGED

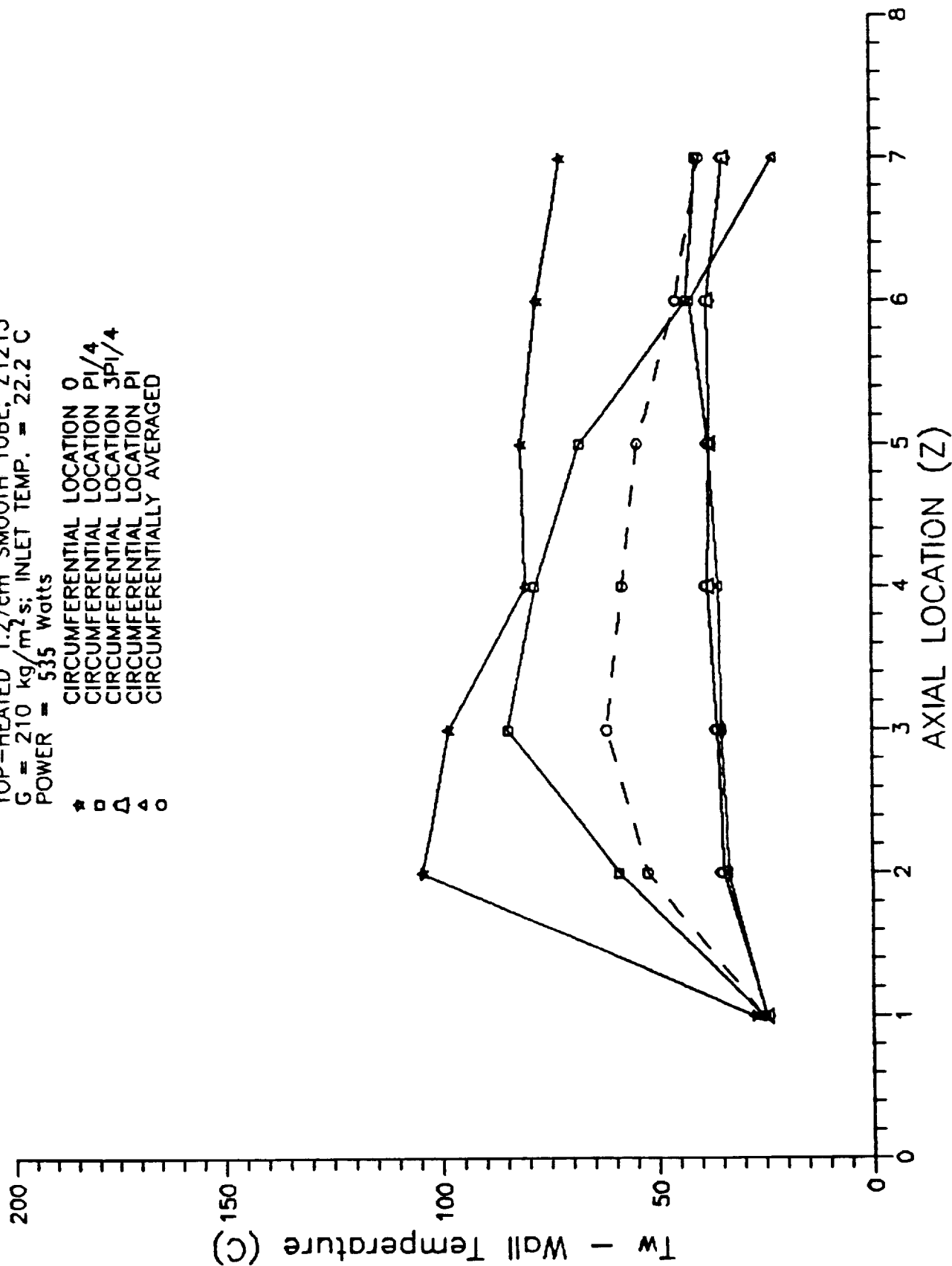


Figure 8. (d) Smooth Tube.

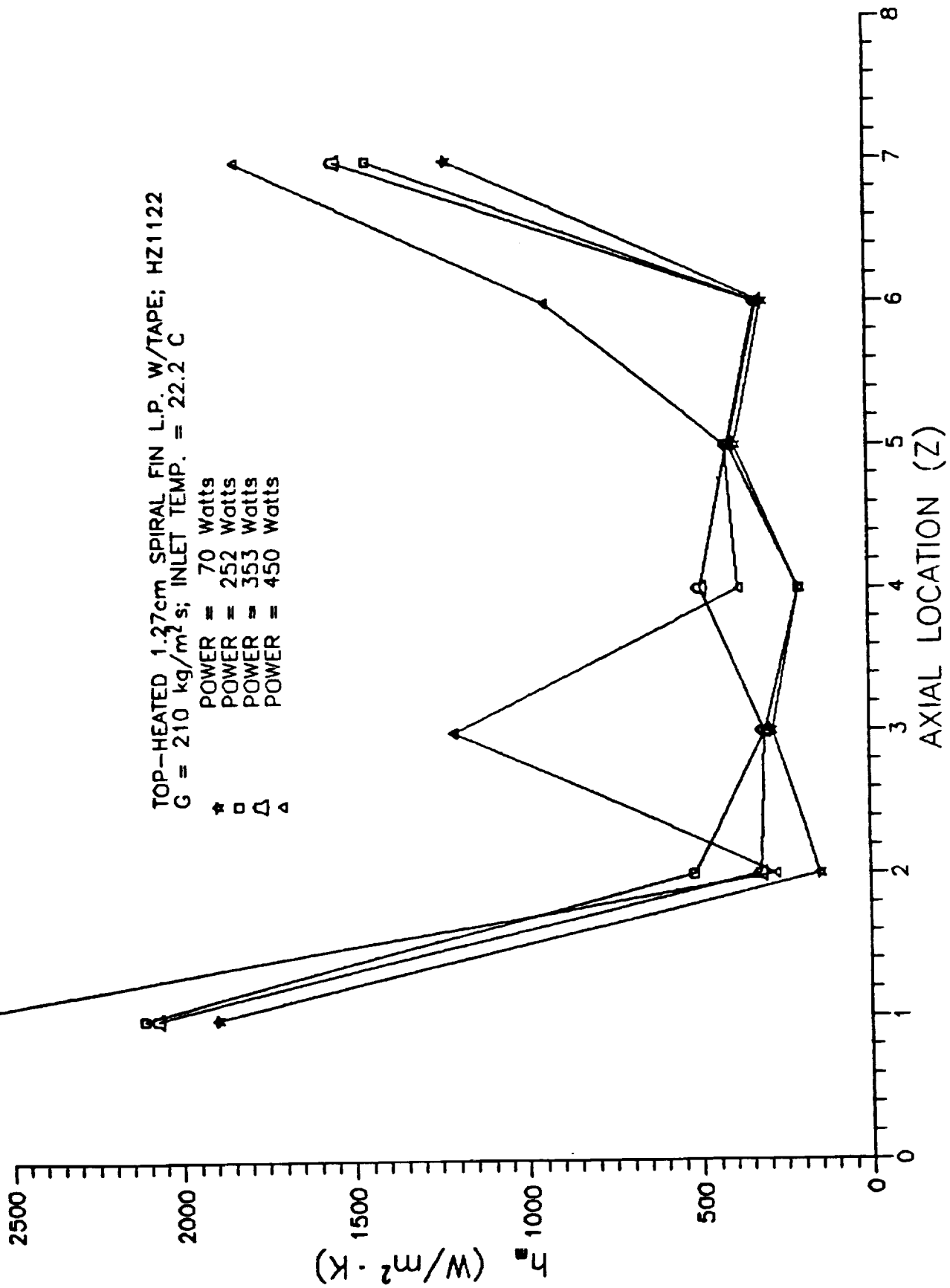


Figure 9 (a) Large Pitch Spiral Fins With a Twisted Tape,



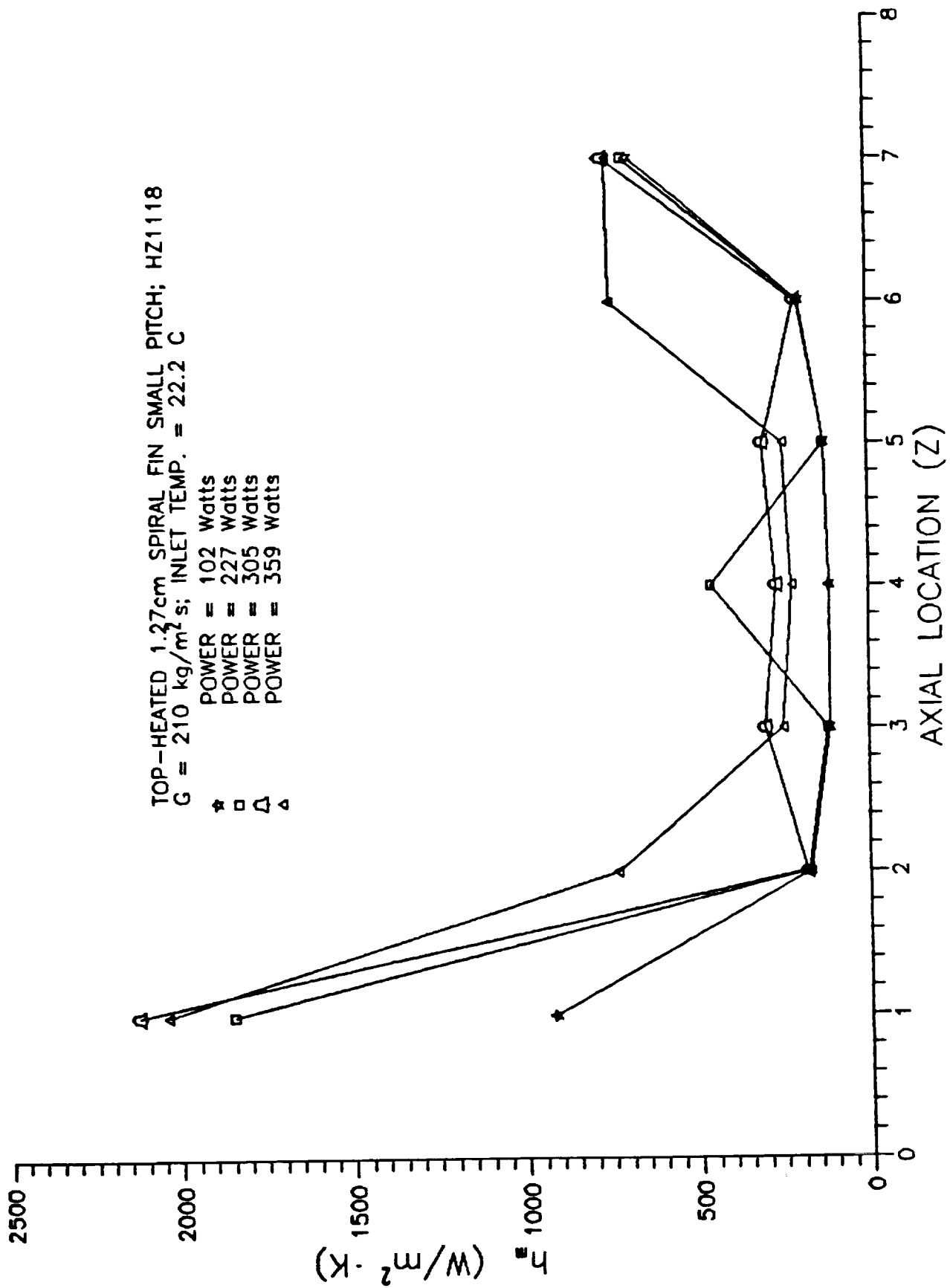


Figure 9 (b) Small Pitch Spiral Fins,

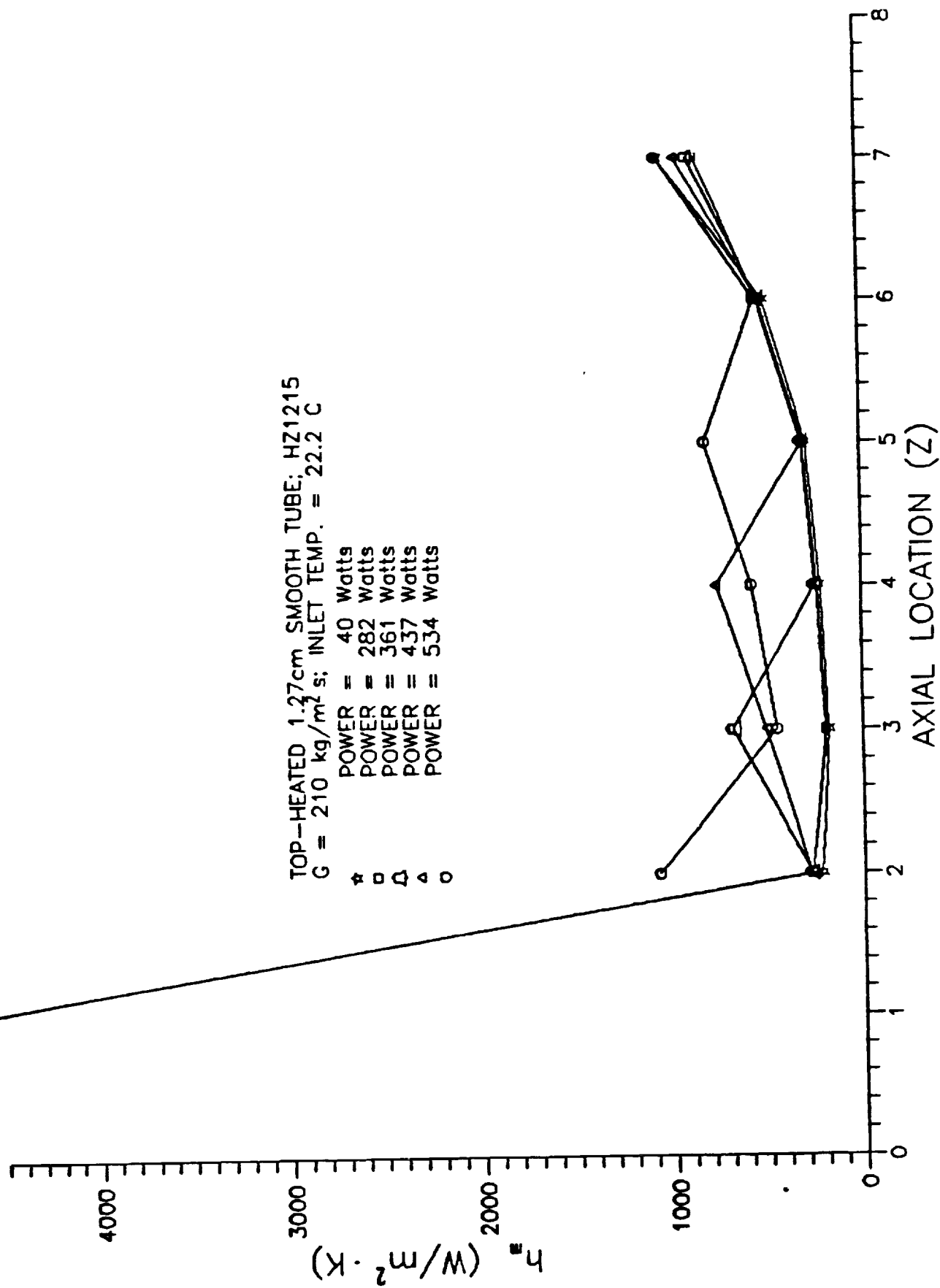


Figure 9 (c) Smooth Wall.

## APPENDIX: Uncertainty Analysis

This study has resulted in the determination of circumferentially mean and axially (and circumferentially) mean heat transfer coefficients from measurements of: (1) the test section outside, local wall temperature (2) the freon-11 flow conditions which include flow rates, exist pressure, and inlet and exit bulk temperatures, and (3) the ambient temperature. The relationships between these quantities are summarized in equations (1) through (5). Following the approach outlined by Moffat [7,8], the uncertainty in the heat transfer coefficient,  $h_m$ , is

$$\delta h_m = [(\frac{\partial h_m}{\partial X_i} \delta X_i)^2 + (\frac{\partial h_m}{\partial C_i} \delta C_i)^2]^{1/2} \quad (A.1)$$

where  $X_i$  represents all independent variables, and  $C_i$  represents corrections used to account for calibration defects, system-senson interactions and system disturbance errors. The double indicies in eq.(A.1) imply summation over all independent or correction variables. If effects of  $C_i$  are neglected,  $\delta h_m$  is given by,

$$\delta h_m \approx [(\frac{\partial h_m}{\partial A} \delta A)^2 + (\frac{\partial h_m}{\partial B} \delta B)^2]^{1/2} \quad (A.2)$$

where A and B are given in equation (1). Since A and B are not actually independent variables, thier relationship with these variables are as follows:

$$\delta A = \text{Function}(T_m, P_p, T_\infty), \text{ so that} \quad (A.3)$$

$$\delta A = [(\frac{\partial A}{\partial P_p} \delta P_p)^2 + (\frac{\partial A}{\partial T_m} \delta T_m)^2 + (\frac{\partial A}{\partial T_\infty} \delta T_\infty)^2]^{1/2}; \text{ and}$$

$$\delta B = \text{Function}(T_\infty, T_m, T_f, P_p), \text{ so that} \quad (\text{A.4})$$

$$\delta B = [(\frac{\partial B}{\partial P_p} \delta P_p)^2 + (\frac{\partial B}{\partial T_m} \delta T_m)^2 + (\frac{\partial B}{\partial T_\infty} \delta T_\infty)^2 + (\frac{\partial B}{\partial T_f} \delta T_f)^2]^{1/2}$$

From equation (1) the partial derivatives shown in equation (A.3) are given by:

$$\frac{\partial A}{\partial P_p} = (\frac{k_A}{k_B})(\frac{r_c}{A_s r_A})[\ln(\frac{r_D}{r_c}) + \frac{k_c}{h_\infty r_D}], \quad (\text{A.5})$$

$$\frac{\partial A}{\partial T_m} = -\frac{k_A k_c B_1}{r_A h_\infty^2 r_D} \frac{\partial h_\infty}{\partial T_m} - \frac{k_c}{r_A}$$

$$\frac{\partial A}{\partial T_\infty} = -\frac{k_A k_c B_1}{r_A h_\infty^2 r_D} \frac{\partial h_\infty}{\partial T_\infty} + \frac{k_c}{r_A}$$

In the above expression,  $A_s = 2\pi DL$ , where  $D = 4r_A$ . The partial derivatives involving B (see equation A.4) can be obtained using equation (1); i.e.

$$\frac{\partial B}{\partial P_p} = \frac{r_c}{A_s k_B} [\ln(\frac{r_c}{r_B}) + \frac{k_B}{k_A} \ln(\frac{r_B}{r_A})] \quad (\text{A.6})$$

$$\frac{\partial B}{\partial T_m} = \Phi - (T_m - T_\infty)(\frac{k_c}{h_\infty^2 r_D}) \frac{\partial h_\infty}{\partial T_m} + (T_f - T_\infty) \frac{k_c}{h_\infty^2 r_D} \frac{\partial h_\infty}{\partial T_m}; \text{ where,}$$

$$\Phi = [\ln(\frac{r_D}{r_c}) + \frac{k_c}{h_\infty r_D} + \frac{k_c}{k_B} \ln(\frac{r_c}{r_B}) + (\frac{k_c}{k_A}) \ln(\frac{r_B}{r_A})]$$

$$\frac{\partial B}{\partial T_\infty} = -\Phi + \ln(\frac{r_D}{r_c}) + \frac{k_c}{h_\infty r_D} + (T_f - T_\infty) \frac{k_c}{h_\infty r_D} \frac{\partial h_\infty}{\partial T_\infty}; \text{ and}$$

$$\frac{\partial B}{\partial T_f} = -[\ln \frac{r_D}{r_c} + \frac{k_c}{h_\infty r_D}]$$

The local fluid bulk temperature was estimated via the First Law of Thermodynamics, the measured values of mass velocity, net power generation, inlet temperature, pressure, and the axial location; i.e.,

$$T_f = \text{Function}(G, P_p, T_{inlet}, P, Z) \quad (A.7)$$

so that,

$$\delta T_f \approx [(\frac{\partial T_f}{\partial P_p} \delta P_p)^2 + (\frac{\partial T_f}{\partial Z} \delta Z)^2 + (\frac{\partial T_f}{\partial G} \delta G)^2 + (\frac{\partial T_f}{\partial T_{sat}} \frac{\partial T_{sat}}{\partial P} \delta P)^2 + (\frac{\partial T_f}{\partial T_{inlet}} \delta T_{inlet})^2]^{\frac{1}{2}},$$

where

$$\frac{\partial T_f}{\partial T_{sat}} = \begin{cases} 0, & \text{for } T_w < T_{womb}; \\ 1, & \text{for } T_w \geq T_{womb}; \text{ and} \end{cases}$$

$$T_f = T_{inlet} + \frac{Z P_p}{\pi L r_A^2 G C_p}$$

The above partial derivatives are given as,

$$\begin{aligned} \frac{\partial T_f}{\partial P_p} &= \frac{Z}{\pi L r_A^2 G C_p} \\ \frac{\partial T_f}{\partial T_{inlet}} &= 1; \end{aligned} \quad (A.8)$$

$$\frac{\partial T_f}{\partial Z} = \frac{P_p}{L A_c G C_p}; \text{ and}$$

$$\frac{\partial T_f}{\partial G} = -\frac{Z P_p}{\pi L r_A^2 G^2 C_p}$$

A complete energy balance of the test section was performed. This required appropriate definition for  $h_\infty$ . The effective external heat transfer coefficient,  $h_\infty$ , was defined in terms of the external natural convective heat transfer coefficient ( $h_c$ ), and the external radiative heat transfer coefficient ( $h_r$ ) by

$$h_\infty = h_c + h_r \approx h_c + \sigma(T_s^2 + T_\infty^2)(T_s + T_\infty), \quad (A.9)$$

where  $\sigma$  is the Stefan Boltzmann constant and  $T_s$  is the outside surface temperature of the test section. The temperature,  $T_s$ , is related to  $T_m$  by the approximate relationship,

$$q_{loss} \approx \frac{2\pi L(T_m - T_s)}{\frac{1}{k_c} \ln(\frac{r_D}{r_C})} = \frac{2\pi L(T_m - T_\infty)}{\frac{1}{k_c} \ln(\frac{r_D}{r_C}) + \frac{1}{h_\infty r_D}} \quad (A.10)$$

Equation (A.10) can be used along with (A.9) to solve for  $T_s$  iteratively for each measured value of  $T_m$ . An iterative analysis is necessary because  $h_\infty$  is a nonlinear function of  $T_s$  via  $h_r$ . The natural convective heat transfer coefficient,  $h_c$ , was determined from the following correlation (for horizontal cylinders)

$$h_c = \frac{k_{air} Nu_D}{2r_D}, \text{ where} \quad (A.11)$$

$$Nu_D = \{0.6 + 0.38 Ra_D^{\frac{1}{4}} [1 + (\frac{0.559}{Pr})^{\frac{4}{9}}]^{-\frac{8}{27}}\}^2,$$

where

$$Ra_D = \frac{\beta g (T_s - T_\infty) D^3}{\nu^2} Pr$$

The partial derivatives of  $h_\infty$  with respect to  $T$  and  $T_m$  appear in equation (A.6) and are given by

$$\frac{\partial h_\infty}{\partial T_\infty} = \frac{\partial h_c}{\partial T_\infty} + \sigma [2(T_s \frac{\partial T_s}{\partial T_\infty} + T_\infty)(T_s + T_\infty) + (T_s^2 + T_\infty^2)(\frac{\partial T_s}{\partial T_\infty} + 1)] \quad (A.12)$$

$$\frac{\partial h_{\infty}}{\partial T_m} = \frac{\partial h_c}{\partial T_m} + \sigma[3T_s^2 + 2T_s T_{\infty} + T_{\infty}^2] \frac{\partial T_s}{\partial T_m},$$

where  $\frac{\partial T_s}{\partial T_m}$  and  $\frac{\partial T_s}{\partial T_{\infty}}$  were obtained from equation (A.10). The resulting expression for  $\frac{\partial T_s}{\partial T_m}$  is

$$\frac{\partial T_s}{\partial T_m} = \frac{\frac{k_c B_5^2}{\ln(\frac{r_D}{r_c})} - B_5 - \frac{T_m - T_{\infty}}{r_D h_{\infty}^2} \frac{\partial h_c}{\partial T_m}}{\frac{B_5^2 k_c}{\ln(\frac{r_D}{r_c})} + \sigma[3T_s^2 + 2T_s T_{\infty} + T_{\infty}^2] \frac{(T_m - T_{\infty})}{r_D h_{\infty}^2}} \quad (\text{A.13})$$

where

$$B_5 = \frac{1}{k_c} \ln \frac{r_D}{r_c} + \frac{1}{h_{\infty} r_D}$$

Sample calculations indicated that  $\frac{\partial T_s}{\partial T_m}$  is about  $1.9 \times 10^{-2}$  at higher power levels ( $P_p = 657.5W$ ), and should be much smaller (nearly zero) at lower power levels. An expression similar to equation (A.13) can be obtained for  $\frac{\partial T_s}{\partial T_{\infty}}$  from equation (A.10) and (A.12). Sample calculations have shown that  $h_{\infty}$  is nearly constant for small changes in  $T_{\infty}$ . Assuming this to be the case, especially at higher power levels,

$$\frac{\partial T_s}{\partial T_{\infty}} \approx \frac{\ln \frac{r_D}{r_c}}{k_c B_5} \quad (\text{A.14})$$

which is slightly less than unity.

One of the last variables for which an uncertainty must be estimated is the net power generation. Since  $T_s$  was near  $T_{\infty}$ ,  $\delta P_p$  will be strongly dependent on the measured



electrical current (I) and voltage (V); i.e.,

$$\delta P_p = [(\frac{\partial P_p}{\partial I} \delta I)^2 + (\frac{\partial P_p}{\partial V} \delta V)^2]^{1/2} \quad (A.15)$$

Here we assume that the uncertainty for the partial derivatives of the power and total power generation are identical. Noting that  $P_p)_{total} = IV$ ,

$$\delta P_p = [V^2 \delta I^2 + I^2 \delta V^2]^{1/2} \quad (A.16)$$

### Sample Calculation

Since the primary objective of this work was to obtain heat transfer coefficients for enhanced and smooth surfaces in the boiling regime, one power level which resulted in localized boiling has been considered. The above equations are being used to develop a computer program so that the uncertainty at every power level can be evaluated. An undergraduate mechanical engineering senior was employed for this purpose.

In particular, selected conditions at a typical high power level was considered for sample calculations. The test section with large pitch fins for  $\phi = 0$ ,  $Z = Z_4$ , and  $P_p = 657.45 W$  [see reference A-1, p. 232]. In addition to  $G = 210 \text{ kg/m}^2 \text{ s}$ ,  $Z_4 = 60.96 \text{ cm}$ ,  $T_f = 314.8 \text{ K}$ ,  $T_\infty = 295 \text{ K}$ , and  $T_m = 376.87 \text{ K}$ .

In the original data reduction used in Part I and [A-1],  $T_s$  was assumed to be  $\frac{T_m + T_\infty}{2}$  and was used in equation (A.9) to compute  $h_r$ . The heat transfer coefficient,  $h_c$ , was assumed to be  $4.24 \text{ W/m}^2 \text{ K}$  for that data reduction. However, the present computations show that  $T_s$  should be  $296.5 \text{ K}$  [obtained from equation (A.10)],  $h_c$  should be

28.6 W/m<sup>2</sup>K, and  $h_{\infty}$  should be approximately 32.3 W/m<sup>2</sup>K. This change has a secondary effect on the uncertainty analysis since  $\frac{k_c}{h_{\infty} r_c}$  was small compared to  $\ln \frac{r_D}{r_c}$ , which is a controlling parameter in this analysis.

The following is representative of the specific characteristics of the test section dimensions, fluids, and thermophysical properties:  $r_A = 6.033 \times 10^{-3}$  m;  $r_B = 6.35 \times 10^{-3}$  m;  $r_c = 6.98 \times 10^{-3}$  m;  $r_D = 3.2385 \times 10^{-2}$  m;  $D = 4r_A$ ;  $L = 1.219$  m;  $k_A = 382.7$  W/mK;  $k_B = 1.038$  W/mK;  $k_c = 0.0303$  W/mK;  $k_{\infty} = 31.3 \times 10^{-3}$  W/mK (Air);  $\nu_{\infty} = 0.2945 \times 10^{-6}$  m<sup>2</sup>/s; (Air);  $\beta = 3.3 \times 10^{-3}$  K<sup>-1</sup> (Air);  $Pr_{\infty} = 0.704$  (Air);  $\rho \approx 1,479$  kg/m<sup>3</sup> (freon-11 density);  $C_p \approx 0.89$  kJ/kgK (freon-11 ).

To complete the specifications for the sample calculations, the measured uncertainties of the independent variables must be determined. The uncertainties for Z and G were :  $\delta Z = 0.0016$  m, and  $\delta G = 8.4$  kg/m<sup>2</sup>s, respectively. The uncertainties in measuring all temperatures were assumed equal and will be denoted by  $\delta T$ . If  $\delta P_p = 0.1$  W,  $\delta T = 10^{-2}$  K, then  $\delta A = 762.3$  W/m<sup>2</sup>,  $\delta B = 0.027$  K,  $\frac{\partial h_m}{\partial A} = 9.92 \times 10^{-3}$  K<sup>-1</sup>,  $\frac{\partial h_m}{\partial B} = -462.6$  W/m<sup>2</sup>K<sup>2</sup>. This results in

$$\delta h_m \approx \pm 14.6 \text{ W/m}^2\text{K}. \quad (\text{A.17})$$

## Discussion

The value of  $\delta h_m$  shown in equation (A.17) is strongly dependent on  $\delta T$  and  $\delta P_p$ . This value would be much smaller for lower values of  $\delta T$  and  $\delta P_p$ , or significantly larger for higher values of these quantities. In the expression for  $\delta B$ , the quantities which have secondary influence were:  $\frac{\partial B}{\partial P_p} = 2.8 \times 10^{-2} \text{ K/W}$ ; and  $\frac{\partial B}{\partial T_\infty} = -1.02 \times 10^{-3}$ . Those quantities with significant influence were:  $\frac{\partial B}{\partial T_m} = 1.534$ ,  $B = 100.8 \text{ K}$ , and  $\frac{\partial B}{\partial T_f} = -1.549$ . There is great concern in the large magnitude of this last quantity; i.e.,  $\frac{\partial B}{\partial T_f}$ . Its magnitude arises from many influences associated with the magnitude of  $T_f$  (the local bulk fluid temperature). For  $T_f < T_{sat}$ ,  $\frac{\partial T_f}{\partial P} = 0$  and the uncertainty in  $T_f$  is  $\delta T$  as noted above. However when  $T_f \geq T_{sat}$ , there is a possibility that  $\delta T_f$  may become large. For example,  $\frac{\partial T_{sat}}{\partial P_{sat}} \approx 180.9^\circ\text{C/MPa} \approx \frac{\partial T_f}{\partial P}$  for boiling around the entire channel. If this condition occurred (e.g., with uniform heating) with only a moderate uncertainty in  $P$  (i.e.,  $\delta P = 0.014 \text{ MPa}$ ),  $\delta T_f$  could be as high as  $2.4 \text{ K}$ . However, in most experiments the bulk fluid temperature remained below the saturation temperature even when there was localized boiling. Under these circumstances,  $\delta T_f$  would be slightly greater than  $\delta T$ , provided  $\delta P \leq 6.8 \times 10^{-5} \text{ MPa}$ .

The uncertainty,  $\delta h_m$ , is also dependent on the parameter  $A$ , which has an unusually large magnitude of  $4.7 \times 10^6 \text{ W/m}^2$  for sample case considered. The uncertainty,  $\delta A$ , is principally affected by  $P_p$ ; so, the effects of  $\frac{\partial A}{\partial T_\infty} = -\frac{\partial A}{\partial T_m} = 116.0 \text{ W/m}^2\text{K}$  are secondary. Accordingly,  $\frac{\partial A}{\partial P_p} = 7,623 \text{ m}^{-2}$ .

## Experimental Design

Many improvements for the existing experimental loop have been enumerated in [A-1]. In addition to those, the heat exchanger for controlling the test section inlet temperature was relocated upstream of the test section. Additional verification runs are planned in anticipation of additional funding to study the vertical flow geometry which has been proposed recently [A-2].

In addition to the above discussed uncertainty sensitivity, this uncertainty analysis suggests some subtle changes in the test section which will reduce the uncertainty in  $\delta h_m$ . In addition to requiring low  $\delta T_m$  and  $k_c$ , if  $r_D/r_c$  was as large as possible, both  $\frac{\partial h_m}{\partial A}$  and  $\frac{\partial h_m}{\partial B}$  would be significantly reduced. This occurs because both of the latter quantities are inversely proportional to  $B$  and  $B^2$ , respectively. The quantity,  $B$ , would increase further if  $T_{sat}$  could be selected to be closer to  $T_\infty$ . The latter requirement would have a significant effect on reducing  $A$ , and hence  $\frac{\partial h_m}{\partial B}$  and  $\delta h_m$ . Another very large contribution to  $\delta h_m$  was due to  $\delta A$ . The quantity most significantly affecting  $\delta A$  was  $\frac{\partial A}{\partial P_r}$ . This latter quantity can be significantly reduced by choosing a low thermal conductivity material for the test section (i.e.,  $k_A$ ). For example, if  $k_A$  is reduced by an order of magnitude,  $\delta A$  will be reduced similarly (i.e., by an order of magnitude). Any one of these effects separately will reduce  $\delta h_m$  by a relatively small amount. However, by employing all of them, significant reductions will occur.

### References

- A-1. "Forced Convective and Flow Boiling with and without Enhanced Devices for Top-Side Heated Horizontal Channels", J. C. Turknett, Jr., MS Thesis, February, 1989, Department of Mechanical Engineering, Prairie View A &M University.
- A-2. "Flow Boiling Enhancement for Thermal Management System" R. D. Boyd, Proposal, Submitted to NASA (Headquarters) May 20, 1991.

**PART II:**

**IMPROVED ANALYTICAL HEAT  
TRANSFER DATA REDUCTION FOR  
A SINGLE-SIDE HEATED COOLANT CHANNEL**

# IMPROVED ANALYTICAL HEAT TRANSFER DATA REDUCTION FOR A SINGLE-SIDE HEATED COOLANT CHANNEL

Ronald D. Boyd<sup>1</sup>, Xiaowei Meng<sup>2</sup>, and  
Sharon Taylor<sup>3</sup>

*Mechanical Engineering Department  
P.O. Box 397*

*Prairie View A&M University  
Prairie View, TX 77446 USA*

## ABSTRACT

A heat transfer model for a single-side, heated, circular coolant channel has been developed and can be used to determine accurate mean heat transfer coefficients from measured wall temperatures. In addition, the circumferential heat flux distribution on the inside wall of the coolant channel was obtained. In previous experiments, steady-state wall temperature measurements were made at various circumferential locations on the outside surface of the channel which was heated from one side and insulated on the other side. The channel was assumed to be cooled internally by a fluid flow field with a bulk temperature,  $T_b$ . In the present work, cases of uniform and nonuniform heat flux were considered for the heated side. The results were presented for the Biot number varying from  $10^{-3}$  to  $10^3$ , and aspect ratio ( $R_o$ , outside to inside radii) varying from 1.04 to 3.0. Using the formulation, the circumferentially mean heat transfer coefficient ( $h_m$ ) can be obtained from specified or measured values of the outside surface temperature  $T(R_o, \phi)$ , and  $T_b$ . If measurements of the local fluid film temperature are made available, the present formulation can be used

---

<sup>1</sup> *Honeywell Endowed Professor of Engineering*

<sup>2</sup> *Graduate Student*

<sup>3</sup> *Research Assistant*

to obtain the circumferential variations of the heat transfer coefficient,  $h(\phi)$ .

Since the results are closed-form analytical expressions, they can be used conveniently for data reduction or for boundary conditions for numerical analyses of the flow field. In cases where axial (local) wall temperature measurements are made along the length of the channel, the present results can be used locally to approximate variations of the mean heat transfer coefficients in the axial direction.

## NOMENCLATURE

$a_n$	Integration parameter; see equation (4)
$B_i$	Biot number, $h_m r_1 / k$
$Bi_n$	$(Bi - n) / (Bi + n)$
$b_n$	Integration parameter; see equation (4)
$h$	Local heat transfer coefficient
$h_m$	Mean circumferential heat transfer coefficient
$k$	Wall thermal conductivity
$m_n$	$= (-h_m r_1^{-n} n k r_1^{-n-1}) / (-h_m r_1^n + k n r_1^{n-1})$
$n$	Eigenvalue
$q''$	Circumferentially varying, outside surface heat flux
$q_o$	Constant heat flux
$r$	Radial coordinate
$R$	$r / r_1$
$R_o$	Aspect ratio, $r_o / r_1$



$r$	Radial coordinate
$r_o$	Outside radius
$r_1$	Inside radius
$T$	Local wall temperature
$T_b$	Bulk fluid temperature
$T^*$	Dimensionless temperature (referred to as T STAR in plots), $\theta/(q_o r_o/k)$
$T_{av}^*(R)$	Average circumferential value of $T^*$ (referred to as AVERAGE T STAR in plots)

#### *Greek*

$\theta(r,\phi)$	Temperature excess above the bulk fluid temperature, $[T(r,\phi)-T_b]$
$\phi$	Circumferential coordinate directed counter-clockwise <sup>1</sup>

---

<sup>1</sup> The origin for  $\phi$  is at: (1) the top of the vertical plane (see Figures 2 and 3) for all plots, **but** at (2) the right-side of the horizontal plane for equations (1) through (14).

## INTRODUCTION

Recently, much attention has been given recently to single-side heated coolant channels. Most practical applications require forced convective cooling (single-phase or two phase) and have coolant channels which have drastic circumferential variation in the applied heat flux. Sometimes, the axial heat flux variations are secondary compared to the circumferential variations. In cases where this is not true, the present data reduction technique must be applied at each local axial location. Because of the simplicity involved, many previous investigators and designers have approximated single side heated coolant channels with an equivalent uniformly heated channel. Since this approximation may not apply in all cases, more investigators are now interested in including the effect of single-side heating in their investigations. With the addition of this needed complexity to many experiments, new and convenient approaches must be identified to reduce heat transfer data. This need is not restricted to experimental investigators. Many numerical analyst neglect the effects of the conjugate nature of their analysis by approximating heat flux boundary conditions rather than using the actual boundary conditions which may have been complicated by multidimensional conduction (and/or radiation) in the solid substrate. Within the scope of the present analytical formulation, the analysis which follows provides a means for those analyst to include more realistic boundary conditions for their study of the fluid flow through non-uniformly heated circular channels.

In many engineering designs, various heat transfer enhancement devices (e.g. fins, twisted tapes, combinations of fins and twisted tapes, etc.) cause very complicated internal velocity and temperature distributions. Consider a circular coolant channel which is: (1)

heated from the outside via a nonuniform heat flux, and (2) cooled from the inside by a complicated convective flow distribution at a bulk fluid temperature,  $T_b$ . Such convective flows are often times too complicated to analyze numerically, especially if the flow is turbulent and/or involves a phase change. The above described configuration models, in two-dimensions, nonuniform heat flux configuration found in electronic devices, reactor components, space cold plates, and many other energy management systems.

For most thermal engineering designs, knowledge of the circumferentially mean heat transfer coefficient,  $h_m$ , is essential and knowledge of the local circumferential heat transfer coefficient,  $h(\phi)$ , and hence the local wall temperature would be desirable. Although previous models [1-4] have been developed for the case of nonuniform surface heat flux, they have either not adequately accounted for the nonuniformity of the heat flux or they were based on laminar flow. Apriori assumptions of such distributions are usually not appropriate.

The objectives of this work were to: (1) establish a convenient technique for determining  $h_m$  from measured or set values of the outside channel wall temperature,  $T(R_o, \phi)$ , and (2) propose a technique for using the external heat flux distribution to infer the inside wall heat flux distribution. These set values for  $T(R_o, \phi)$  or  $q''$  may either be experimental measurements or critical design constraints.

## PROBLEM SPECIFICATION AND FORMULATION

The model to be studied consists of a nonuniformly heated coolant channel (see Figure 2) which is heated from one side and insulated (perfectly) on the opposite side. The thermophysical properties of the channel material were assumed constant. The mean circumferential heat transfer coefficient,  $h_m$ , was assumed to adequately describe the convective heat transfer from the inside surface of the channel to the bulk fluid. Although not used directly in this formulation, this does allow for the existence of circumferentially varying heat transfer coefficient,  $h(\phi)$ . This latter coefficient can only be found by determining the circumferential variation in the "local" fluid film temperature necessary for the definition of  $h(\phi)$ . The wall temperature is characterized by the following differential equation:

$$\frac{1}{r} \frac{\partial^2 T}{\partial \phi^2} + \frac{1}{r} \frac{\partial}{\partial r} \left( r \frac{\partial T}{\partial r} \right) = 0, \quad (1)$$

However, note that for the formulation, the circumferential coordinate,  $\phi$ , is directed counter-clockwise with its origin ( $\phi = 0$ ) on the right side of a horizontal plane. The origin for  $\phi$  will be changed to that shown in Figures 2 and 3 for all plots in Figures 10 through 13. The boundary conditions are

$$T(r, \phi) = T(r, \phi + 2\pi), \quad \frac{\partial T(r, \phi)}{\partial \phi} = \frac{\partial T(r, \phi + 2\pi)}{\partial \phi} \quad (2a)$$

$$-h_m [T(r, \phi) - T_b] + k \frac{\partial T}{\partial r}(r, \phi) = 0, \text{ and} \quad (2b)$$

$$-k \frac{\partial T(r_o, \phi)}{\partial r} = \begin{cases} -q''(\phi), & 0 \leq \phi \leq \pi; \\ 0, & \pi < \phi \leq 2\pi, \end{cases} \quad (2c)$$

After these equations were nondimensionalized and restructured using the standard separation of variables technique, the following temperature profile was obtained:

$$\theta = \theta_o + \sum_{n=1}^{\infty} (r^{-n} - m_n r^n) (a_n \cos n\phi + b_n \sin n\phi), \text{ and} \quad (3)$$

$$\theta_o = A_o \left[ \frac{1}{Bi} + \ln R \right],$$

where  $n=1,2,3,4,5,\dots$ , which reflects all boundary conditions having been applied except the last. The first term,  $\theta_o$ , would have described the radial temperature profile for the case of a completely uniform heat flux around the circumference of the flow channel. The second term is therefore the required correction due to the nonuniform heat flux. Application of the last boundary condition results in expressions for the constants  $a_n$  and  $b_n$  in terms of the nonuniform heat flux distribution; i.e.,

$$\begin{aligned} (r_o^{-n-1} + m_n r_o^{n-1})a_n &= \frac{-1}{\pi n} \int_0^{2\pi} \frac{q''(\phi)}{k} \cos n\phi d\phi, \\ (r_o^{-n-1} + m_n r_o^{n-1})b_n &= \frac{1}{\pi n} \int_0^{2\pi} \frac{q''(\phi)}{k} (\sin n\phi) d\phi, \text{ and} \\ \frac{kA_o}{r_o} &= \frac{1}{2\pi} \int_0^{2\pi} q''(\phi) d\phi \end{aligned} \tag{4}$$

Case I:  $q''(\phi) = q_o$

The case of  $q''(\phi)$  having a constant magnitude of  $q_o$  on one side of the channel and a zero heat flux on the remaining side is applicable to electronic cooling, space cold plates, and is an approximation for reactor component heat loading and many other applications. For the latter application, a sinusoidal heat flux distribution, which will be covered in Case II (below), is more applicable of fusion reactor components. For the case of a uniform heat flux on one side of a channel, the dimensionless temperature distribution is:

$$T^*(R, \phi) = \frac{\theta(r, \phi)}{\frac{q_o r_o}{k}} = \frac{1}{2} \left[ \frac{1}{Bi} + \ln R \right] + \sum_{n=1}^{\infty} \frac{2 \sin n \phi}{\pi n^2} \frac{R^n}{R_o^n} \frac{[1 - Bi_n R^{-2n}]}{[1 + Bi_n R_o^{-2n}]}, \quad (5)$$

where  $a_n=0$ ,  $A_o = \frac{q_o r_o}{k}$ , and  $b_n = \frac{-2q_o}{n\pi k}$ ,  $n=1,3,5,7,\dots$ . It is instructive to examine the validity of this equation with respect to the limits of the Biot number, Bi. For  $R=1$ ,

$$T^*(1, \phi) = \frac{1}{2Bi} + \sum_{n=1}^{\infty} \frac{4 \sin n \phi}{\pi n R_o^n [(Bi + n) + (Bi - n) R_o^{-2n}]}. \quad (6)$$

As Bi approaches infinity, the convective transport mode predominates. In that case, both terms in equation (6) approach zero and this implies that  $T(r, \phi)$  approaches  $T_b$ . In a similar fashion,  $T(r_o, \phi)$  approaches a temperature above  $T_b$  as  $Bi$  approaches infinity.

The radial temperature gradient is given by

$$\frac{\partial T^*}{\partial R}(R, \phi) = \frac{1}{2R} + \sum_{n=1}^{\infty} \frac{2 \sin n \phi}{\pi n} \frac{R^{n-1}}{R_o^n} \frac{[(Bi + n) + (Bi - n) R^{-2n}]}{[(Bi + n) + (Bi - n) R_o^{-2n}]} \quad (7)$$

The temperature gradients at  $R=1$  are especially important since they represent the effective circumferential heat flux at the inside wall of the coolant channel. Therefore, for  $R=1$ ,

$$\frac{\partial T^*}{\partial R} = \frac{1}{2} + \sum_{n=1}^{\infty} \frac{4 \sin n \phi}{\pi n R_o^n} \frac{Bi}{[(Bi + n) + (Bi - n) R_o^{-2n}]}$$

For  $Bi=0$ , the lowest achievable dimensionless temperature gradient at the boundaries occurs under the conditions of very high channel thermal conductivity or very low heat transfer coefficient. Therefore,  $\frac{\partial T}{\partial R}$  is given by

$$\frac{\partial T^*}{\partial R} = \begin{cases} \frac{1}{R_o} \left[ \frac{1}{2} + \sum_{n=1}^{\infty} \frac{2 \sin n \phi}{\pi n} \right], & \text{for } R = R_o \text{ and any } B_i; \\ \frac{1}{2}, & \text{for } R = 1 \text{ and for } B_i = 0; \\ \frac{1}{2} + \sum_{n=1}^{\infty} \frac{4 B_i \sin n \phi}{\pi n R_o^n [(B_i + n) + (B_i - n) R_o^{-2n}]}, & \text{for } R = 1 \text{ and any } B_i. \end{cases} \quad (8)$$

The first equation in equation (8) should satisfy equation (2c).

Two additional relationships will be of interest: (1) the average circumferential dimensionless temperature excess,  $T_{av}^*(R)$ , and (2) the ratio of the inside wall temperature to the outside wall temperature.  $T_{av}^*$  is defined as

$$T_{av}^*(R) = \frac{1}{\pi} \int_{\frac{\pi}{2}}^{\frac{3\pi}{2}} T^*(R, \phi) d\phi, \text{ or} \quad (9)$$

$$T_{av}(R) = \frac{1}{2} \left[ \frac{1}{B_i} + \ln R \right] \quad (10)$$

Therefore, if  $T_{AV}$  is measured experimentally the mean heat transfer coefficient,  $h_m$  can be obtained from equation (10). In cases where measurements of  $T(R_o, \phi)$  are made, it may be important to relate this measurement directly to  $T(1, \phi)$ . In this instance, it will be important to know the ratio of the inside to outside channel wall temperatures. These quantities are related to the ratio of  $T^*(1, \phi)/T^*(R_o, \phi)$ . It is very important to note that this ratio is completely independent of the magnitude of  $q_o$  and is only implicitly related to the thermal conductivity of the channel,  $h_m$ , and the geometry via the Biot number; i.e.,

$$\frac{T^*(1, \phi)}{T^*(R_o, \phi)} = \frac{\frac{1}{2B_i} + \sum_{n=1}^{\infty} \frac{4 \sin n \phi}{\pi n R_o^n [(B_i + n) + (B_i - n) R_o^{-2n}]}}{\frac{1}{2} \left[ \frac{1}{B_i} + \ln R_o \right] + \sum_{n=1}^{\infty} \frac{2 \sin n \phi}{\pi n^2} \frac{[(B_i + n) - (B_i - n) R_o^{-2n}]}{[(B_i + n) + (B_i - n) R_o^{-2n}]}} \quad (11)$$

As will be displayed shortly, the above equations can be used to either: (1) obtain the temperature distribution for given values of  $q_o$ ,  $h_m$ ,  $k$ , geometry, etc., or (2) obtain the

mean circumferential heat transfer coefficient,  $h_m$ , from measurements of the outside wall temperature for given values of  $q_o$ ,  $k$ , and the geometry.

Case II:  $q''(\phi) = q_o \sin(\phi)$

There are many applications where the flow channel is irradiated from one side by a heat source, and shielded on the other side. Equations (3) and (4), which apply equally to this case, reduce to the following after equation (2c) is applied by allowing for  $q''(\phi) = q_o \sin \phi$ ,

$$T^*(R, \phi) = \frac{1}{\pi} \left\{ \left[ \frac{1}{Bi} + \ln R \right] + \frac{1}{2} \sum_{n=2}^{\infty} \frac{(R^{-n} Bi_n - R^n)}{2n(R_o^{-n} Bi_n - R_o^n)} \left[ \frac{\{(-1)^{n-1} - 1\}}{n-1} + \frac{\{(-1)^{n+1} - 1\}}{n+1} \right] \cos n\phi \right. \\ \left. - \frac{\pi}{2} \left[ \frac{R^{-1} - R \left\{ \frac{Bi-1}{Bi+1} \right\}}{R_o^{-1} + R_o \left\{ \frac{Bi-1}{Bi+1} \right\}} \right] \sin n\phi \right\}, \quad (12a)$$

$$\frac{\partial T^*}{\partial R}(R, \phi) = \frac{1}{\pi} \left\{ \frac{1}{R} + \frac{1}{2} \sum_{n=2}^{\infty} \frac{(R^{-n-1} Bi_n + R^{n-1})}{(R_o^{-n} Bi_n - R_o^n)} \left[ \frac{1}{(n-1)} + \frac{1}{n+1} \right] \cos n\phi \right. \\ \left. - \frac{\pi}{2} \left[ \frac{-R^{-2} - \left\{ \frac{Bi-1}{Bi+1} \right\}}{R_o^{-1} + R_o \left\{ \frac{Bi-1}{Bi+1} \right\}} \right] \sin n\phi \right\} \quad (12b)$$



### Formulation Verification

The heat transfer coefficient  $h_m$  can be defined as,

$$h_m = \frac{k \frac{\partial T}{\partial r}(1, \phi)}{[T(1, \phi) - T_b]}, \quad \text{or} \quad (13a)$$

$$1.0 = \frac{B_i^{-1} \frac{\partial T^*}{\partial R}(1, \phi)}{T^*(1, \phi)}, \quad (13b)$$

which reduces to,

$$1 = \frac{\frac{1}{2} + \sum_{n=1}^{\infty} \frac{4B_i \sin n\phi}{\pi n R_o^n [(B_i + n) + (B_i - n) R_o^{-2n}]}}{\frac{1}{2} + \sum_{n=1}^{\infty} \frac{4B_i \sin n\phi}{\pi n R_o^n [(B_i + n) + (B_i - n) R_o^{-2n}]}} \quad (14)$$

This equation represents one of the boundary conditions. All computations must exactly satisfy this equation for all values of  $B_i$ ,  $R_o$ , and  $\phi$ . This is just one of many ways the computed results were verified.

### RESULTS\*

The results are presented in a dimensionless form involving parametric variations of the averaged wall temperature, wall temperature distributions, and the radial temperature gradient at the inside surface of the coolant channel. This gradient is most important because it is directly related to the local (circumferential) heat flux. For cases involving a non-uniform external heat flux distribution, most designers are quite interested in the corresponding non-uniform heat flux distribution at the inside boundary. This heat flux is equal to  $-k \frac{\partial T(r_1, \phi)}{\partial r}$ . A closed-form solution for the temperature gradient in this

---

\* See the nomenclature list to note the differences in the origin for  $\phi$  for the formulation equations and the plots, which are contained in this section.

latter equation has been given above, and corresponding circumferential distributions are presented below as functions of  $Bi$  and  $R_o$  for the case of  $q'' = q_o$ .

### Parametric Temperature Distribution

Closed-form two-dimensional analytical temperature distributions have been obtained for two cases involving single-sided heat flux distribution. In both cases the heat flux was applied on one side; i.e., half of the perimeter of the circular coolant channel was heated while the remaining half was insulated. In one case the heat flux distribution was constant (see equation (5)); and in the other, a sinusoidal heat flux distribution was used with the maximum heat flux occurring on the plane of symmetry (see equation (12) and Figure 2). In the latter case, a zero heat flux existed from  $\phi = \frac{\pi}{2}$  to  $\phi = \frac{3\pi}{2}$ . This analytical approach is an improvement over the previous data reduction technique, which employed the heated hydraulic diameter model used in Part I.

The improved technique for determining the circumferentially mean heat transfer coefficient,  $h_m$ , is based on equation (10). This simple equation relates the circumferentially averaged temperature at any  $R$  to  $B_i$ , and hence  $h_m$ . In the experiments described in Part I, local temperature measurements were made at  $R = R_o$ , and the averaged temperature was computed from these measurements. Figure 10 shows the dimensionless, averaged temperature as a function of both  $B_i$  and  $R_o$ . For the experiments in Part I,  $B_i$  was less than  $3.0 \times 10^{-3}$  and  $R_o$  was near 1.1. From Figure 10, this indicates that measured values of  $T_{av}^*$  above 0.5 give good resolution for corresponding values of  $B_i$  (or  $h_m$ ).

The local variations of the coolant channel wall temperature are presented in Figures 11 ( $\phi = 0$  and  $\pi$ ) and 12. Figures 11a-c ( $\phi = 0$ ; center of the heated side) appear to show

that there are negligible variations of  $T^*$  for all  $R$  and  $Bi$ . However, closer inspection is provided by Figures 11d-f, where it is shown that at all values of  $R_o < 1.04$  and  $Bi < 0.01$ , there are negligible variations of  $T^*$  with respect to  $R$ . Figures 11g-l show similar results for  $\phi = \pi$  (center of the insulated side). The circumferential variation of  $T^*$  is shown in Figure 12 in terms of the ratio of  $T^*(R = 1, \phi)/T^*(R = R_o, \phi)$  for  $R_o = 3.0$ . The maximum value of this ratio is 1.0, which is approached when: (1)  $Bi$  becomes small (i.e.  $< 0.005$ ), and (2) as  $R_o$  approaches 1.0. The minimum value of this ratio always occur at  $\phi = 0$  (Heated side). This corresponds with  $T(R_o, \phi)$  being a maximum and  $T(1, \phi)$  being a minimum. The maximum value of the ratio occurs at  $\phi = \pi$ , which is on the line of symmetry of the insulated portion of the channel.

#### Inside Wall Heat Flux Distribution

The heat flux distribution at the inside wall of the coolant channel is proportional to the local radial temperature gradient at  $R=1.0$ . Figures 13a-c show that there are no substantial heat flux variations on the inside wall when: (1)  $Bi < 10^{-3}$  for  $R_o = 1.04$ , (2)  $Bi < 10^{-2}$  for  $R_o = 1.34$ , and (3)  $Bi < 5.0 \times 10^{-2}$  for  $R_o = 3.0$ . Notice that this  $Bi$  limit increases with  $R_o$ . Hence for  $Bi$  greater than the above limits, the circumferential variation of the inside wall heat flux becomes progressively larger as  $Bi$  increases.

Because the analytical results are in form of infinite series, the convergence of the series requires more and more terms: (1) as  $R_o$  approach 1.0, and (2) as  $Bi$  becomes larger (e.g., greater than 0.2 for  $R_o=1.04$ , and greater than 10.0 for  $R_o=1.34$ ). Let  $\epsilon$  be defined as the difference in the infinite series of equation (8) which is computed by using "n"-terms in

one case and "n+1" terms in the other. When  $\epsilon = 10^{-3}$ , poor convergence resulted for the above noted intervals of  $Bi$ . The results in Figures 13a-c required  $\epsilon = 10^{-7}$  for acceptable convergence. A number of approaches were used to check and verify the results. As noted above, convergence was assumed when all boundary conditions were computed within a minimal error. the boundary condition shown in equation (2b).

## CONCLUSIONS

An improved technique has been developed for obtaining circumferentially mean heat transfer coefficients from measured wall temperature data for circular coolant channels which are heated externally from one side and insulated externally on the other. Although two cases for the outside heat flux distribution were considered (constant and sinusoidal) a parametric analysis was presented for the cases of constant heat flux. For both cases, closed-formed analytical solutions were obtained.

Detail results were presented for the case of constant outside heat flux. The technique has good resolution for  $Bi < 0.5$  and should result in minimal error in the heat transfer coefficient for a dimensionless temperature,  $T^*$ , greater than 0.5 for  $Ro < 1.5$ . Quantitative profiles were computed for the effective inside heat flux circumferential distribution, which is proportional to  $\frac{\partial T^*(1,\phi)}{\partial R}$ . Significant circumferential heat flux variations occurred at higher  $Bi$  as  $Ro$  increased. For example, significant variations occurred for: (1)  $Ro = 1.04$ , when  $Bi > 10^{-3}$ ; (2)  $Ro = 1.34$ , when  $Bi > 10^{-2}$ ; and (3)  $Ro = 3.0$ , when  $Bi > 5.0 \times 10^{-2}$ .

## ACKNOWLEDGMENTS

The PI would like to acknowledge Dr. Joseph Atkinson, John Thornborrow and NASA(JSC and Headquarters) for their assistance and for supporting this work under contract NAG 9-310. In addition, the PI is grateful to: Dana Brooks (undergraduate), Byran Curtis (undergraduate), and Fred Smith (undergraduate) for their assistance and their willingness to consider research and a graduate education. Finally, a special thanks goes to Mrs. Margie Lewis and Ms Wei Cui whose help in typing segments of this manuscript came at a critical time. Above all, I would like to acknowledge the friendship of all the above students and assistants listed in Parts I and II, and the co-authors of Parts I and II.

## REFERENCES

1. Hasan, M.Z., "Effects of Nonuniform Surface Heat Flux and Uniform Volumetric Heating on Blanket Design for Fusion Reactors", Fusion Technology, Vol 16, 1989, pp. 44-52.
2. Boyd, R.D. and Turknett, J.C., "Forced Convection and Flow Boiling With and Without Enhancement Devices for Top-Side-Heated Horizontal Channels", Space Science and Engineering Research Forum Proceedings, Alabama A&M University, Normal, Alabama, 1989 (March), pp. 363-370.
3. Reynolds, W.C., J. Heat Trans. ASME, Vol 82(2), 1960, pp. 108-112.
4. Reynolds, W.C., Int J. Heat and Mass Transfer, 6, 1963, pp. 445-454.

## Figure Captions

Figure 10. Circumferentially Averaged Temperature, at  $R = R_o$  Versus the Biot Number, Bi.

Figure 11. Local Dimensionless Temperature Versus R With Bi as a Parameter for:

- (a)  $R_o=1.04$ , and  $\phi=0$  (center of the heated side); (b)  $R_o=1.34$ , and  $\phi=0$ ; (c)  $R_o=3.0$ , and  $\phi=0$ ; (d)  $R_o=1.04$ ,  $\phi=0$ , and reduced range for  $T^*$ ; (e)  $R_o=1.34$ ,  $\phi=0$ , and reduced range for  $T^*$ ; (f)  $R_o=3.0$ ,  $\phi=0$ , and reduced range for  $T^*$ ; (g)  $R_o=1.04$ ,  $\phi=\pi$  (center of the insulated side); (h)  $R_o=1.34$ , and  $\phi=\pi$ ; (i)  $R_o=3.0$ , and  $\phi=\pi$ ; (j)  $R_o=1.04$ ,  $\phi=\pi$ , and reduced range for  $T^*$ ; (k)  $R_o=1.34$ ,  $\phi=\pi$ , and reduced range for  $T^*$ ; and (l)  $R_o=3.0$ ,  $\phi=\pi$ , and reduced range for  $T^*$ .

Figure 12. Circumferential Variation of the Ratio of the Inside to Outside Wall Temperatures as a Function of Bi for  $R_o=3.0$ .

Figure 13. Circumferential Variation of the Local Dimensionless Radial Temperature Gradient as a Function of Bi for: (a)  $R_o=1.04$ , (b)  $R_o=1.34$ , and (c)  $R_o=3.0$ .

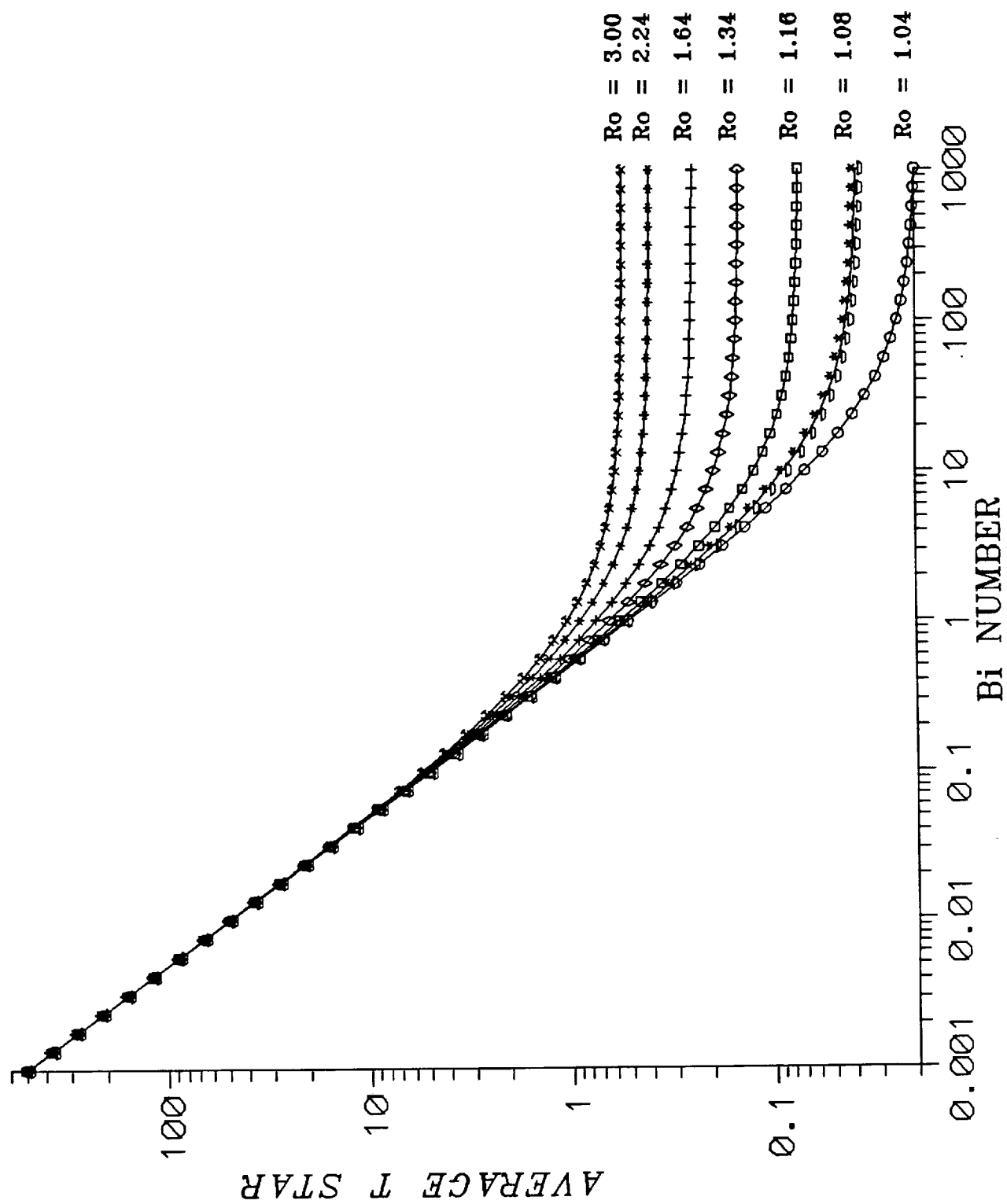


FIG. 10

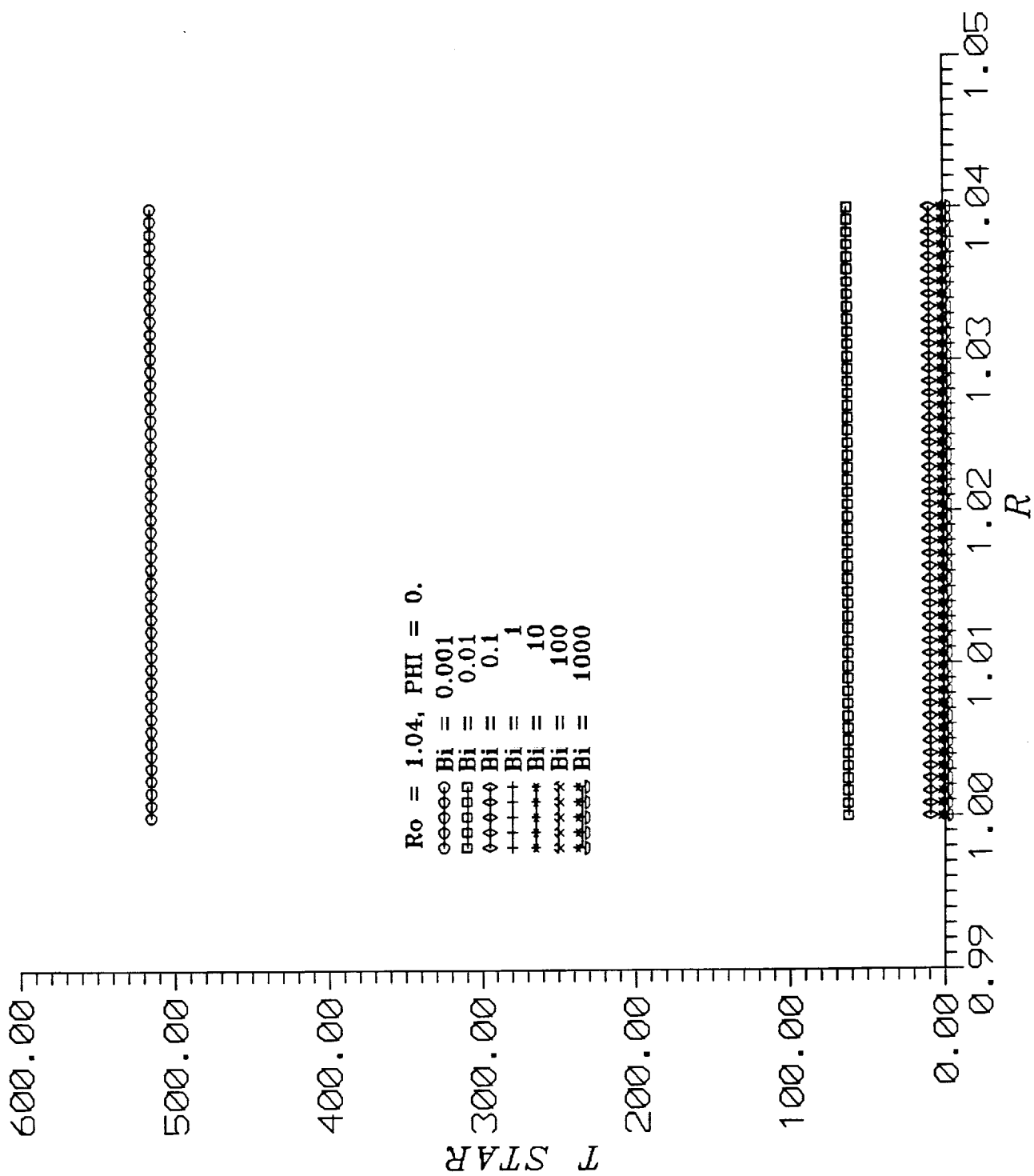


FIG. 11a



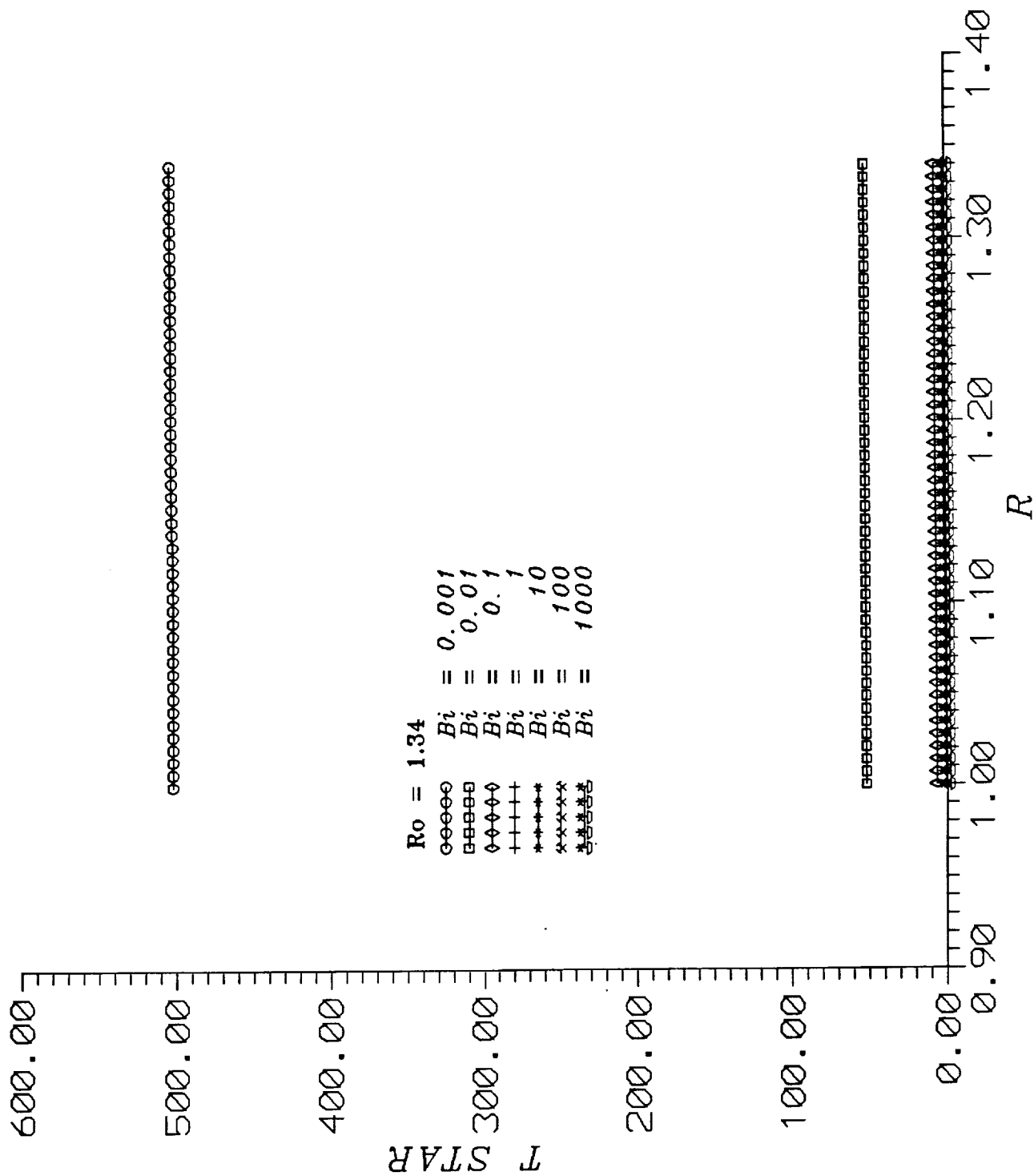


FIG. 11b

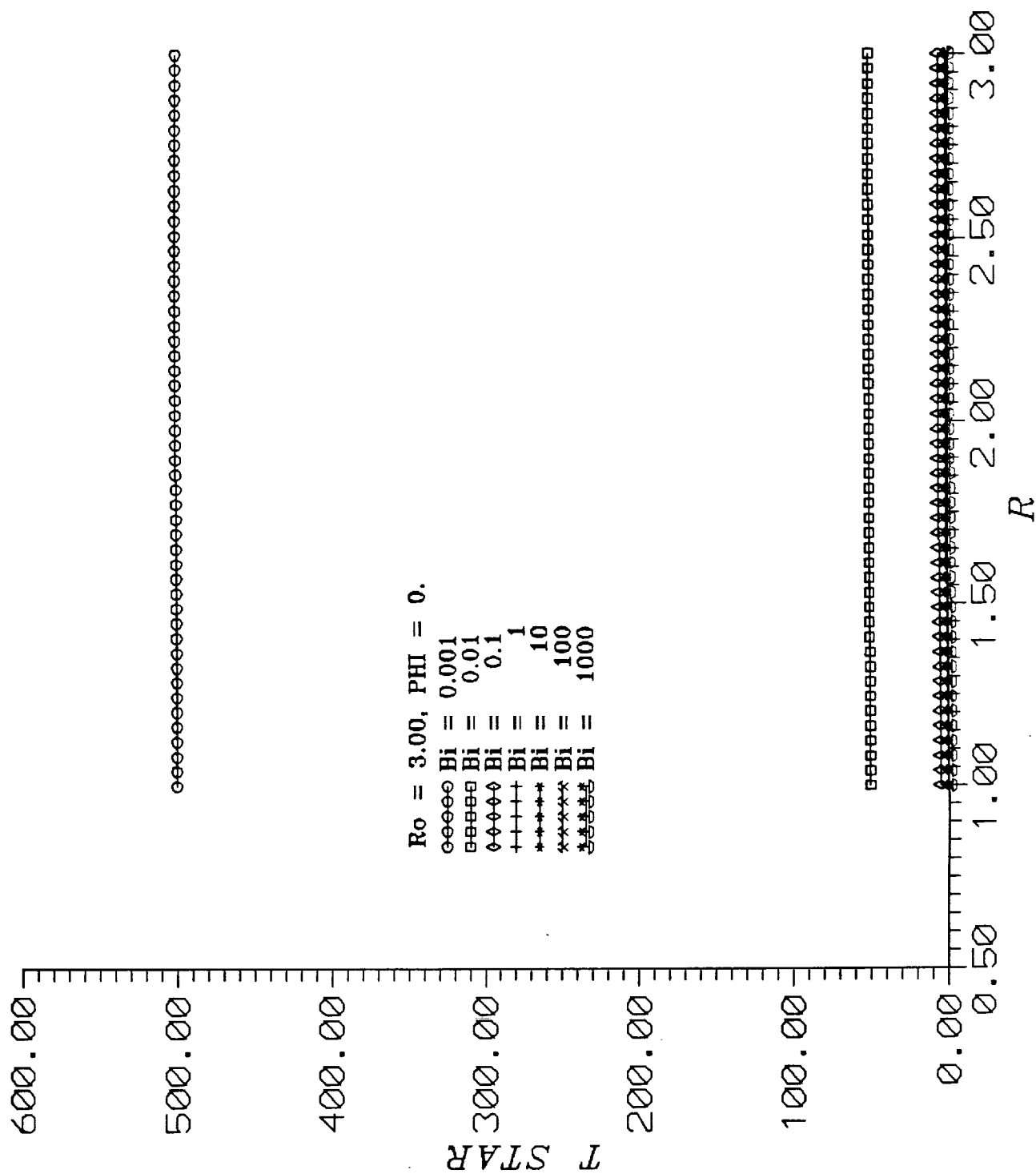


FIG. 11c

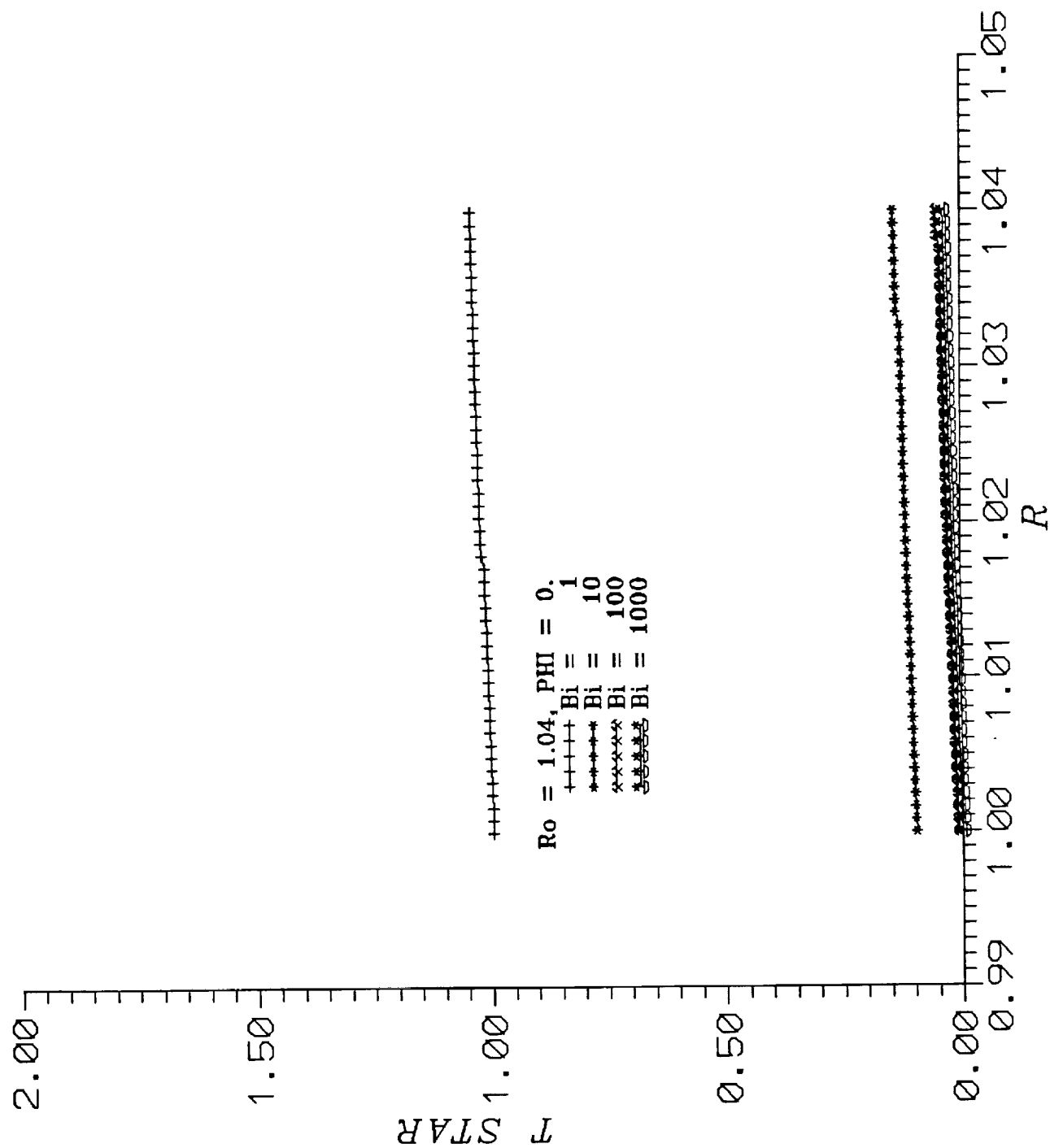


FIG. 11d

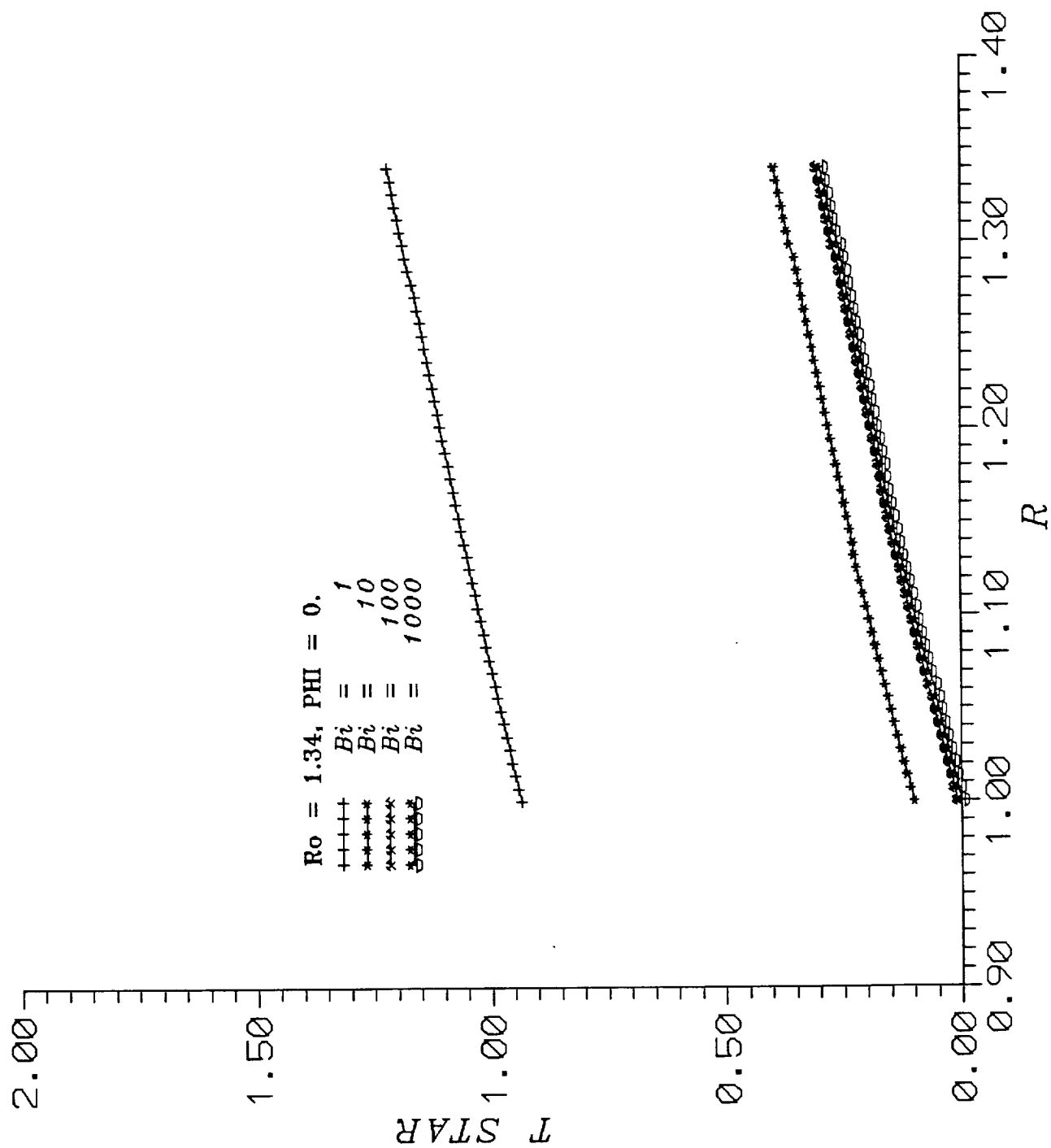


FIG. 11e

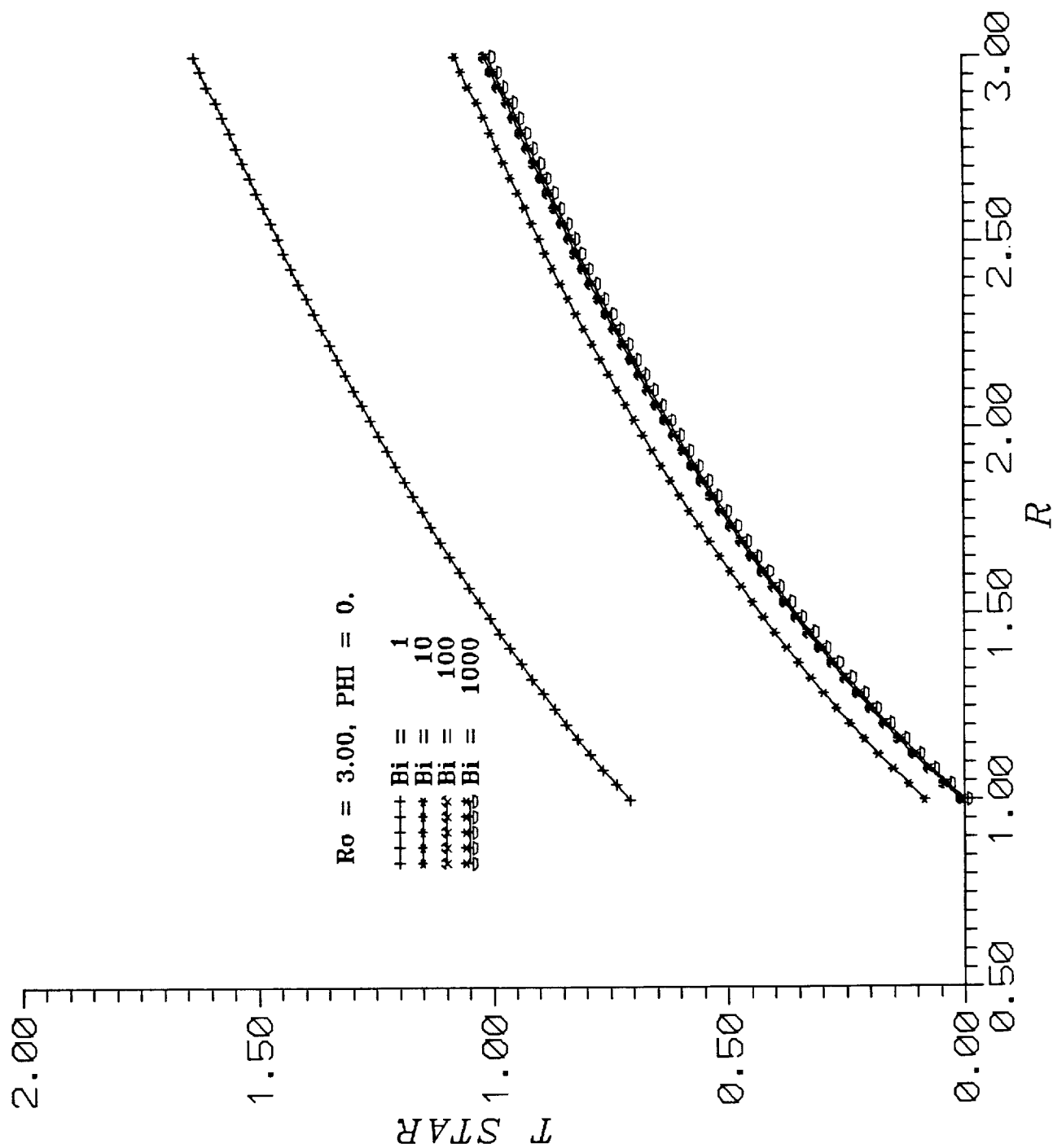


FIG. 11f

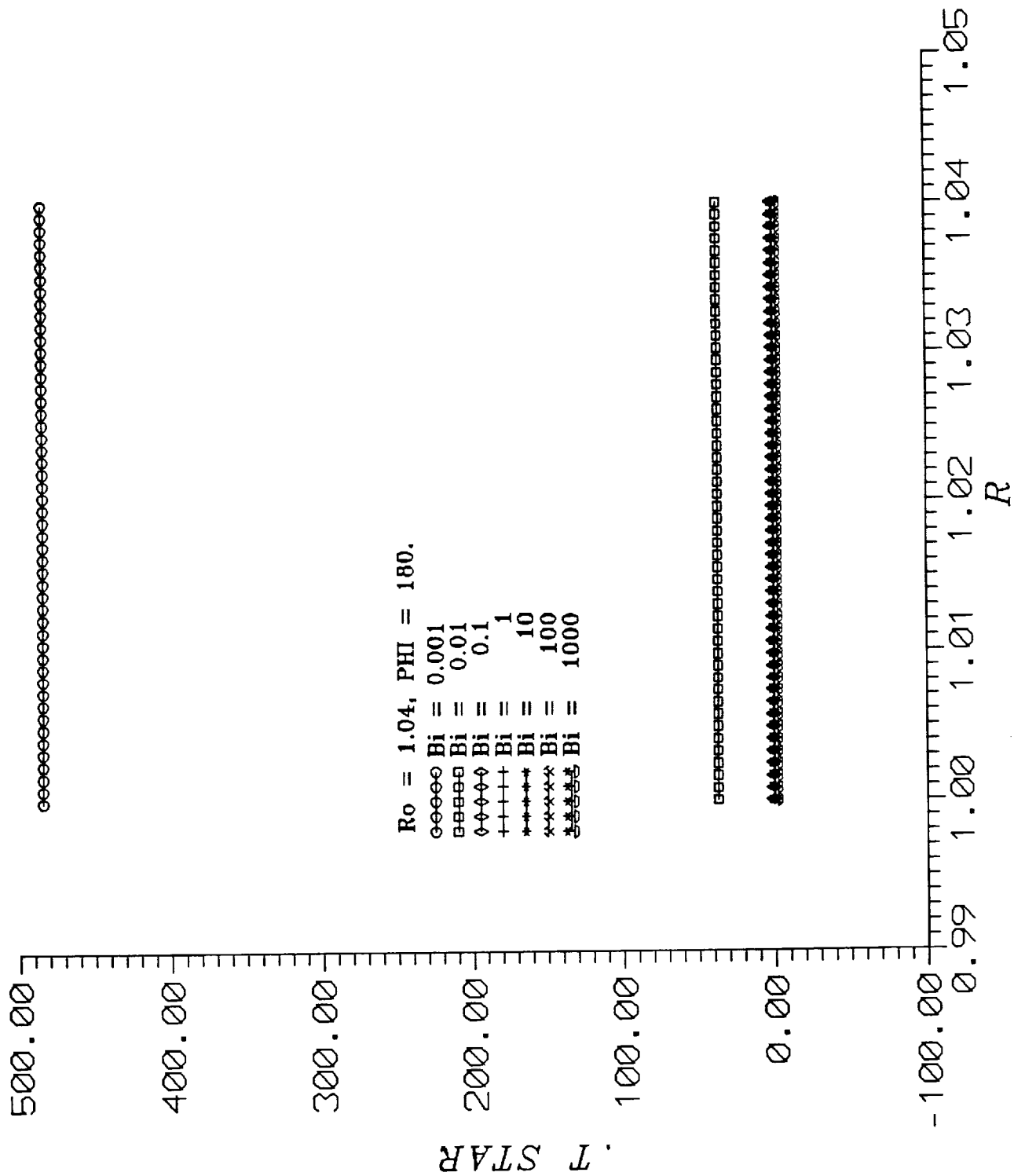


FIG. 11g

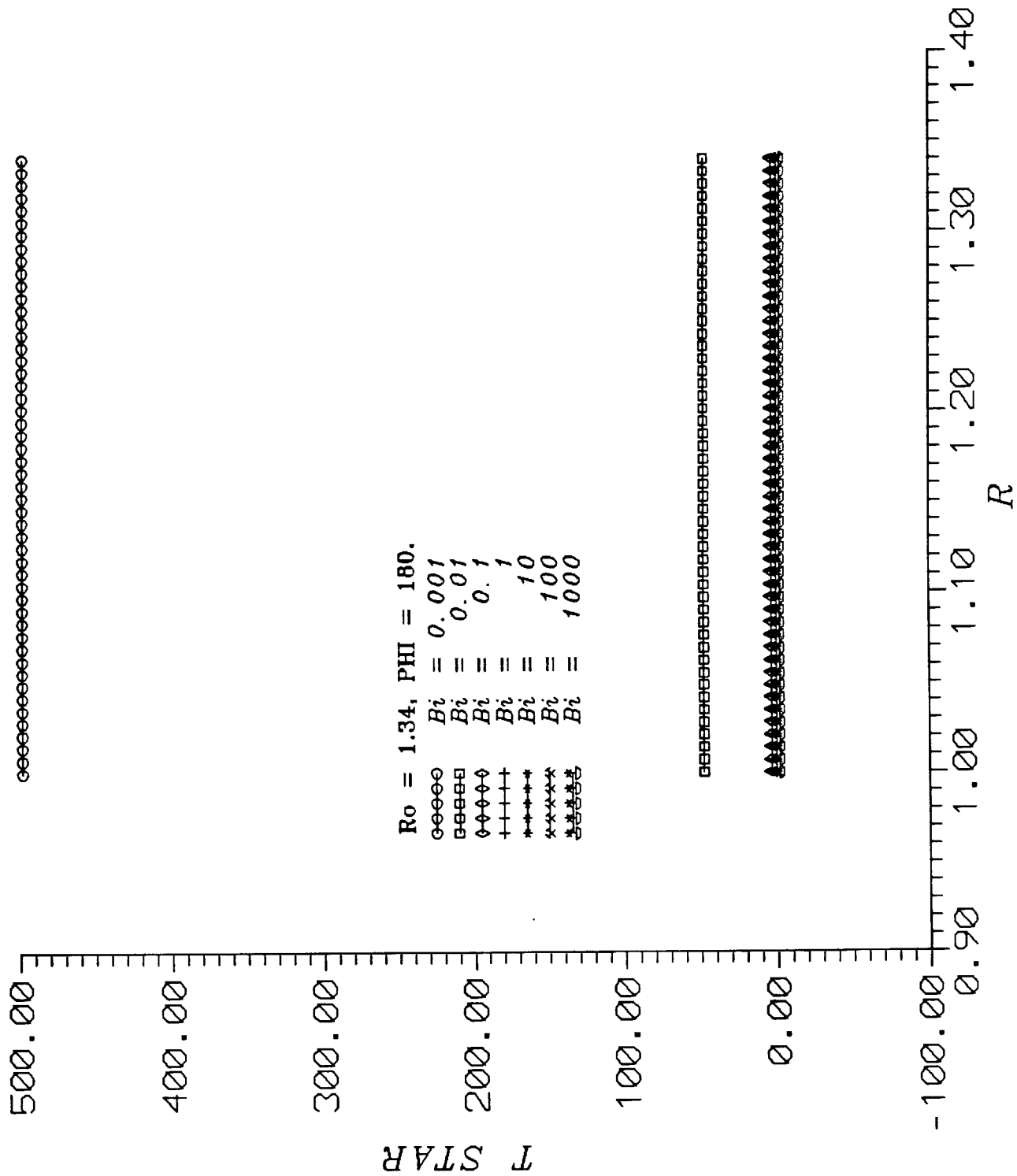


FIG. 11h

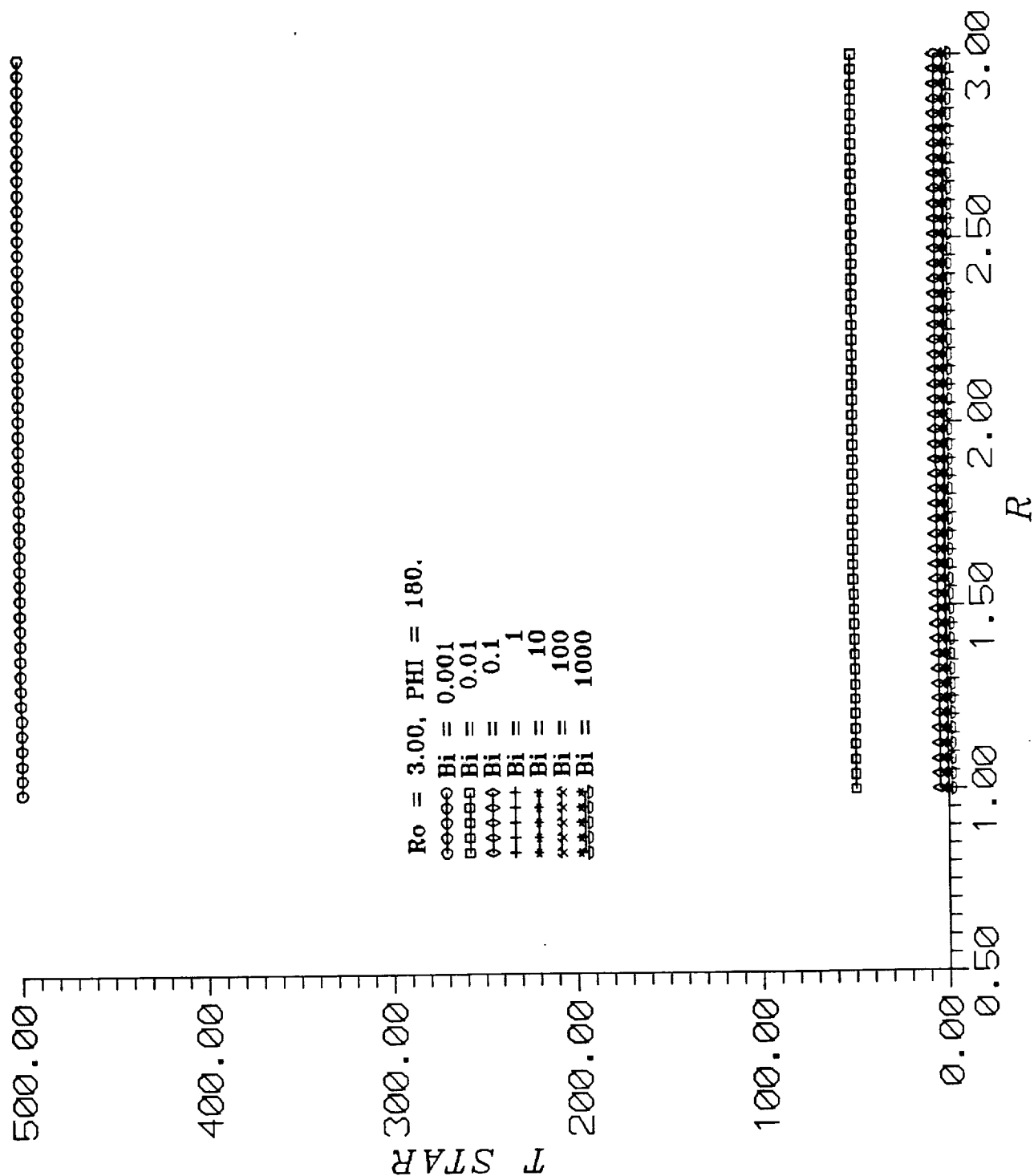


FIG. 11i



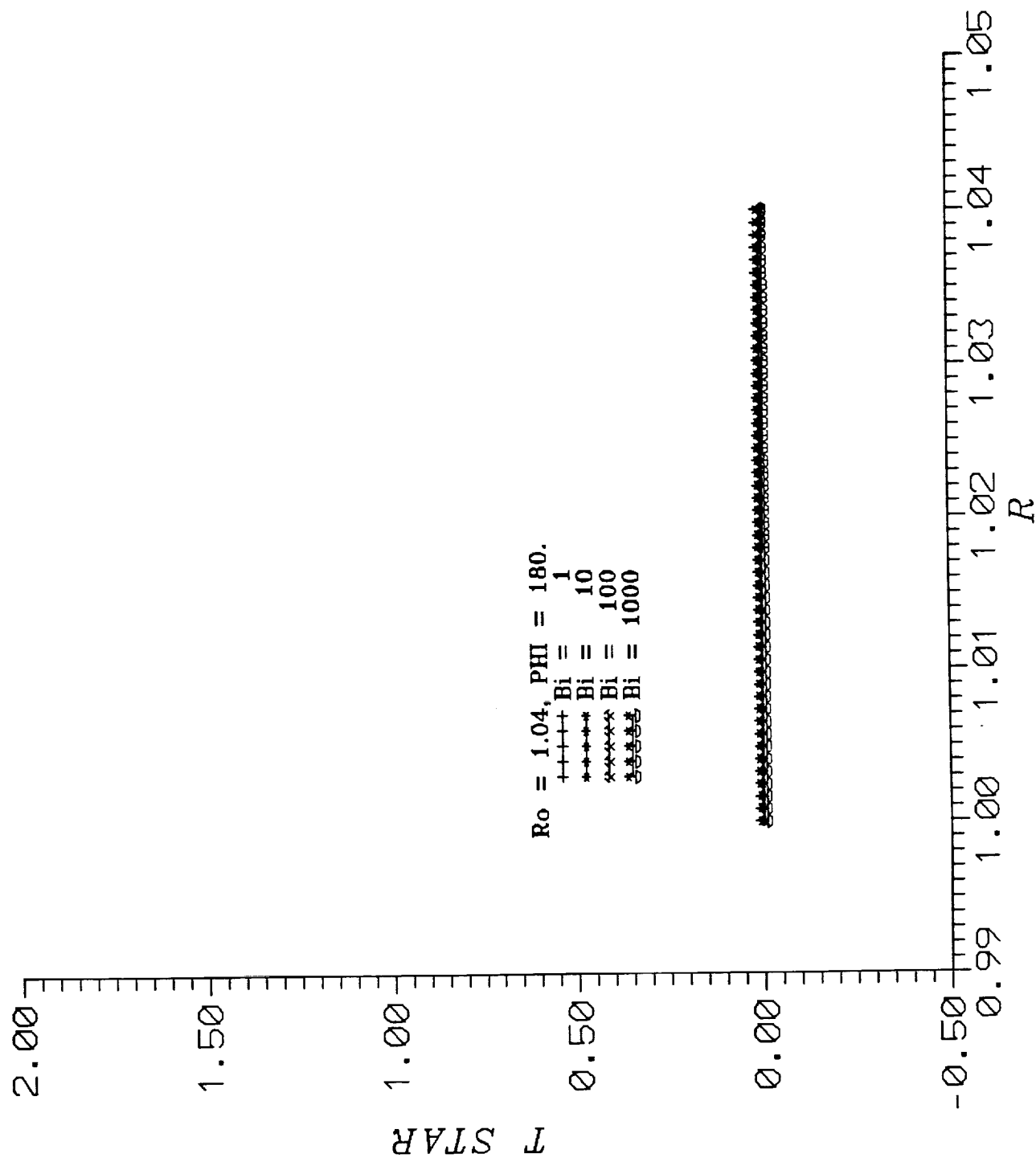


FIG. 11j

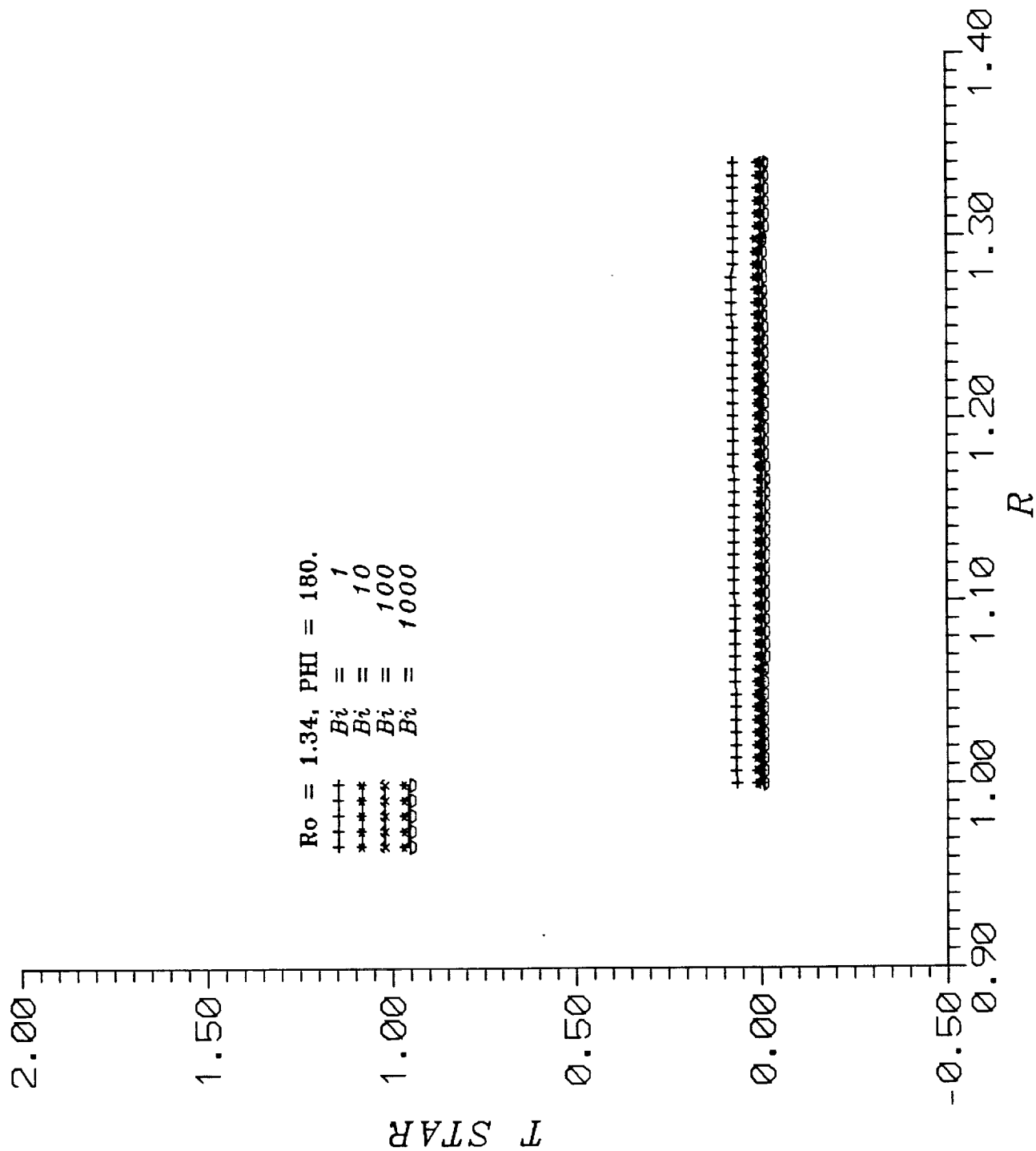


FIG. 11k

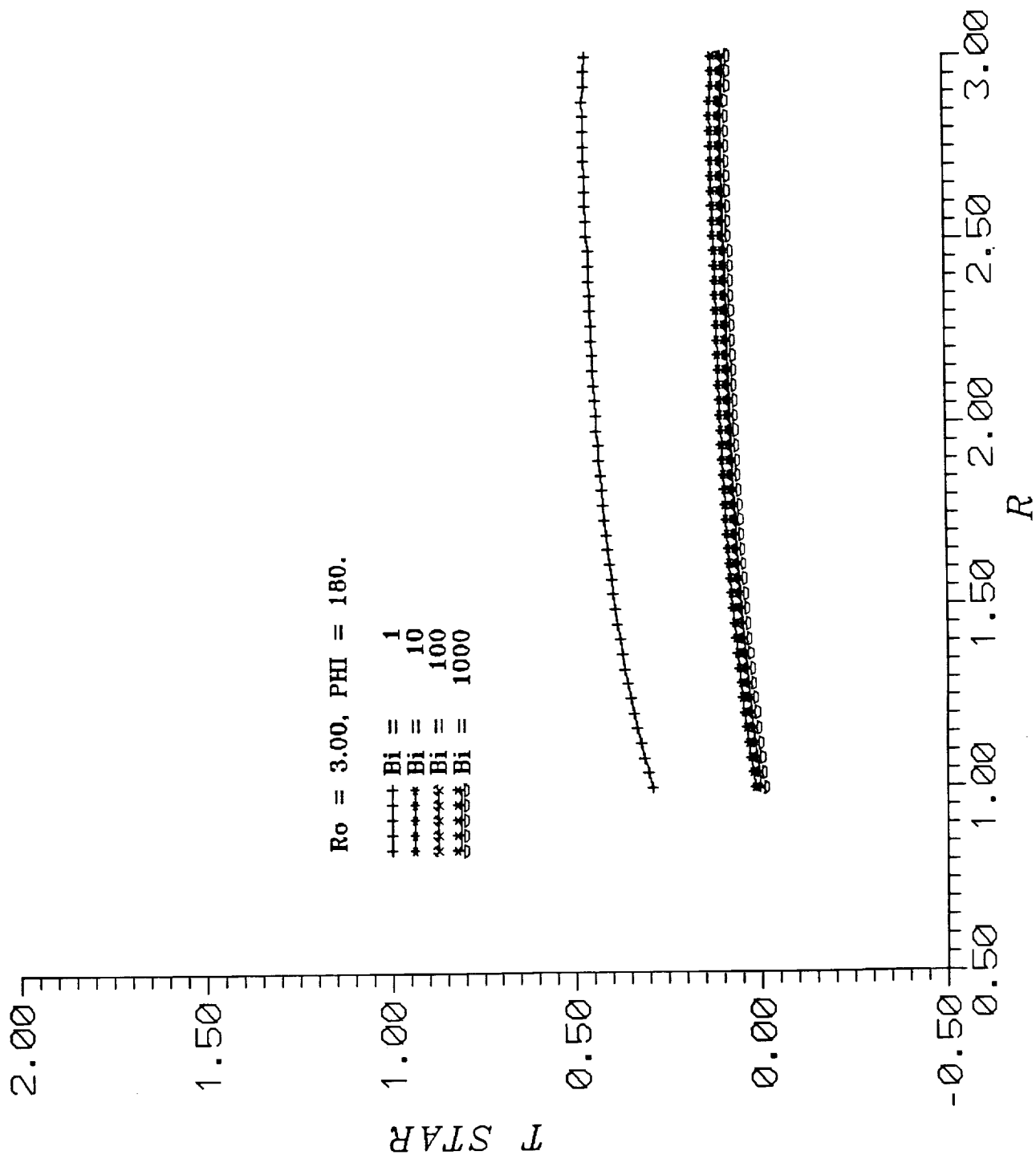


FIG. 111

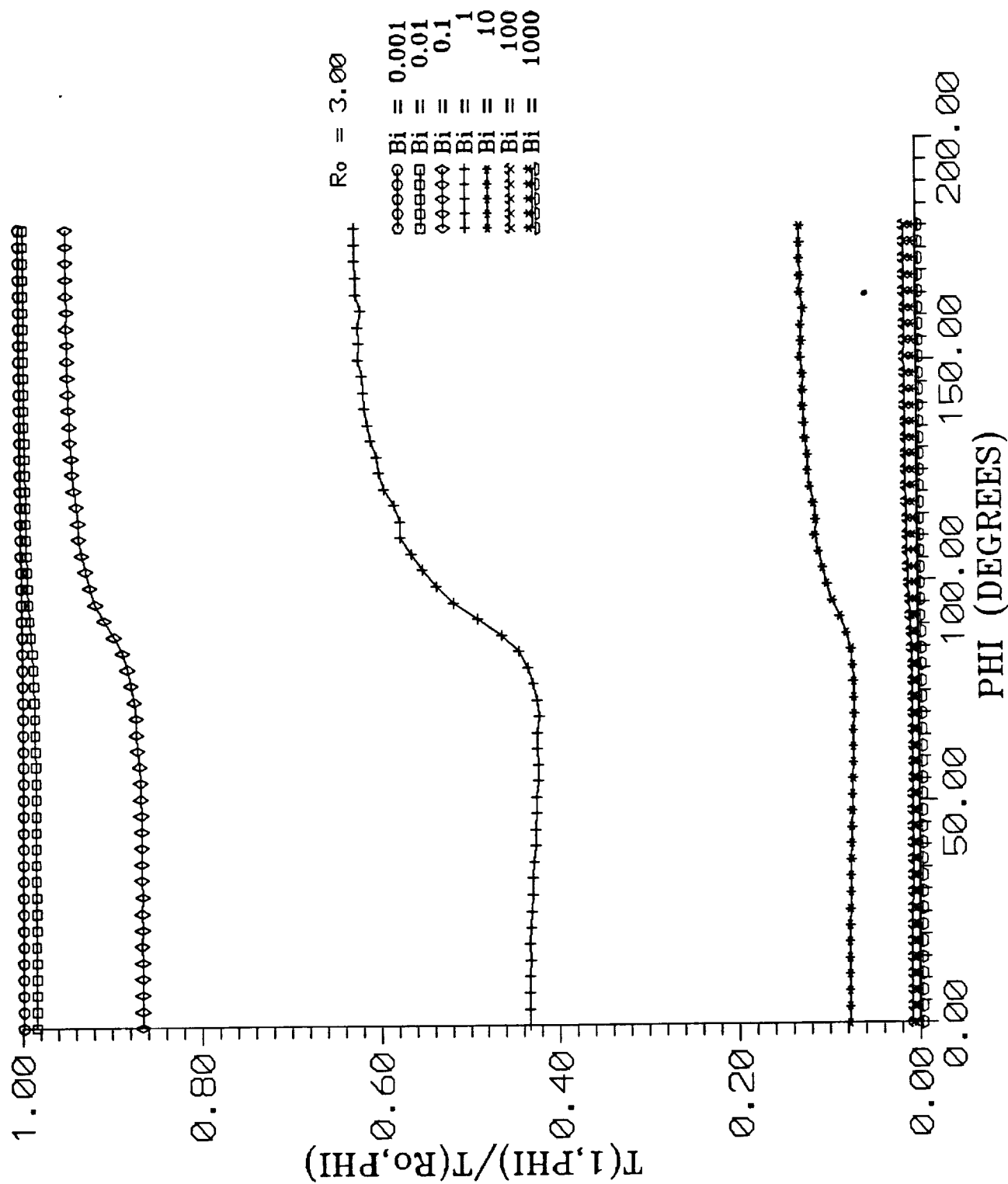


FIG. 12

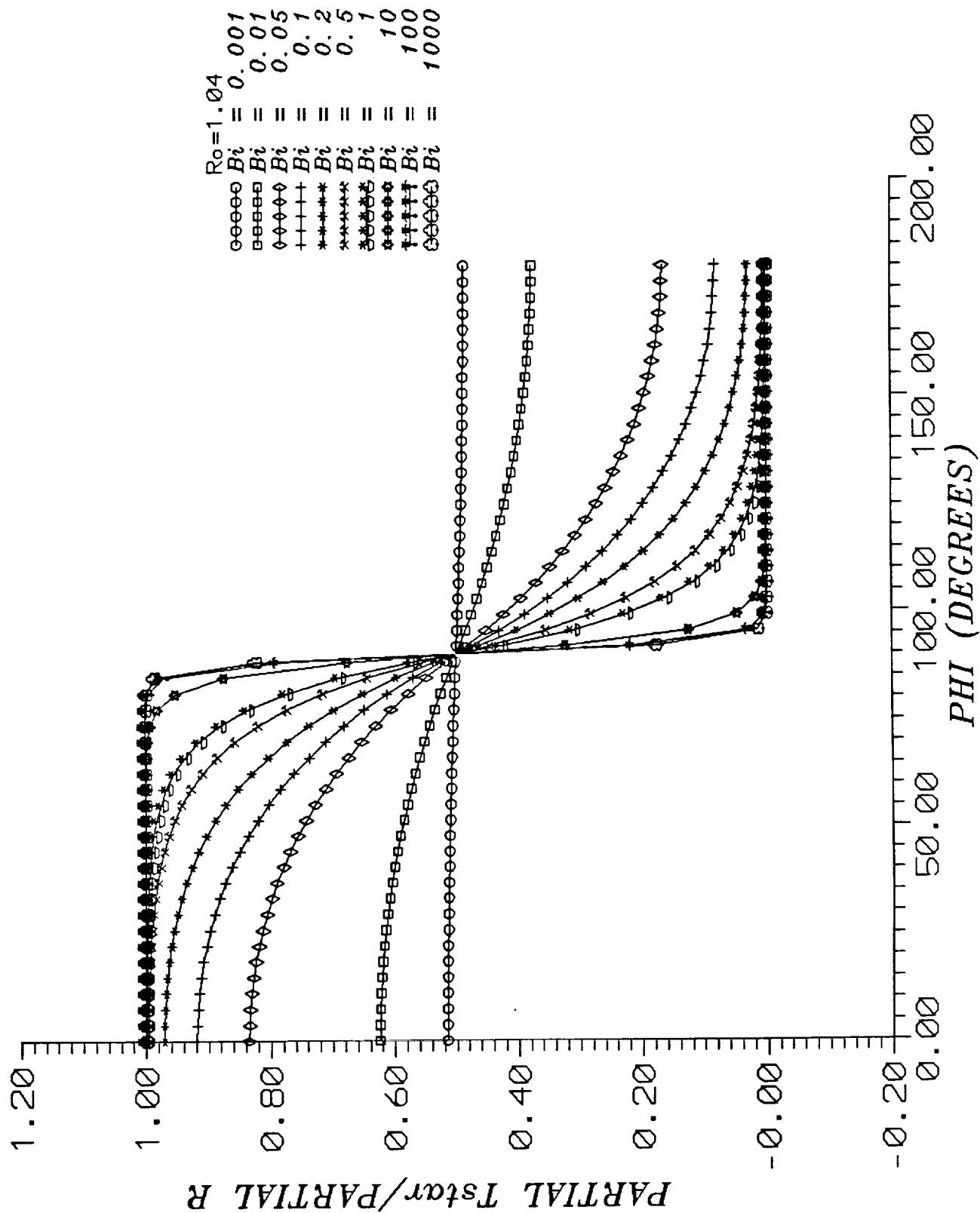


FIG. 13a

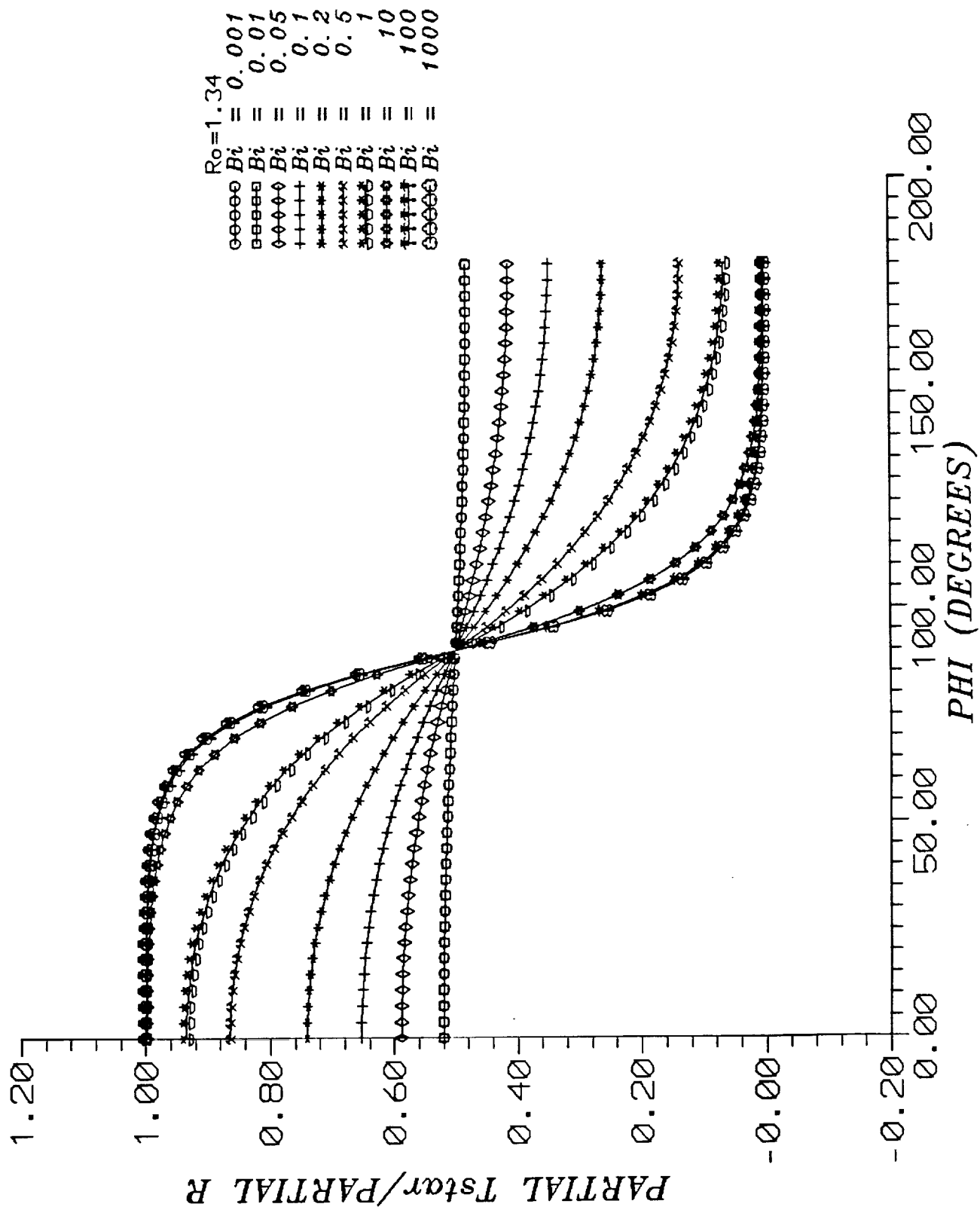


FIG. 13b

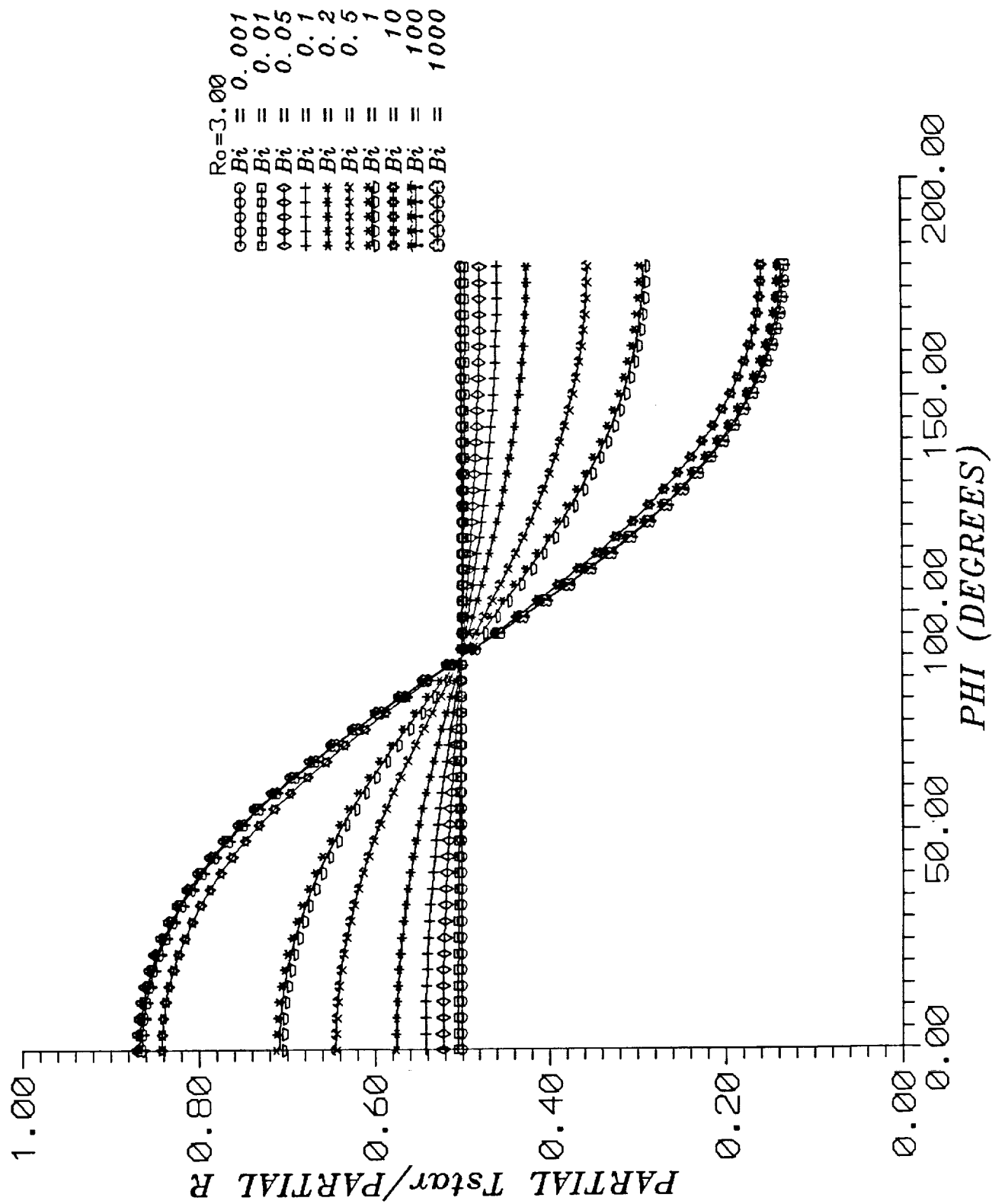


FIG. 13c

## DISTRIBUTION

Mr. John Thornborrow, (3)  
Technical Officer  
(Research Grant # NAG 9-310)  
Mail Code: EC5  
NASA Johnson Space Center  
Houston, TX 77058

NASA Scientific & Information Facilities (2)  
P. O. Box 8757  
Baltimore-Washington Airport  
Baltimore, MD 21240

Dr. Ronald D. Boyd, (10)  
Honeywell Endowed Professor of Engineering and  
Director of the Thermal Science Research Center  
P. O. Box 397  
Department of Mechanical Engineering  
Prairie View A&M University  
Prairie View, TX 77446

Mr. Alvin Smith,  
Graduate Student

Mr. Xiaowei Meng,  
Graduate Student

Dr. Joseph Atkinson,  
Director  
Equal Opportunity Employment Office  
Mail Code AJ  
NASA Johnson Space Center  
Houston, TX 77058

Mr. Robert Effinger,  
Project Specialist  
Prairie View A&M University  
Research Foundation  
Rm 104A, Anderson Hall

Dr. F. Byrd  
Vice President For Academic Affairs  
Administration Building  
Prairie View A&M University



Dr. J. Foster,  
Dean  
College of Engineering And Architecture  
Prairie View A&M University

President J. Becton, Jr.  
Prairie View A&M University

End Date Feb 8, 1992